Gasification and Pyrolysis of Eucalyptus, Prickly Pear, Gumweed, and Lignin for Biofuels and Chemical Intermediates

by

Phillip James Cross

A dissertation submitted to the Graduate Faculty of
Auburn University
in partial fulfillment of the
requirements for the Degree of
Doctor of Philosophy

Auburn, Alabama
August 4th, 2018

Keywords: Gasification, Pyrolysis, Eucalyptus, Prickly Pear, Gumweed, Lignin

Approved by

Sushil Adhikari, Chair, Professor of Biosystems Engineering
Oladiran Fasina, Professor of Biosystems Engineering
Brian Via, Professor of School of Forestry and Wildlife Sciences
Yi Wang, Assistant Professor of Biosystems Engineering

Abstract

This focus of this dissertation is to advance our understanding of how the chemical makeup of feedstocks alters the performance of thermochemical conversion and alters the production of biofuel and chemical intermediates. In doing so we also develop strategies for obtaining a chemical makeup more suitable for producing the desired product slate. The large-scale use of non-food biomass as a source of renewable carbon for fuels and specialty chemicals will require the development of dedicated feedstocks with cell wall characteristics optimized for growth and efficient conversion (high carbon and hydrogen retention, low catalyst deactivation). Additionally, intensification of biomass production and reduction in water and nutrient consumption is crucial. Therefore, this dissertation is focused on understanding the thermochemical conversion of advanced feedstocks which will include woody biomass grown using state of the art agricultural practices, drought tolerant biomass species, and chemically isolated lignin's. Harvesting age and presence/absence of bark have been selected as parameters to improve the agricultural practices and chemical makeup of short rotation *Eucalyptus benthamii* (*E. benthamii*). Additionally, *Opuntia ficus-indica* (prickly pear) and *Grindelia squarrosa* (gumweed), exceptionally drought tolerant plants, are converted to biofuels using thermochemical processes for the first time. Finally, chemically isolated lignin's from hardwood and softwood species are a promising feedstock for the production of phenolic compounds as specialty chemicals for polymers and resins.

Thermochemical gasification and pyrolysis of *E. benthamii* showed that by selecting the age at which *E. benthamii* was harvested and altering the presence/absence of bark, tar profiles of gasification can be altered. Older trees without bark produced more naphthalene and indene while younger trees produced more benzene and toluene. Additionally, syngas profiles from gasification are affected by these parameters.

Older 7 year *E. benthamii* without bark (7EWoB) generated higher levels of CH_4 leading to a higher heating value of the syngas compared to both younger samples harvested at 2 years with and without bark (2EWoB and 2EWB). The presence of bark was found to increase the H_2 yield which leads to a higher H_2: CO gas ratio with the 2EWB sample. By selecting the appropriate growth cycle and altering the presence/absence of bark, the product slate and kinetics of fast pyrolysis can be altered. Older samples had a higher CrI of the cellulose leading to the production of d-Allose while this compound was not observed in measurable quantities from younger samples. Additionally, the phenolic-monomers produced through fast pyrolysis were different for these samples.

To further asses the formation of gasification tar as one of the main hurdles to the industrialization of the gasification technology, model lignin dimers were used to evaluate how different linkages of lignin and S, G, and H type lignin alter the reaction network and tar compounds. Pyrolysis at 850°C showed that S type dimers produce more indene and 2-ring aromatics through radical condensations. G type lignin was found to generate more furans and 3-ring tars while H type lignin produces more phenolics and 1-ring aromatics.

Opuntia ficus-indica (prickly pear) and *Grindelia squarrosa* (gumweed) are two types of biomass that possess unique cell wall architectures tailored for prolific growth in arid and semi-arid climates. Fast pyrolysis of these feedstocks has potential as the unique carbohydrates and resins have been found to be efficiently converted to hydrocarbons and generate their own slate of oxygenates not yet observed in the catalytic fast pyrolysis of biomass. Vapor phase upgrading of these drought-tolerant feedstocks using zeolite catalyst was shown to be an effective method of reducing the oxygen content of the pyrolysis vapors and generating hydrocarbons and valuable chemicals. Pyrolysis vapors from prickly pear were effectively converted to aromatics and olefins with slightly lower yields than that of pine. The higher H/C_{eff} values lead to lower yields of aromatics even for the in-situ configuration and therefore ex-situ catalyst used to produce larger C3+ olefins are recommended. The ex-situ deactivation and coke formation were observed to be less severe for prickly pear than other feedstocks and is attributed to the higher H/C_{eff} values and elevated CO_2 yields of non-catalytic pyrolysis vapors. Gumweed produced high levels of aromatics, moistly

naphthalene's and toluene with in-situ catalyst placement. Ex-situ catalyst can be used to produce high levels of olefins and potentially valuable oxygenates such as 3,3,5,6-tetramethyl-1-indanone. Ex-situ deactivation showed that these oxygenates can be produced even at a catalyst to biomass ratio of 1:2 while yields of light olefins and aromatics decreased.

High-value chemicals are the leading area of research to make biofuels more economical. Phenolic compounds are produced from the lignin fraction of biomass and can be used in resins and specialty chemicals. Ethanol organosolv and ionosolv are two strategies to remove lignin from biomass and do so by different reactions. By evaluating the different structures of the resulting lignin using 2D-HSQC NMR and ^{31}P NMR it is possible to correlate the interunit linkages to the pyrolysis products and determine which structures are more suitable for thermochemical conversion and production of higher value chemicals. Ionic liquid lignin was found to generate higher yields of phenolic monomers and also produced a much simpler product slate than whole biomass or EOL lignin

Dedicated to my loving and supportive wife and family

Acknowledgments

I would like to thank my advisor, Dr. Sushil Adhikari for his continued patience, understanding, guidance, and support. I would also like to thank Dr. Oladiran Fasina, Dr. Brian Via, and Dr. Yi Wang, for serving as committee members and Dr. Carlos Carrera for serving as Graduate School reader. I am thankful for the opportunity Dr. Adhikari provided by allowing me to travel to the National Renewable Energy Laboratory (NREL) as a visiting scholar. I would like to thank the scientists are NREL including, Calvin Mukarakate, Mark Nimlos, Daniel Carpenter and Brian Donahue. I am thankful to all of my colleagues at Auburn University especially, Hyungseok Nam, Avanti Kulkarni, Rajdeep Shakya, Zhouhong Wang and Vivek Patil.

Table of Contents

List of Figures

List of Tables

Chapter 1 Introduction

Biofuels and bio based chemicals represent the harmonization of capitalism with environmentalism. Biofuels are not simply a replacement for fossil fuels they represent a shift in our perception of how societies function. Moving from linear thought processes comprised of extraction, utilization and dumping to a cyclic mindset where waste streams are as important as the raw materials. Biofuel research has been driven by the notion that they are carbon neutral and better for the environment. However, this fact alone cannot sustain a biorefinery. Research has to overcome significant technical hurdles not only in the conversion of biomass but also in the cultivation and chemical makeup of feedstocks.

In this work, a biofuel is any chemical or mixture of chemicals that is a suitable replacement for hydrocarbon fuels. A biofuel intermediate is a group of chemicals that can be easily upgraded to a fuel source. Examples of this include syngas (CO, H_2) which can be used in Fischer Tropsch reactions to produce gasoline type fuels which are a mixture of hydrocarbons that are 5-10 carbons in length, or diesel fuels that are a mixture of hydrocarbons 11-20 carbons in length. Biofuel intermediates can also be the oxygenated bio-oils which are a mixture of Furnas, phenols, carbonyls, acids, methoxyl phenols and many other oxygenates. These oxygenated bio-oils can be deoxygenated through many processes to obtain a hydrocarbon mixture suitable for gasoline or diesel fuel blends. Both examples show bio fuel intermediates that can be upgraded to what is known as a "drop-in" biofuel. These are different than biofuels such as ethanol, methanol or butanol because they are fully compatible with existing petroleum refineries.

A chemical intermediate is a single compound or group of compounds that will be used to produce bioproducts. Some examples of chemical intermediates that are believed to have near-term marketability are benzene, phenol, acetic acid, butanediols, furfural, and xylene. These can be used to produce plastics or other polymers or may be used as resins, solvents or additives. Bioproducts is a broad term and in general includes any value-added chemical produced from renewable sources.

The source of biomass is important to the overall success of the biofuels industry because it decides the theoretical potential of any conversion process.[1] Additionally, feedstock cost is one of the main factors driving the final fuel selling price.[2] By making the amount of desired plant material more abundant through improved agricultural practices and densification of crops we can improve the supply of biomass. By

making it easier to convert biomass into a desired product through optimization of cell wall architecture it reduces the intensity and therefore the cost of the conversion process. The combination of these ideas is expressed as the improvement of biomass supply and composition, the main goal of feedstock technologies. Feedstocks have been categorized into 1st, 2nd, and 3rd generation biomass categorizing materials by their composition which intern leads to the intensity of the conversion process. [3,4] 1st generation biofuels are those which are primarily starch and have limited amounts of other materials present in their cell wall architecture. [5] These 1st generation biomass plants are technologically easy to convert to a combustible fuel. The leading 1st generation biofuel in the U.S. is corn (maize) which provides 95% of fuel ethanol production in the USA. Globally this accounts for more than 50% of the worlds ethanol production. [6] 2nd generation biomass feedstocks include lignocellulosic plants such as woody biomass and switchgrass. [3] Woody biomass contains approximately 45% cellulose, 25% lignin and 25% hemicellulose with the remaining fractions being extractives and ash. Switchgrass is composed of 35% cellulose, 26% hemicellulose and 18% lignin with larger portions of ash. 3rd generation feedstocks are alga. [3] There are different strains of alga being developed and the main objective is to get lipids which are longer hydrocarbons that can be easily converted to fuels. Alga can generate up to 50% lipids by mass and the remaining percent is biomass which can be used to generate fuels through other conversion processes. Alga can generate higher densities of biomass; however, alga can be difficult to grow without contamination if large ponds are used and the development of closed systems have not found a method that is as cheap as growing crops using traditional agricultural methods. Another challenge of the algal feedstock is they require large volumes of water and nutrients. [7]

Figure 1.1. The three generations of biofuel feedstocks

Drought resistant plants such as *Opuntia ficus-indica* (prickly pear) and *Grindelia squarrosa* (gumweed) use up to 4 times less water than other types of biomass used for biofuels. This comes from the photosynthetic mechanism used by these types of plants known as Crassulacean acid metabolism (CAM).

[8] CAM photosynthesis limits the amount of transpiration as compared to C3 and C4 photosynthesis by only opening the plant stoma to take in CO_2 at night when temperatures are lower. [9] This greatly reduces the amount of water wasted and also leads to very efficient growth which is surprising for desert plants. Both prickly pear and gumweed have been cited as having the potential to produce approximately 11 Mg ha^{-1} yr^{-1} which rivals that of switchgrass while grown in semi-arid climates where the average rainfall is only 400-600mm. [10] While the dry weight yields of these plants are not yet higher than other types of biomass they can be grown in regions of the Southwest where farmland is extremely cheap and uncompetitive. For example, New Mexico can be as low as $500 per acre for farmland while regions like Iowa are as much as $8000 per acre. The carbon content of prickly pear and gumweed is still within the range of other biomass types and therefore the theoretical energy content generated by growing these plants is not significantly changed.

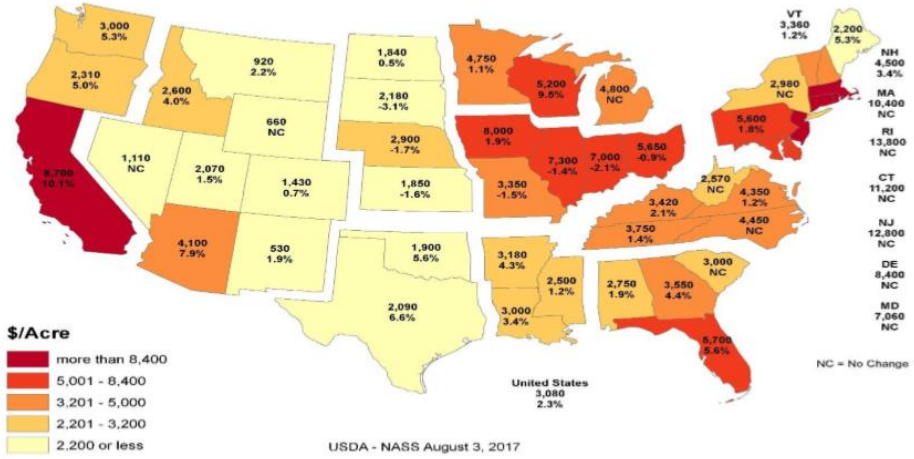

Figure 1.2. 2017 Farm real estate value by state and percent change from 2016 [11]

Conversion technologies are broken down into biochemical and thermochemical groups. Within the vast amount of processes available the main objective is to produce a molecule with either a high fuel value or a high chemical value. Producing fuel is the main goal as the driving factor for biofuels is to replace petroleum-based fuels that are harmful to the environment. However, the economics of the biofuels industry can be improved if valuable oxygenated products are made as co-products. These molecules have a higher value than fuel in many cases and they are not competing directly with petroleum markets. [12] Petroleum is fully deoxygenated and therefore chemical reagents are synthesized and not simply distilled. Molecules such as acetone, phenol, furan, furfural, and diols are wanted co-products that can add a great deal of value to the process. [13] There are a lot more compounds that can be added to the list of value-added chemicals and it should be noted that the biochemical and thermochemical routes generate different value-added chemicals. Other CO-products can include lubricating oil and hydraulic fluids.

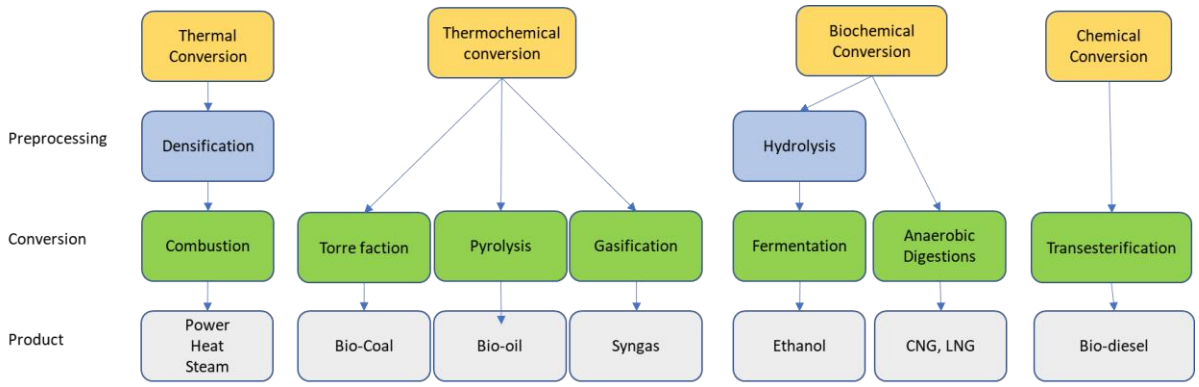

Figure 1.3. Conversion technology flowchart

The biochemical processes consist of three main stages; pretreatment, hydrolysis, and fermentation or chemical processing. Pretreatment aims to break the plant cell wall and increase the accessibility of catalyst (enzymes) to the sugars available in the feedstock. A few examples of pretreatments are; ionic liquids, dilute acid, ammonia fiber explosion, steam explosion, organosolv or alkaline treatments just to name a few. [14] Another function of the pretreatment is to separate the lignin from the feedstock. Lignin is mostly detrimental to the fermentation processes because it cannot be converted to a usable chemical. Typically, lignin is burned to recover the energy as heat. However, there is a growing field of research around converting lignin into valuable chemicals. [15] Pretreatment is an expensive processes [4] and therefore thermochemical conversion which negates pretreatment has an advantage over biochemical in this respect.

Thermochemical conversion uses high temperatures to convert biomass and covers three main processes; pyrolysis, gasification, and combustion. Oxygen or air are used in the case of gasification and combustion to act as an oxidizing agent are partially combust biomass. Gasification can also use carbon dioxide as an oxidizing agent. Pyrolysis does not use an oxidizing agent, but it can use hydrogen in some cases. These processes although all categorized the same give very different products. Combustion is the cleanest processes and converts most of the biomass into CO_2, water, ash, and heat. This process is technically simple and can be used to generate steam which in turn is used with steam turbines to generate electricity. The downfall of this process is that it does not generate a liquid transport fuel and therefore does not address the key motivation of the biofuels industry. Gasification is similar to combustion but uses slightly lower temperatures and levels of oxygen so that the biomass is converted to carbon monoxide, hydrogen, methane, and carbon dioxide. This mixture of gasses is known as syngas and is analogs to natural gas. It can be used with either a Fischer-Tropsch reaction to generate linear alkanes or in a dimethyl either to triptane process. Within the scope of this process, the technical hurdle is contaminants produced during gasification. These lead to expensive downstream cleaning of the syngas. These contaminate consisted of tar, sulfur compounds, nitrate compounds, and halides. These would coke and poison reforming catalyst, again making the cleanup processes expensive. Pyrolysis uses an inert atmosphere and temperature of

around 500°C to partially deconstruct biomass. This leads to the production of bio-oil which can contain hundreds of chemicals. These chemicals may be further upgraded through vapor phase upgrading with a catalyst or a hydrotreating process to give mostly deoxygenated molecules. Pyrolysis gives the most chemically diverse product slate of all the conversion processes. This has the potential to generate valuable oxygenated co-products as listed earlier.

1.1 Research Problem

The US contains roughly 2.5 billion acres within its boards and only 56% remains as forest-use-land and grassland pasture and range. [16] The remaining land is accounted for as cropland, urban areas, and special-use areas. Therefore, to realistically expand the use of biofuels the growth of biomass feedstocks must be optimized for these areas and produce high yields while maintaining a suitable chemical makeup. Intensification of land use through short rotation forestry is an excellent way to improve yields as well as selectively harvest and process biomass to give better conversion performance. Utilizing arid and semi-arid deserts and grasslands can greatly increase the availability of land for bioenergy crops. Exploration into the conversion of drought-tolerant biomass is a novel field of research with great potential to expand the portfolio of biomass available for biofuels. By determining how the chemical makeup of these feedstocks influences the product slate we can better account for the variability in biomass and produce a more desirable product slate of biofuel and chemical intermediates.

1.2 Research Proposal and Objectives

Objective 1. Bubbling fluidized bed gasification of short rotation *Eucalyptus*: effect of harvesting age and bark.

Goal: Improvement of syngas production and reduction of tar contaminants from biomass gasification by altering feedstock age and the presence/absence of bark in combination with adjusting the amount of bed material within the bubbling fluidized bed reactor.

Rational: Eucalyptus is an energy crop that can grow prolifically in the Southeast and through the practice of short rotation coppicing it is possible to control the growth conditions to give a predictable annual yield. However, the variable of the growth cycle has never been addressed with regards to gasification products and tar constituents. Consequently, it is difficult to advise on the best practice for obtaining a feedstock with the optimal chemical composition for gasification. Therefore, the rationale for this objective is to provide a detailed account of the gasification syngas profile and tar contaminants and correlate them with biomass properties so that growth cycles of *E. benthamii* in the south-east can be optimized for non-catalytic, oxygen fed, bubbling fluidized bed gasification.

Objective 2. Spectroscopic characterization and non-catalytic fast pyrolysis of Eucalyptus: Effect of harvesting age and bark.

Goal: Further analyze the structure of eucalyptus and utilize pyrolysis as an intermediate step of gasification to better understand the gasification behavior.

Rational: Subtle chemical differences in biomass characteristic can potentially be determined through spectroscopic characterization that cannot be seen with methods used in objective one. Additionally, pyrolysis can be used as an intermediate step of gasification to observe compounds that may influence the tar compounds generated.

Objective 3. Tar formation from lignin model dimers containing the β-O-4 and biphenyl linkage with different methoxyl content representing the H, G, and S lignin types.

Goal: Identify how H, G, and S type lignin dimers alter the formation and selectivity of tars from gasification/ pyrolysis.

Rationale: Lignin is the main source of larger aromatic tars generated during gasification. The β-O-4 linkage is the most abundant linkage in lignin's and is also easily fragmented during pyrolysis/gasification to ultimately generate H, G, or S monomers. The homolytic cleavage of methoxyl groups is the main step in the polymerization of lignin derivatives to generate soot and larger aromatic compounds. Therefore, using these model compounds and obtaining a detailed product slate with Py-GC/MS/FID/TCD the mechanism of tar formation from different types of lignin can be understood and ultimately determine what causes the different aromatic tar compounds to be formed during gasification.

Objective 4. Fast pyrolysis of *Opuntia ficus-indica* (prickly pear) and *Grindelia squarrosa* (gumweed).

Goal: Evaluate the pyrolysis product slate of novel, drought tolerant feedstocks *Opuntia ficus-indica* (prickly pear) and *Grindelia* squarrosa (gumweed) at 450°C, 550ºC, and 650°C and show how their unique composition leads to unique product slates.

Rationale: The large-scale use of non-food biomass as a source of renewable carbon for fuels and chemicals will require the development of dedicated feedstocks co-optimized for growth and efficient conversion (high carbon and hydrogen retention, low catalyst deactivation). The benefits of drought-tolerant plants as feedstocks for biofuels and biochemicals have been identified by other groups [8, 17] who stressed that increasing global temperature, drought, and soil-drying conditions caused by global warming will increase competition for agricultural freshwater and cultivated soils. Expanding available biomass resources to include plants with exceptional drought tolerance complements traditional lignocellulosic resources and has the advantage of lower water requirements and the use of arid and semi-arid lands, potentially opening up large areas of the western U.S. to biofuel and biochemical production. The use of marginal lands with

low water availability will be a crucial component to the success and ecological sustainability of a future bioeconomy.

Objective 5. Catalytic fast pyrolysis of drought-tolerant biomass: Optimal catalyst configuration and evaluation of deactivation patterns

Goal: Monitor the deactivation of HZSM-5 during catalytic fast pyrolysis of *Opuntia ficus-indica* (prickly pear) and *Grindelia* squarrosa (gumweed).

Rationale: The adaptation of these plants to harsh climates has generated cell wall architectures composed of complex matrices that hold different compositions of lignocellulosic biopolymers (cellulose, hemicellulose, and lignin) while additionally utilizing alternative carbohydrates and resins to thrive in these climates. Most notably these plants have developed much lower levels of lignin. This characteristic alone can lead to improved zeolite lifetime and limit the deactivation of zeolites through coke forming lignin condensation reactions.

Objective 6. Effect of lignin isolation technique on structure and pyrolysis.

Goal: Determine the feasibility of producing a phenolic based oil from lignin that has low variability in chemical constituents.

Rational*:* The phenolic nature of lignin makes it a suitable intermediate for chemicals if the lignin can be isolated and liquified. Additionally, a low variability in the product slate makes it easier for adhesive manufactures to utilize this chemical intermediate. In order to investigate methods of improving yield and lowing variability three sources of lignin and two isolation techniques are used to determine how differences in lignin structure influence yield and selectivity.

References

1. Mu, D.; Seager, T.; Rao, P.; Zhao, F. Comparative life cycle assessment of lignocellulosic ethanol production: Biochemical versus thermochemical conversion. *J. Environ. Manage.* **2010,** *46*, 565-578.

2. Jones, S.; Meyer, P.; Snowden-Swan, L.; Padmaperuma, A.; Tan, E.; Dutta , A.; Jacobson, J.; Cafferty, K. Process design and economics for the conversion of lignocellulosic biomass to hydrocarbons fuels: Fast pyrolysis and hydrotreating bio-oil pathway*;* National Renewable Energy Laboratory (NREL): Golden, CO, 2013.

3. Perlack, R. Biomass as feedstock for a bioenergy and bioproducts industry the technical feasibility of a billion-ton annual supply. United States. Dept. of, E.; United States. Dept. of, A.*;* Oak Ridge National, L., 2001.

4. Humbrid, D. Process design, and economics for biochemical conversion of lignocellulosic biomass to ethanol: Dilute-acid pretreatment and enzymatic hydrolysis of corn stover*;* Technical Report; National Renewable Energy Laboratory: Golden, 2011.

5. Demirbas, A. Progress and recent trends in biofuels. *Prog. Energy Combust.l Sci* **2007,** *33,* 1-18.

6. Souza, G. M.; Victoria, R.; Joly, C.; Verdade, L. Bioenergy & Sustainability: Bridging the gaps. Paris: SCOPE. ISBN 978-2-9545557-0-6 72, 779.

7. Davis, R. Process design, and economics for the production of algal biomass: Algal biomass production in open pond systems and processing through dewatering for downstream conversion*;* Technical Report; National Renewable Energy Laboratory: Golden, 2016.

8. Cushman, J.; Davis, S.; Yang, X.; Borland, A. Development and use of bioenergy feedstocks for semi-arid climates. *Journal of Experimental Botany* doi:10.1093/jxb/erv087.

9. Mason, M. The potential of CAM crops as a globally significant bioenergy resource: moving from 'fuel of food' to 'fuel and more food'. *Energy Environ. Sci.* **2015**.

10. Hoffman, J. Potential cash crop for the arid southwest. *Economic Botany* **1986,** 162-169.

11. *Land Values 2017 Summary (August 2017);* USDA, National Agricultural Statistics Service.

12. Iisa, K. Improving biomass pyrolysis economics by integrating vapor and liquid phase upgrading. *Green Chemistry* **2017,** 10.1039/C7GC02647K.

13. Vispute, T. Renewable chemical commodity feedstocks from integrated catalytic processing of pyrolysis oils. *Science* **2010,** *330,* 1222-1227.

14. Kumar, A. Recent updates on different methods of pretreatment of lignocellulosic feedstocks: A review. *Bioresour Bioprocess* **2017,** 10.1186/s40643- 10.1017-0137-9.

15. Ragauskas, A. Lignin valorization: Improving lignin processing in the biorefinery. *Science* **2014,** 10.1126/science.1246843.

16. Daniel, B.; Borchers, A. Major uses of land in the United States, 2012. *EIB-178, U.S. Department of Agriculture, Economic Research Service, August 2017*.

17. Yang, X. A roadmap for research on crassulacean acid metabolism (CAM) to enhance sustainable food and bioenergy production in a hotter, drier world. *New Phytologist* **2015,** *207,* 491-504.

Chapter 2 Bubbling fluidized bed gasification of short rotation Eucalyptus[2]

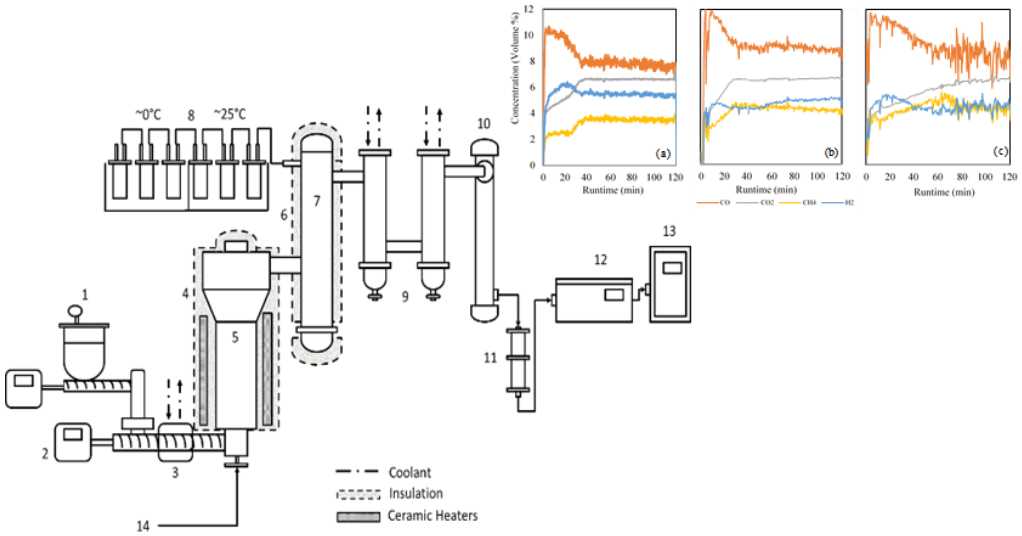

2.1 Abstract

The improvement of syngas production and reduction of tar contaminants from biomass gasification is the focus of this work. Altering the chemical makeup of the feedstock was achieved by altering feedstock age and the presence/absence of bark. *Eucalyptus benthamii* is a promising biomass source for the gasification process and can be grown as a short rotation bioenergy crop allowing for selective growth cycles. Three *E. benthamii* samples harvested at two years with bark (2EWB) two years without bark (2EWoB) and seven years without bark (7EWoB) were used for this work. Upon gasification, the highest CH_4 gas concentration was obtained from 7EWoB sample. Alternatively, the highest H_2 gas yield was obtained from 2EWB sample. The presence of bark also significantly affected CO and CH_4 gas yields. Major tar compounds in the syngas were benzene, naphthalene, toluene, and indene. Almost twice the amount of naphthalene and indene was obtained with older samples (7EWoB) compared to young samples

[2] Cross, P.; Kulkarni, A.; Nam, H.; Adhikari, S.; Fasina, O. Bubbling fluidized bed gasification of short rotation Eucalyptus: Effects of harvesting are and bark. *Biomass and Bioenergy* **2018,** *110,* 98-104.

(2EWoB and 2EWB). This observation motivated further investigation. Spectroscopic characterizations of the wood cell wall architecture were conducted using CP/Mas ^{13}C NMR, XRD, and ATR-FTIR. Pyrolysis at 500ºC was used as an intermediate step of gasification. It was observed that the degree of crystallinity was higher for the older (7EWoB) E. benthamii (CrI = 52 vs CrI = 49) and correspondingly resulted in carbon yield of D-Allose to be 0.23% versus 0.13%. Higher yields of certain S type lignin derivatives were observed for samples with bark, including 2,6-dimethoxyphenol and 2,5-dimethoxybenzaldehyde-4-methyl. The pyrolysis work was unable to explain differences in the tar slate observed during gasification, therefore, tar forming reactions were studied using lignin model dimers with the β-O-4and biphenyl linkage with different methoxyl content representing H, G, and S type dimers. A tandem microreactor Py-GC/MS/FID/TCD system was used to characterize and classify tar compounds and evaluate differences in reaction pathways based on the structural changes of the model compounds. It was determined that the methoxyl groups of S and G lignin which are more abundant in older *E. benthamii* leads to higher levels of larger tar compounds.

2.2 Introduction

Gasification of lignocellulosic biomass for the production of renewable fuels and chemicals is somewhat mature technology. [1,2,3] Gasification is a partial combustion of biomass, which produces valuable gases to be used as a direct fuel source or upgraded to more valuable liquid fuels and chemicals. [4,5] Using high temperatures (600 °C-1000 °C), low oxygen levels (0.20-0.45 of equivalence ratio, ER), gasification deconstructs and converts the main substituents of biomass (cellulose, hemicellulose and lignin) into gas product, known as syngas, solid char, liquid tar, and other contaminants (ammonia, hydrogen sulfide, and others). [1,2,3,6,7,8] Pressure has also been studied for this technology. [9] Several reactor designs exist for biomass gasification. [10,11] Fluidized beds are of primary interest for this technology and mainly consist of circulating flow gasifiers [12] and bubbling fluidized bed gasifiers. [13] A major hurdle for gasification comes from the complexity of biomass leading to mixed reactions and the formation of aromatic contaminants that are costly to eliminate. These organic compounds with a molecular weight equal to or greater than benzene (78 g $mole^{-1}$) are classified as tar. The reduction of tar is the most important hurdle in the industrialization of gasification technology. [2,3] Lowering the level of tar can be somewhat accomplished by selecting appropriate biomass and reaction conditions. Carpenter et al. [4] studied the gasification of different biomass (hardwood, softwood, herbaceous grasses and agricultural residues). Biomass type was shown to alter the abundance of aromatic tar compounds generated during gasification along with primary gas yield. In their study, the highest observed tar yield from wood was 270 g m^{-3} (0°C, 101 kPa abs) while corn stover, switchgrass, and wheat straw reached 370 g m^{-3} (0°C, 101 kPa abs). Wood also showed a higher hydrogen mass yield of approximately 13% on average, and a higher total gas yield of 31% on average.

In the southeastern United States, *E. benthamii* is an emerging short-rotation bioenergy crop. Plantations can produce a volume of 5120 m^3 km^{-2} of *E. benthamii* after 34 months, while that of *Pinus radiata* is 2970 m^3 km^{-2} at an equivalent age. [14] *E. benthamii*, grown in southern Florida by ArborGen (ArborGen, Inc., Ridgeville, SC), can produce 2700 - 3500 tonne km^{-2} $year^{-1}$ on a 7-year rotation, and 3100 - 4000 tonne km^{-2} $year^{-1}$ on a 3-year rotation. [14] Short rotation also provides the possibility of harvesting trees at a specific age to alter the chemical makeup and thus potentially changing the product slate of gasification. Rencoret et al. [15] studied the effects of harvesting age on chemical compositions of *Eucalyptus globulus*. Samples harvested after 1 month, 18 months and 9 years were evaluated. The mass fraction of lignin varied from 16% with 1-month old trees to 25% with 9-year-old trees. Also, the lignin composition of syringyl (S), guaiacol (G) and p-hydroxyphenyl (H) content were changed as well. S/G ratio was 1.4 for the youngest samples (1 month) and 3.8 for the oldest (9 years). The amount of H type lignin fell from 9% to 2% with age. Indicating that lignin monomers are deposited at different times of the trees life, first H type lignin is deposited then G, and finally S. Additionally, there was a decrease in acetone extractives, water-soluble material and ash with increasing age. Senelwa et al. [16] studied fuel characteristics of twelve different woody biomass at different ages; 3 years, 4 years and 5 years. This work also investigated differences in fuel characteristics of bark versus the inner wood including the heartwood and sapwood. It was found that the only differences between whole wood samples (heartwood, sapwood, and bark) of different age were the basic density and the mass fraction of bark. Average wood basic density increased from 362 kg m^{-3} at 3 years to 376 kg m^{-3} at 5 years. The mass fraction of bark present in the different samples decreased from 14% at 3 years to 11% at 5 years, which affects the fuel properties of the sample due to the different chemical composition of bark compared to inner wood (sapwood and heartwood). Bark tends to have a high lignin content as well as alkali and alkaline earth metal salts, which affect the results of proximate analysis and higher heating value. Hanaoka et al. [17] determined that the light gas yield from Japanese red pine bark gasification was similar to the lignin gasification with respect to the CO, H_2 and CH_4 yields. Additionally, the total gas and tar yields from bark samples were lower than that of the whole Japanese oak due to a high lignin and low sugar content of bark.

In combination with feedstock selection, the amount of bed material is one parameter that can influence the formation of tar and syngas during bubbling fluidized bed gasification. [18,19] Mayerhofer et al. [19] studied the formation of tar and syngas at different heights of a bubbling fluidizing bed. The bed height to inner diameter of the reactor (H/D) ratio was varied at two points (3.25 and 5.84) showing different syngas samples. At higher H/D ratios the syngas yields increased, however, there was also an increase in the total tar yields. Wan Ab Karim Ghani et al. [18] studied the syngas production using palm kernel shells and coconut shells in a bubbling fluidized bed reactor by varying the H/D from 0.167 to 0.583. CO_2 yield

increased at different ratios while the trends of other gases were dependent on the feedstock. Palm kernel shells have a proximate analysis more closely related to that of woody biomass and showed a decrease in H_2 yields while CO, CO_2, and CH_4 yield increased. Thus, the previous studies suggest that H/D ratio is an important parameter in the optimization of gasification performance with results dependent on feedstock and therefore further gasification study using short rotation biomass, *E. benthamii*, is of value to this technology.

Biomass properties are an important aspect of any conversion process. The standard methods for characterizing biomass are proximate and ultimate analysis, heating value determination, and wet chemical analysis. [20] However, these can be time consuming and there are still characteristics of biomass that can alter the tar slate not determined by these methods. Spectroscopic characterization such as Solid-State CP/Mas ^{13}C NMR, ATR-FTIR, and XRD can be used to determine additional information about characteristics of biomass and represent a way of characterizing the whole biomass without any alteration of its physical or chemical properties. Solid-state NMR was recently shown to be a fast and accurate way of determining lignin content of lignocellulosic biomass by Fu et al. [21] FTIR in combination with partial least squares regression was shown to accurately predict extractives and lignin content as well as carbohydrates and did very well at predicting thermochemical properties of volatile matter and fixed carbon (R^2> 0.80, RPD > 2.0). [22] XRD can show the crystallinity index of biomass as described by Park et al. [23]

The global kinetics of pyrolysis and gasification shift the conversion and product slates. Studying the thermal degradation kinetics and determining kinetic parameters can aid in the design of reactors and reaction conditions. Van de Velden et al. mention that pyrolysis and gasification should be operated on biomass with a particle size of <200 μm or 0.2 mm with a heating rate of at least 80 K min^{-1} and a reaction environment where the Biot-number is less than 1.0. [24] TGA is therefore offered as a suitable system to perform the kinetic analysis given the other conditions are met. Model-free kinetics are commonly used to determine kinetic parameters of biomass pyrolysis because they allow for the reaction mechanism to change during the course of the reaction and they can reduce the mass transfer limitations by using multiple heating rates. [25] Activation energy (E_a, kJ mol^{-1}) and the pre-exponential factor (A min^{-1}) are the main kinetic parameters determined for biomass pyrolysis. These are often determined by the Flynn-Wall-Ozawa method (FWO), the Kissinger-Akahire-Sunose (KAS) or the Kissinger methods. [25,26] Kinetic parameters have been determined for a range of biomass and generally have a large range. E_a can range from 100 kJ mol^{-1} to 240 kJ mol^{-1} while A can range from 8.1E+11 min^{-1} to 5.2E+14 min^{-1}. How these parameters change based on age is yet to be evaluated and it will be helpful in optimizing the selection of short rotation eucalyptus benthamii for use as biofuel feedstocks.

Lignin model compounds have been used to study tar formation to simplify reaction networks and identify possible devolatilization reactions. One of the main compounds studied to date has been 2-phenethyl phenyl ether (PE) which represent a simplified β-O-4 linkage. Pyrolysis of this compound between 500°C-600°C has shown that concerted retro-ene and Maccoll reactions are dominant. [27,28] At higher temperatures (over 1000°C) hemolytic cleavage will become more dominant. [28] Additional work on fully substituted β-O-4linkages have been conducted both computationally and experimentally and concluded that the retro-ene fragmentation was most favorable. [29] The main products from a retro-ene fragmentation of 2-phenoxyphenyl-1,3-propanediol are phenol and benzaldehyde along with potentially 6 other products. [30] Secondary reactions to generate soot and tar formation from lignin model compounds with β-O-4 linkages have also been evaluated and propose that the majority of reactions are dominated by free radical pathways. [31] Additionally, a main step to the polymerization of larger aromatic compounds is hemolytic cleavage of methoxyl groups. [32,33] These model compound studies have largely used monomeric lignin derivatives such as guaiacol to study the reaction pathways.

The objectives of the current study are to investigate 1) gasification performance of short rotation *E. benthamii* biomass as energy crop in terms of product yields, 2) syngas composition as well as tar content with regards to tree harvested age and the presence/absence of bark, and 3) the effect of alteration of fluidized bed H/D ratio on syngas for a non-catalytic bubbling fluidized bed bench-scale reactor with O_2 as oxidizing medium.

2.3 Experimental

2.3.1 Feedstock and characterization

Eucalyptus benthamii (*E. benthamii*) samples were obtained from ArborGen's plantation in South Florida and included 2-years old with bark (2EWB), 2-years old without bark (2EWoB), and 7-years old without bark (7EWoB). Additionally, *Pinus taeda* (loblolly pine) was used as an alternative woody biomass feedstock. Samples were air dried to have a moisture content less than 15% before being ground with a hammer mill (C.S. Bell Co., model 10HBLPK, Tiffin, OH, USA) and sieved with a screen size of 1.58 mm. Proximate, ultimate, and chemical analyses were performed to characterize biomass samples. A detailed description of the bubbling fluidized bed reactor equipment and methods can be found in a paper by Abdoulmoumine et al. [34] In addition to biomass analysis, elemental compositions of the inorganic ash were also conducted using ICP-OES, PerkinElmer Life Sciences 9300-DV system. Pyrolysis gas chromatography (Py/GC-MS) was used to study the lignin monomers released during mild pyrolysis. This method has been used to estimate S, G and H type lignin. [15]

Solid State CP/Mas ^{13}C NMR was conducted on a Bruker Avance III 400Mhz using the method previously described by Neupane et al. [35] FTIR spectrum on E. Benthamii samples was collected on a Perkin Elmer Spectrum model 400 (Perkin Elmer CO., Waltham, MA). Spectra were recorded using 32 scans in the range 4000 to 650 cm^{-1}. Characterization of cellulose crystallinity was performed on a Bruker D2 Phaser X-Ray Diffractometer (Bruker, Billerica, MA). The diffraction intensities of biomass samples were measured in the 2θ-range of 10 to 40° using a scan time of 0.5 s taken at every 0.01415°. The crystallinity index was calculated according to Equation (2.1).

$$CrI = \frac{I_{002} - I_{am}}{I_{002}} * 100\% \quad (2.1)$$

I_{002} (at 2θ = ~22°) is the maximum peak intensity and I_{am} (at 2θ = ~18°) is the minimum intensity between peaks at 2θ = ~15.5° and ~22°.

2.3.2 Gasification unit and operation

The bubbling fluidized bed gasifier used in this study is shown in Figure 2.1. *E. benthamii* sample stored in the hopper was continuously fed using a screw feeder. An average biomass feed rate of 5.8 g min^{-1} was used. Equivalence ratio (ER) was maintained at 0.22 by feeding a mixture of nitrogen and oxygen to the bottom of the reactor. Specific details of the reactor dimensions can be found in a paper by Abdoulmoumine et al. [34] Gasification was carried out at 935°C with a static bed height of 6.4 cm (1.8 H/D) unless otherwise noted. Non-catalytic silicon sand with an average particle diameter of 0.03 cm was used as bed material. For comparison purpose, *P. taeda* was gasified at the same operating conditions. Bed height experiments used the same flow rate (15 L min^{-1} N_2) for all experiments and no attempt was made to adjust fluidization mechanics to offset the effects of altering bed height.

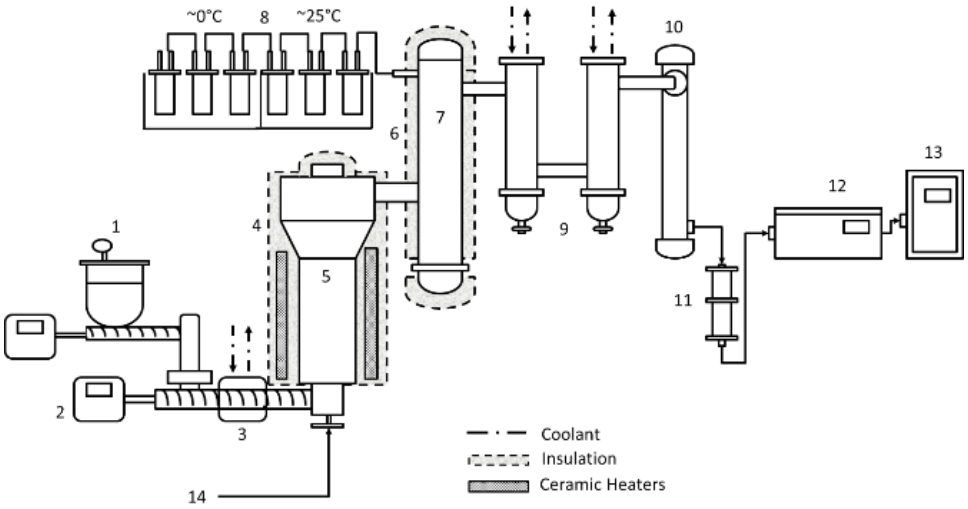

Figure 2.1. Schematic of gasification unit. 1. Biomass hopper; 2. Injection screw; 3. Heat exchanger; 4. Insulation and heaters; 5. Fluidized bed reactor; 6. Insulation and heaters; 7. High temperature filter; 8. Impinger train; 9. Condensers; 10. Electrostatic precipitator (ESP); 11. Charcoal filter; 12. FTIR gas analyzer; 13. NOVA gas analyzer; 14. O2 and N2 gas inlet.

All solid, liquid and gas streams in and out of the reactor were measured to obtain a material mass balance. Solid and liquid product streams were collected from the high-temperature filter (HTF) and condensers. Collected materials were then weighed to determine the yield per dry biomass (g kg^{-1}). The gas product yield was calculated with the steady state gas data, collected from online gas analyzers. In this work, steady state is defined as a constant mole fraction percent of syngas with respect to time. It should be noted that all experiments were monitored to ensure that steady state was achieved and used for calculations.

The gas yield was calculated using Equation 2.2, the weight of each product gas was summed and then divided by the total feed of biomass and oxygen into the reactor. Carbon conversion was calculated using Equation 2.3, the total moles of carbon in the product gas were summed and taken over the total carbon in the biomass feed.

$$\text{Gas yields} = \text{mass}_{\text{product gas}} / (\text{mass}_{\text{oxygen}} + \text{mass}_{\text{biomass}}) \quad (2.2)$$

$$\text{Carbon conversion} = (\text{Mole C}_{\text{product gas}}/\text{mass}_{\text{biomass}}) / (\text{Mole C}_{\text{biomass}}/\text{mass}_{\text{biomass}}) \quad (2.3)$$

2.3.3 Tar collection and analysis

A method of tar collection was imported from the "CEN accredited and approved technical specification for the measurement of tar in biomass gasification." [36] In short, the tar measurement system consisted of six impingers, the first five were filled with 50 cm^3 isopropanol, the first three at 25 °C, the last three maintained at 0 °C in an ice bath; the sixth impinger was used as a moisture trap. The tar yield (mg kg^{-1} dry biomass) was determined after a sample mixture of all six impingers was analyzed using an

Agilent GC-FID (Agilent Technologies, Santa Clara, CA) equipped with a DB-1701 column. GC inlet and FID detector were both maintained at 250°C. The temperature ramping program was set at 4°C min^{-1} to 250°C and held for 20 minutes. Eleven tar compounds were used for the quantitative analysis and consisted of; benzene, toluene, O-xylene, styrene, indene, phenol, naphthalene, 2 methylnaphthalene, and biphenyl. These are the major tar compounds, formed in air blown fluidized bed gasification.[37] Standards were used to determine the retention time for identification and to build a calibration curve for quantification.

2.3.4 Tandem Micro Reactor Py-GC/MS/FID/TCD

The pyrolysis reactor, as shown in Figure 2.2, was a tandem micro pyrolyzer (Rx-3050TR, Frontier Laboratories, Japan) equipped with an autosampler (AS-1020E) and microjet cryotrap (MJT-1030Ex) held at -96 °C inside the GC oven. The gas chromatography unit (7890B, Agilent Technologies, USA) used a dean switch to direct vapors into three columns. Condensable vapors were split and sent to two columns (Ultra Alloy-5, Frontier Laboratories, Japan) with a 5 % diphenyl and 95 % dimethylpolysiloxane stationary phase. One column was connected to a mass spectroscopy unit (5977A, Agilent Technologies, USA) and the other column was connected to a flame ionization detector (FID). Non-condensable gases were sent to a different column (GS-GASPRO, Frontier Laboratories, Japan) and vapors were sent to a thermal conductivity detector (TCD). The GC oven program held at 40°C for 4.5 min and then heated to 300°C at a rate of 20C min^{-1}.

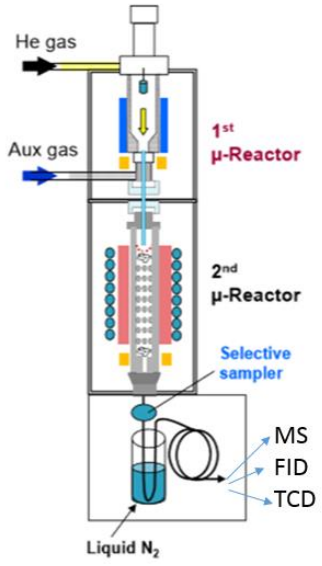

Figure 2.2. Schematic of the tandem microreactor illustrating the two reaction chambers, helium and auxiliary gas inlets, selective sampler, liquid N_2 cryotrap and MS/FID/TCD detectors.

Pyrolysis experiments were replicated three times, samples of 0.5 mg were loaded into small deactivated stainless-steel cups and charged into the first pyrolysis chamber maintained at a set point of 500°C for analytical pyrolysis. Heating rate estimations for this furnace style reactor can be found in a

publication by Proano-Aviles et al. [38] Pyrolysis vapors were identified using the NIST GC-MS library. Carbon yield for analytical pyrolysis of feedstocks was calculated using a method similar to Lisa et al. [39] and Xu et al. [40] The retention times of the compounds identified by MS were used to determine the corresponding FID peaks. 17 compounds were used to generate mass based linear calibration curves to compile FID response factors correlating the FID peak integration area to µg of carbon. The carbon yield of non-calibrated compounds was determined using the normalization method where the response factor from a compound with the closet structure is used and the relative response factor is set to 1. [41] The carbon yield is defined by the Equation (2.4.).

$$C\ yield = \frac{\sum_j m_j [C]_j}{m_f [C]_f} \quad (2.4)$$

where j = product j

$[C]_j$ = C content of product j, g C/g product j

$[C]_f$ = C content of feed, g C/g feed

m_j = mass of product j, g product j

m_f = mass of feed, g feed

The list of standards used can be found in the supplementary information (Table S3.5), additionally, results are also given in average FID area percent of each peak in the SI. Approximately 10mg of each lignin model compound was obtained as a gel. To transfer the samples to the deactivated stainless-steel cups used in pyrolysis, the gel samples were mixed with acetone to obtain the desired concentration. Small aliquots were then taken and pipetted into the samples cups and the acetone was allowed to evaporate at room temperature over 1 hour. The target weight of each model compound used in pyrolysis was 1 mg. In this work, pyrolysis results are presented in FID area percent.

2.3.5 TGA Kinetics

Kinetic analysis was conducted using a Pyris 1 TGA—thermogravimetric analyzer (PerkinElmer, Shelton, CT). Biomass samples weighing 2.5 mg and a particle size >0.5mm were placed into aluminum crucibles for the analysis. The temperature program was set to ramp from 30°C to 800°C with varying ramp rates of 10, 15, and 50°C min^{-1}. Nitrogen was used as the carrier gas with 20 mL min^{-1} flow rate. Three model free kinetic equations were used to calculate the activation energy (E_a) of the feedstocks: Kissinger, Flynn-Wall-Ozawa and the Kissinger-Akahira-Sinose. The equations for these three methods are shown below, Equation (2.5-2.7).

$$\text{Kissinger: } \ln\left(\frac{\beta}{T_m^2}\right) = \ln\left(\frac{AR}{E}\right) - \frac{E}{RT_m} \quad (2.5)$$

$$\text{Flynn-Wall-Qzawa: } \ln(\beta_i) = \ln\left(\frac{A_\alpha E_\alpha}{R_g(\alpha)}\right) - 5.331 - 1.052\frac{E_\alpha}{RT_{\alpha i}} \quad (2.6)$$

$$\text{Kissinger–Akahira–Sunose: } \ln\left(\frac{\beta_i}{T_{\alpha i}^2}\right) = \ln\left(\frac{A_\alpha R}{E_\alpha g\alpha}\right) - \frac{E_\alpha}{RT_{\alpha i}} \quad (2.7)$$

2.3.6 Lignin model compounds

Model compounds containing the most abundant linkage of lignin the β-O-4were provided by Rui Katahira of the National Renewable Energy Laboratory (Golden, CO.). In total five model compounds were used and represent the different types of lignin monomers, syringyl (S), guaiacol (G), and P-hydroxyphenyl (H) as shown below in Figure 2.3. In addition to the β-O-4linkage of S, G, H lignin monomers, the linkage at the C4 position is varied between a phenol group and phenyl group.

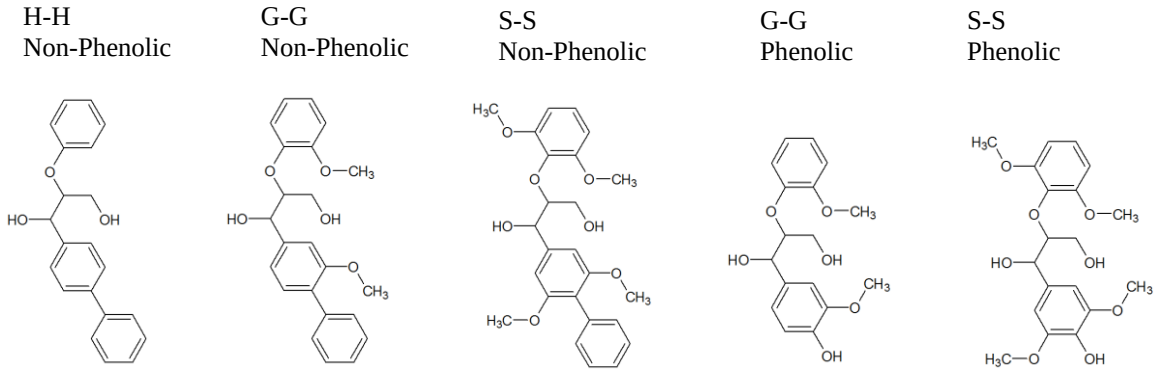

Figure 2.3. Structure of lignin model compounds

2.4 Results and Discussion

2.4.1 Biomass characterization

The properties of different *E. benthamii* samples were characterized based on the heating value, proximate analysis, ultimate analysis and chemical analysis as indicated in Table 2.1. The proximate analysis showed the proportion of volatile matter (VM), fixed carbon (FC) and ash on a dry basis. The VM decreased in the following order of 2EWoB (87.4%) > 7EWoB (85.4%) > 2EWB (83.0%). The highest ash content was 0.85% in 2EWB followed by 0.27% for 2EWoB and 0.22% for 7EWoB. Statistical analysis determined that ash content is significantly higher in 2EWB samples but is not significantly different for 2EWoB versus 7EWoB. Jin et al. [42] also reported similar results of higher ash in the bark from red oak and yellow-poplar. The major ash-forming elements of *E. benthamii* biomass were made up of alkali and alkaline earth metal salts including Ca, K, Mg and Na as shown in Table 2.2. Other major ash-forming elements present in the samples were Al, Fe, Mn, Ba, B, and Zn at very low concentrations. Organic elements, Si, P and S and halogens, Cl, were not analyzed in this work. Ultimate analysis showed the mass

fractions of carbon, hydrogen, nitrogen, and oxygen in the feedstocks. The amount of carbon on a dry basis is used to determine the carbon conversion as detailed in Equation 2.3. There was an important trend in the mass fraction of hydrogen in the feedstock, 2EWB (6.55 %) ≥2EWoB (6.45 %) ≥7EWoB (6.32 %). This trend is believed to have affected syngas yields and is further discussed in the following sections. In comparison to the elemental composition of *P. taeda*, *E. benthamii* had lower carbon mass fraction (less than 46 %) vs 47 % and higher levels of oxygen (over 47%) vs. 45.5 %. Chemical analysis imported from Goncalves et al.[43] showed the distribution of sugars, lignin, and extractives. The most significant trend here was the total mass fraction of lignin and extractives, 2EWoB (27.8 %) > 7EWoB (26.5 %) > 2EWB (26.0 %). These fractions of biomass are typically associated with tar yields.[44] Interestingly, *P. taeda* had much higher levels of extractives and lignin which combined account for 32.5%. Results of Py-GC/MS found that the lignin structure of 2 and 7-year *E. benthamii* sample is not statistically different in regard to the lignin monomer compositions (P=0.97). The relative amount of syringyl (S) and guaiacol (G) derivatives was used to determine an S/G ratio. The ratios were 1.45±0.4 for 2EWB, 1.37±0.5 for 2EWoB, and 1.38±0.3 for 7EWoB.

Table 2.1. Chemical characterization of *E. benthamii* biomass samples. reported as mass fraction[a]

	2EWB	2EWoB	7EWoB	*P. taeda*
Moisture (wet basis)	14.0	8.7	11.9	7.9
Higher Heating Value (MJ kg^{-1})	19.4 a	20.0 b	19.6 a	20.2b
Proximate analysis (dry basis)				
Volatile matter	83.0 a	87.4 b	85.4 c	83.1a
Ash content	0.9 a	0.3 b	0.2 b	0.3b
Fixed carbon	16.2	12.3	14.4	16.5
Ultimate analysis (dry basis)				
C	45.7 a	45.9 a	46.1 a	47.1
H	6.6 a	6.5 ab	6.3 b	6.5
N	0.3 b	0.3 a	0.3 a	0.4
O*	47.5 a	47.4 a	47.3 a	45.5
S/G ratio	1.5 a	1.4 a	1.4 a	-
Chemical analysis[b] (dry, ash free basis)[43]				
Glucose	53.7	51.3	50.0	45.3
Galactose	1.8	1.7	1.5	3.0
Xylose	14.5	13.6	12.6	4.9
Lignin	23.8	25.5	25.0	26.3
Extractives	2.2	2.3	1.5	6.2

[a]Values in the same rows with the same letter (a,b or c) are not statistically different (P>0.05). [b]Imported from Goncalves et al. [43] [*] Oxygen is calculated by difference.

Table 2.2. Major ash-forming elements in *E. benthamii* samples

	Ash (mg kg^{-1})					
Feedstock	Ca	K	Mg	Na	Fe	Al
2WEB	1261	1227	271	544	187	91
2EWoB	660	507	102	250	85	39
7EWoB	853	398	129	350	73	15

Spectroscopic characterization of three *E. benthamii* samples using SSNMR, FTIR, and XRD were performed. The properties of these samples were also previously characterized based on heating value, proximate analysis, ultimate analysis and chemical analysis. [45] The spectroscopic and physical characterizations of these three samples were well aligned. SSNMR results are shown in Figure 2.4. The single peak at 105 ppm (4) indicates that cellulose type I is present for all three samples. [46] A higher degree of crystallinity for the cellulose in 7EWoB was observed based on the more intense signal at 89 ppm (4) which correlates with the C-4 carbon of crystalline cellulose and the less intense signal at 84 ppm (5), which is the C-4 carbon of amorphous cellulose and is highest for the 2EWoB sample. The signal at 56 ppm (10) which is related to the aryl methoxyl carbons of lignin is higher for 2EWoB. The signal at 154 ppm (2), related to the C-5 carbon of lignin aromatic rings containing a methoxy group, is also higher for 2EWoB. This could suggest a higher abundance of S type lignin. However, Rencoret et al. [15] found that S type lignin was higher in older samples. Additionally, the lignin derivatives detected from pyrolysis do not show increased S content from 2EWoB. Therefore, the more abundant signal can only be used to confirm the previous chemical analysis of these samples that showed slightly higher levels of lignin for 2EWoB. The signals from 63-66 ppm (9) are background of the C-6 carbon of hemicellulose. These signals were lower for 7EWoB. The signal at 21.5 ppm (11) is also less intense for 7EWoB and relates to the acetate groups in hemicellulose. Additionally, a lower signal intensity was found for 7EWoB at 174 ppm (1) which correlates to carbonyl groups of lignin and carboxyl groups of hemicellulose. Previously, the values of xylose and galactose were also found to be lower for 7EWoB indicating a lower hemicellulose content. [45]

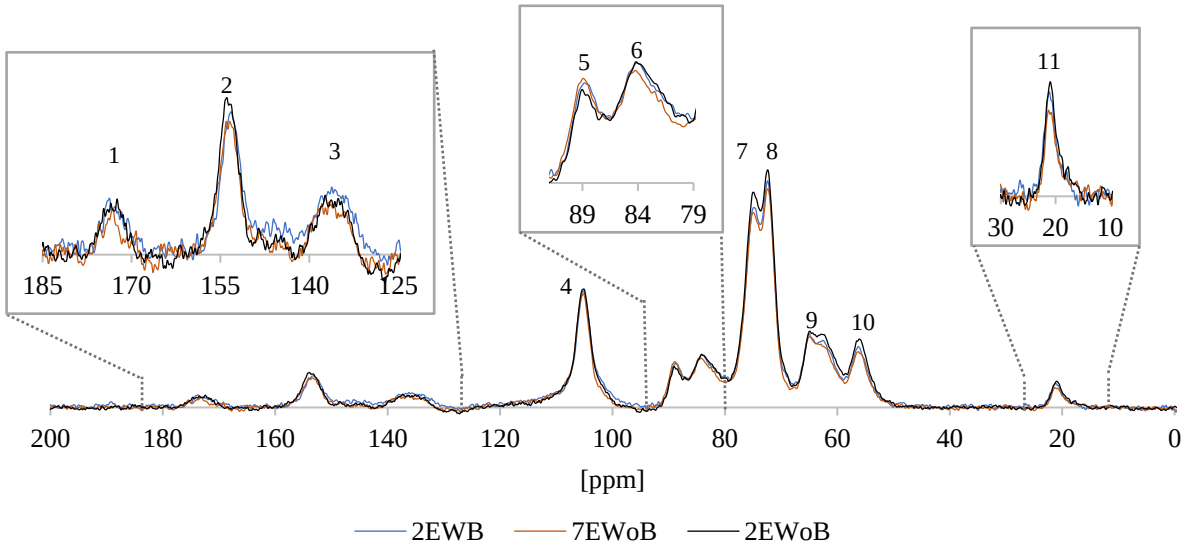

Figure 2.4. Solid-state NMR spectrum of 2EWoB, 2EWB, and 7EWoB

ATR-FTIR spectra of the three samples 2EWoB, 2EWB and 7EWoB are shown in Figure 2.5. Major differences between the FTIR spectrum of these three samples included the lower intensity of the peak at 1738-1734 cm^{-1} (1) for 7EWoB, as compared to the others. This peak is from unconjugated C = O bonds, which can be found in xylans. These results coincide with the SSNMR results and previous physical characterizations of 7EWoB. [45] A higher hydrogen content was previously determined for 2EWB [45] and similarly C-H deformations from cellulose and lignin at 1454 cm^{-1} (5) and 1420 cm^{-1} (6) are higher for 2EWB. Additional C-H deformation from lignin and carbohydrates observed from the signal at 1367 cm^{-1} (7) as well as the signal from C-H vibration in cellulose at 1325 cm^{-1} are more intense for 2EWB. A higher lignin content was also determined for 2EWB which can be seen in the FTIR shoulder signal at 1228 cm^{-1} (9), which is from guaiacol ring breathing, C-O stretching in lignin and for C-O linkage in guaiacol aromatic methoxy groups. Also, the signal at 1228 cm^{-1} for syringyl ring and C-O stretch in lignin and xylan is higher for 2EWB. The intensities of the signals at 1021 cm^{-1} (12) for the C-O stretch in cellulose and hemicellulose follow the same trend that was observed for the physical characterization of cellulose and hemicellulose for these samples: 2EWB > 2EWoB > 7EWoB.

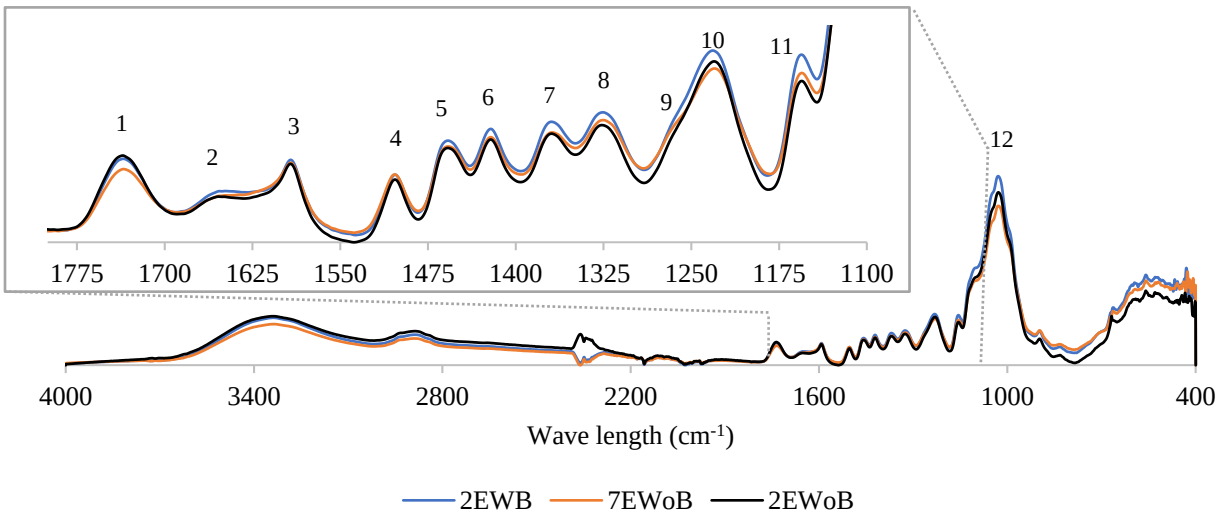

Figure 2.5. FTIR spectrum of 2EWoB, 2EWB, and 7EWoB.

XRD results are shown in Figure 2.6 and illustrate a higher I_{002} value for 7EWoB leading to a higher crystallinity index of 53 compared with 49 for the younger samples calculated using Equation (2.1). Also, the presence or absence of bark didn't make any difference to the crystallinity index. These results are in agreement with what was observed in the SSNMR. These CrI values are within the range of values determined by Mukarakate et. al, [47] (low 34 and high 62) for cellulose type I.

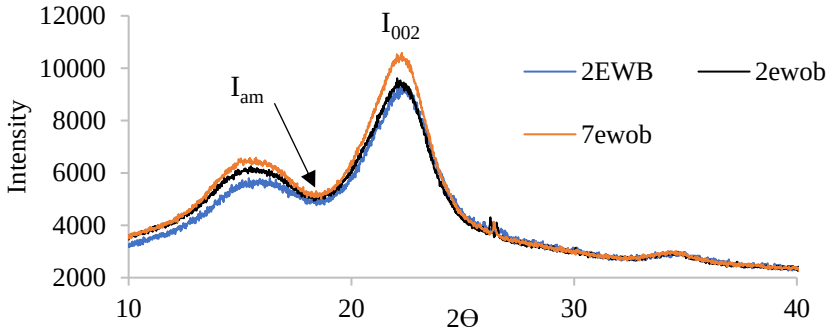

Figure 2.6. XRD illustrating I_{002} and I_{am} used in calculating the CrI of 2EWoB (CrI=49), 2EWB (CrI=49) and 7EWoB (CrI = 53).

2.4.2 Carbon balance and product distribution

The mass balance for the gasification of three *E. benthamii* samples (2EWB, 2EWoB, and 7EWoB) was over 90% as shown in Table 2.3. Gasification carbon conversions defined in Equation 2.3 ranged from 83.6% to 91.1%, which was less than the carbon conversion of *P. taeda* gasification (95%). These values appeared to emulate what was seen in the volatile matter content determined by the proximate analysis. The char yield from *E. benthamii* was most affected by the age of the sample. The highest char yield was obtained with 7EWoB (55.3 g kg^{-1}) possibly due to a higher bulk density (225 kg m^{-3}) of biomass compared

to younger samples (2EWB 205 kg m^{-3} and 2EWoB 203 kg m^{-3}). A higher bulk density for older woody biomass was also observed by Senelwa et, al. [16] The higher bulk density of 7EWoB biomass may have negatively affected the mechanics of the bubbling fluidized bed leading to lower conversion and large deviations between replicate experiments. Interestingly, the char yield from *P. taeda* gasification was similar to young *E. benthamii* without bark, 33.3 g kg^{-1} vs 34.9 g kg^{-1}.2EWB produced more char (42.9 g kg^{-1}) than 2EWoB (33.3 g kg^{-1}) due to the higher amount of fixed carbon and ash.

The total gas yields from *E. benthamii* were significantly affected by the presence/absence of bark. 2EWoB showed the highest gas yields (832.5 g kg^{-1}) followed by 7EWoB, which is likely due to the higher mass fraction of extractives and volatile matter which is related to the amount of hemicellulose and cellulose. These gas yields are close to what was obtained from *P. taeda* gasification (829 g kg^{-1}), *P. taeda* samples had high amounts of extractives and volatile matter as well. The liquid condensate collected in the two condensers of the gasification unit reflected the moisture content of the samples as 2EWB showed the highest amount (226 g kg^{-1}).

Table 2.3. Summary of the overall performance of *E. benthamii* gasification.

Feedstock	Mass Balance (%)	Carbon Conversion (%)	Gas yield * (g kg-1)	Syngas Heating Value (MJ m-3)	Condensate (g kg-1)	Char (g kg-1)
2EWB	91	83.6±1.3 a	738.2±7.3 a	3.08±0.02 a	225±6.5 a	42.9±2.6 a
2EWoB	92	91.1±5.1 b	832.5±39 b	3.48±0.07 b	125±4.5 b	33.3±1.9 b
7EWoB	92	85.7±0.1 a	786.8±25 ab	3.83±0.2 c	159±26.6 b	55.3±5.5 c
P. taeda	-	95.0	829.0	4.98	-	29.7

Values in the same column with the same letter (a, b or c) are not statistically different (P>0.05). *Gas yield is based on the amount of oxygen and biomass flow rates, kg min^{-1}.

2.4.3 E. benthamii gasification syngas profiles

The concentration (volume %) of CO, CO_2, H_2 , and CH_4 from different *E. benthamii* samples is presented in Figure 2.7. Syngas concentrations were stable (within 1% variation) after approximately 35 minutes of runtime for the younger samples (2EWB and 2EWoB) and approximately 60 minutes for the adult sample (7EWoB). The different duration of time needed to reach steady state was possibly due to the high density of older samples (7EWoB). [16] The production of syngas was dependent on several simultaneous and competing reactions. The extent to which each reaction progresses was dictated by reactor operating conditions and feedstock. [48] In a system operating at a high gasification temperature (935 °C) and achieving high carbon conversion (>80%), the heterogeneous reactions are shown below as Equation (2.8), (2.9) and (2.10) were essentially completed. Therefore, the final syngas composition is determined by the homogeneous gas phase reactions given in Equation (2.11) and (2.12) [48] and the initial feedstock composition. As mentioned previously the amount of hydrogen in the *E. benthamii* samples was 2EWB ≥ 2EWoB ≥ 7EWoB, a similar trend is observed in the formation of H_2 gas. The formation of hydrogen-

containing syngas species is a result of hydrogen in the feedstock being converted to CH_4 during the heterogeneous methanation reaction and subsequently being converted to H_2 during the homogeneous steam methane reforming reaction in the gas phase. [48] The overall gas yields and progression of the final gas phase reactions and is believed to shape the syngas profiles. The overall trend in H_2 gas yields was 2EWB ≥ 2EWoB ≥ 7EWoB, which was inversely correlated to CH_4 yields of 7EWoB > 2EWoB ≥ 2EWB. The concentration of H_2 gas was much higher as compared to the concentration of CH_4 for 2EWB whereas H_2 and CH_4 concentrations were similar for 2EWoB and 7EWoB samples (Figure 2.7). Therefore, the steam methane reforming reaction seems to be more active with the 2EWB samples.

$C + H_2O \leftrightarrow CO + H_2$	(+131 MJ kmol-1)	Water-gas reaction	(2.8)
$C + CO_2 \leftrightarrow {}_2CO$	(+172 MJ kmol-1)	Boudouard reaction	(2.9)
$C + 2\ H_2 \leftrightarrow CH_4$	(-75 MJ kmol-1)	Methanation reaction	(2.10)
$CO + H_2O \leftrightarrow CO_2 + H_2$	(-41 MJ kmol-1)	Water-gas shift reaction	(2.11)
$CH_4 + H_2O \leftrightarrow CO + 3\ H_2$	(+206 MJ kmol-1)	Steam reforming reaction	(2.12)

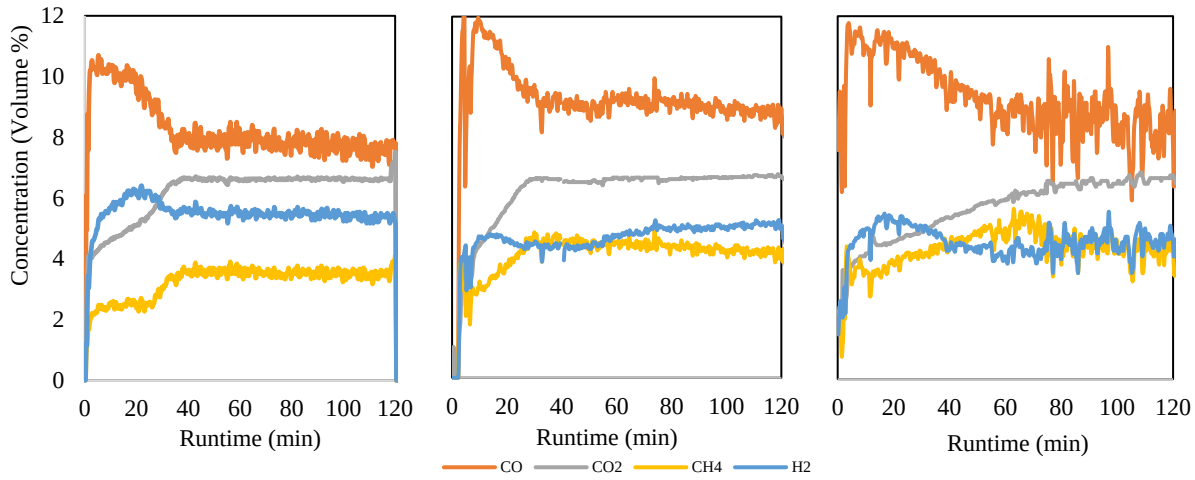

Figure 2.7. Syngas profiles from air blown bubbling fluidized bed gasifier (a) 2EWB, (b) 2EWoB, (c) 7EWoB.

CO is a valuable chemical produced by gasification and can be used in the Fischer-Tropsch process along with H_2 for liquid transportation fuel production. [49] Syngas from 2EWB contained the most H_2 and the lowest CO gases, which can be explained by the higher moisture content that affected the water-gas shift reaction. However, the water-gas shift reaction is not favorable at this high temperature due to its exothermic nature. The lower CO yield may also be linked to the lower carbon conversion for 2EWB samples. [34] The lower CH_4 with higher CO_2 and H_2 from 2-years old *E. benthamii* gasification suggested

an active reaction of wet reforming. At the same time, the presence of bark further propagated the water-gas shift reaction. Ultimately, the trend of H_2: CO ratio was 2EWB (0.05)>2EWoB (0.039) >7EWoB (0.035), which is essential to the downstream application of syngas to the Fischer-Tropsch reaction for liquid fuel production. As compared to *E. benthamii* syngas composition, *P. taeda* behaved differently in syngas production. Although it had high amounts of hydrogen in the feedstock, H_2 yield was lower than all *E. benthamii* gasification syngas. CO yield for *P. taeda* was comparable to 2EWoB and slightly higher than 7EWoB. H_2: CO ratio of *P. taeda* syngas was 0.033, which was lower than the ratio of the current study syngas ratio.

Table 2.4. Distribution of light gasses for all *Eucalypts* samples and literature values for *P. taeda*[34]

	Gas Yields* (g kg^{-1})					
Feedstock	H_2	CO	CO_2	CH_4	C_2H_2	C_2H_4
2EWB	12.7 ± 0.2 a	254.2 ± 8.1 a	341.3 ± 4.50 a	66.0 ± 3.4 a	3.2 ± 0.1 a	56.3 ± 3.4 a
2EWoB	11.2 ± 0.8 ab	288.0 ± 11.0 b	322.2 ± 17.6 a	77.2 ± 0.4 b	3.8 ± 0.4 a	61.4 ± 17.0 a
7EWoB	9.89 ± 1.0 b	281.8 ± 10.5 b	317.3 ± 15.4 a	95.9 ± 13.9 b	2.5 ± 0.1 b	52.9 ± 6.5 a
P. taeda	9.5	286.6	342.0	85.2	3.3	67.1

Values in the same column with the same letter (a,b or c) are not statistically different (P>0.05) using one way ANOVA and post-hoc test of summary statistics (mean, standard deviation). *Yield is based on the amount of oxygen and biomass flow rates, kg min^{-1}.

2.4.4 Gasification tar analysis

The formation of tar during gasification is one of the major hurdles for further applications. A detailed list of quantified tar compounds from *E. benthamii* gasification can be found in Table 2.5. The overall tar yields for *E. benthamii* samples were 2EWoB (1.69 g kg-1), 7EWoB (1.50 g kg-1) and, 2EWB (1.32 g kg-1). This trend is correlated with the combined mass fractions of extractives and lignin, which are understood to generate higher levels of tar during gasification. [50] In addition to differences in the total yield of tar, a noticeable difference can be found in types of tar compounds formed for *E. Benthamii* samples. 2EWoB samples generated more benzene while 7EWoB produced more naphthalene, and indene tars. The higher yields of polycyclic aromatic hydrocarbons (PAH) for 7 years old samples may be due to multiple factors. The formation of tar is believed to be through three main mechanisms; (i) direct combination of aromatic rings, (ii) H2 abstraction C2H2 addition, and (iii) phenol precursor for PAH formation. [50] The favorability of these tar forming pathways are dictated by factors such as reactor temperature, pressure, residence time and feedstock. [2] It is noted that the yields of C_2H_2 are statistically lower for 7EWoB and may, therefore, suggest that the indene and naphthalene tars are generated through the H2 abstraction C_2H_2 addition mechanism. PAH tars are more difficult to process as compared to benzene because their high

boiling point can cause them to condense on colder sections of the unit. Therefore, although 2EWoB has a higher total amount of tar, it will still be less challenging to utilize the produced syngas.

Table 2.5. Tar yield and profile for three *E. benthamii* samples

	Tar Yield (mg kg^{-1})		
Tar Compound	2EWB	2EWoB	7EWoB
Benzene	910.1±3.2	1268.4±2.1	806.2±4.0
Toluene	110.4±0.4	116.6±0.3	93.6±0.8
O-xylene	19.4±0.7	25.8±0.1	18.6±2.5
Styrene	50.1±0.2	49.5±0.2	44.1±1.1
Indene	76.9±0.3	80.6±0.1	204.6±2.0
Phenol	5.7±0.1	5.4±0.1	5.3±0.3
Naphthalene	137.3±0.5	129.8±0.3	314.0±0.8
2 methyl naphthalene	5.7±0.1	6.9±0.1	18.3±0.2
Biphenyl	0.0±0.0	4.4±0.1	0.0±0.0
Total (mg kg^{-1})	1314.5±4.6	1686.6±3.0	1622±10.8

The presence of bark lowered the yields of almost all tar compounds detailed in this study, which is likely correlated to the lower overall gas yield for 2EWB. However, there was a slight increase in the amounts of phenol and naphthalene. Phenol can be produced through the reaction of water and benzene, [51] therefore, the difference between 2EWoB and 2EWB may be due to the higher moisture content of 2EWB. The increased yields of naphthalene for 2EWB is interesting because alkali and alkaline earth metal salts in the ash can act as a cracking catalyst for naphthalene. [52] However, this may be more applicable to feedstock with higher ash content (>1%). The yield of tar was much higher for *P. taeda* than *E. benthamii*, reported as 2.24 g kg $biomass^{-1}$. [34] These results were attributed to a higher lignin and extractives content in *P. taeda*. Ultimately, the results showed that young samples (2 year) produced more tar than old samples (7 year) primarily due to the much higher yields of benzene for younger samples. It should be considered that the total tar yields without benzene were 7EWoB (0.70 g kg^{-1}), 2EWB (0.41 g kg^{-1}) and 2EWoB (0.42 g kg^{-1}). If benzene is not problematic for the utilization of gasification syngas, young *E. benthamii* samples (2EWB and 2EWoB) are the more favorable feedstock.

2.4.5 Effect of bed heights on syngas and tar formation

The amount of non-catalytic silicon sand used as bed material in the bench scale reactor was varied to achieve an H/D ratio (height/diameter) of 1.26, 1.89 and 2.52. These experiments were conducted using the 2EWB feedstock and resulted in noticeable effects on syngas, char and tar yields. As the static bed height ratio increased from the lowest (1.26) to the highest (2.52), the primary gas yields increased by 7%

as shown in Table 2.6. A lower char yield was also found with the higher H/D ratio and is correlated with the improved carbon conversion.

Table 2.6. Overall performance metrics for all bed height experiments.

H/D	Overall Performance Metrics					
	Mass Balance (%)	Carbon Conversion (%)	Char (g kg^{-1} feed[1])	Gas yield * (g kg^{-1} feed)	Liquid Condensate (g kg^{-1} biomass)	Syngas Heating Value (MJ m^{-3})
1.3	90.8	83.5±1.3a	36.9±0.2a	738.3±7.9 a	277.2±5.3a	3.1±0.1a
1.9	93.7	81.2±2.7a	36.6±0.5a	774.3±13.9ab	238.6±10.4b	3.2±0.1a
2.5	95.3	85.4±5.9a	23.3±0.4b	791.8±21.1 b	253.4±3.5b	3.3±0.1a

*Gas yield is based on the oxygen and biomass flow rates, kg min^{-1}.

Syngas compositions are summarized in Table 2.7. The largest difference in gas composition distributions was found between the lowest (1.26) and the highest (1.89) H/D ratio. H_2 and CO yields decreased while CO_2 and CH_4 increased. The syngas heating value subsequently increased from 3.08 MJ m^{-3} to 3.25 MJ m^{-3}. Similar trends were observed by Wan Ab Karim Ghani for two different feedstocks over an H/D range of 0.16 to 0.5. This may be due to the increase in pressure caused by the greater bed weight. Although pressure was not monitored in this work the relation of bed height and pressure is well documented. [53] A study by Kitzler et al. [9] looked at varying the pressure during fluidized bed biomass gasification and found CO and H_2 concentrations decreased while CO_2 and CH_4 increased over the pressure range of 1-3 bar abs. These trends are similar to those observed in the current study. The relation to pressure has an optimal point as discussed by Kitzler et al. therefore, these trends in syngas concentrations may not hold over a wide range of H/D ratios. However, H/D ratio is useful in shifting products from H_2 and CO to CH_4 for 2EWB over the mentioned ranges and may be employed when a pressurized system is not available.

Table 2.7. Light gas yields for all bed height experiments.

H/D	Gas Yields (g kg^{-1} feed*)					
	H_2	CO	CO_2	CH_4	C_2H_2	C_2H_4
1.26	12.7±0.1 a	254.2±6.6 a	341.4±2.0 a	66.0±3.0 a	3.24±0.1 a	56.3±2.2 a
1.89	10.9±0.7 b	236.5±6.7 b	361.4±9.8 b	71.8±2.5 b	2.75±0.1 b	39.7±5.6 b
2.52	9.06±0.5 c	239.0±15 ab	367.8±11 b	78.4±2.4 c	2.57±0.1 ab	43.9±8.2 ab

Values in the same column with the same letter (a,b or c) are not statistically different (P>0.05). *feed is defined as the oxygen and biomass flow rates, kg min^{-1}.
Tar was characterized and quantified by GC-FID.

Tar yields were determined for each H/D ratio and are shown in Figure 2.8. An increase in tar yield was observed as the H/D ratio was increased from 1.26 to 1.89 primarily due to an increase in benzene, toluene, and indene. As the H/D ratio was further increased to 2.52, the tar yield slightly decreased as a

result of lower phenol, naphthalene, and benzene yields, while other tar compounds were relatively unchanged. Tar compounds can be formed through multiple reaction pathways [50] and their initial increase may be linked to the improved conversion of biomass and increased overall production of gas. The trend in tar yields is reflected in the yields of C_2H_4 and suggest some correlation.

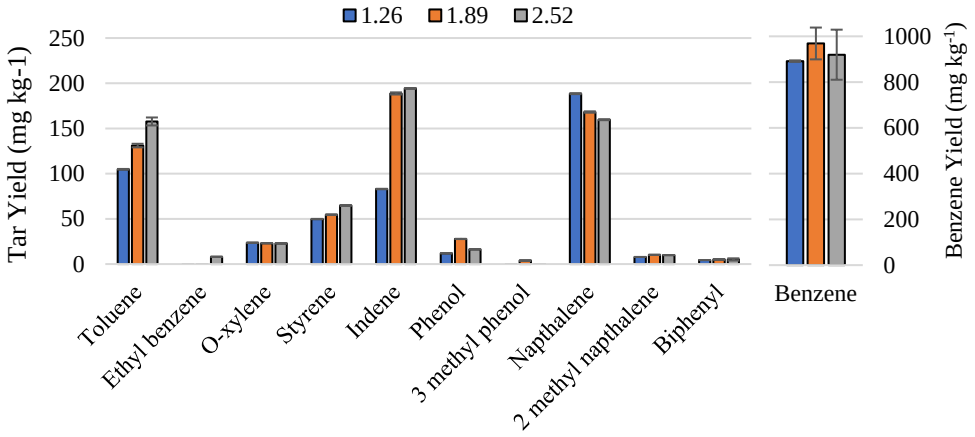

Figure 2.8. Tar yield during gasification of 2EWB with increasing H/D ratio (1.26, 1.89, 2.52).

2.4.6 Micro pyrolyzer GC-MS-FID-TCD

Microscale pyrolysis conducted at 500°C was performed on the three eucalyptus samples with varying harvesting age and presence/absence of bark. The carbon yields of the major products are shown in Table 2.8. The total carbon yield obtained with these samples ranged from 42% to 47%. The main types of compounds detected are light gases including CO, CO_2, and light hydrocarbons. Condensable vapors included methoxy phenols, acids, ketones, aldehydes, and furans. The carbon yields for these individual groups of compounds can range from around 8% for methoxy phenols, light gases and acids to 4% for aldehydes, and ketones to 2% or less for furans and alcohols. There are noticeable differences in the yields of each of these classes of compounds depending on the feedstock selected, 2EWB, 2EWoB or 7EWoB.

Light gases are one of the end products of many different reactions that occur during fragmentation and depolymerization of biomass, with decarboxylation and decarbonylation being the main two reactions that produce CO and CO_2. Therefore, CO and CO_2 carbon yields are good indicators of major differences in reaction pathways. The similar yields of non-condensable gases observed here indicate that there are only subtle differences in these feedstocks and the resulting pyrolysis products from them. There is a statistical difference between the yields of 7EWoB and 2EWoB and this is thought to be caused by the different characteristics of the cellulose. According to Mamleev et al. an additional source of H_2O and CO_2 from cellulose is the dehydration of non-reducing ends. The spectroscopic analysis of these feedstocks was

not able to show a strong correlation between the carbonyl and carboxylic groups and the CO and CO_2 yields, as these signals were far weaker for 7EWoB in CP/Mas ^{13}C NMR, as well as in ATR-FTIR analysis. However, lower amounts of acids are produced with 7EWoB and may indicate that the carboxyl groups that are present in the hemicellulose are being converted to CO_2 instead of being converted to larger molecules.

Phenolic lignin monomers are abundant products of biomass pyrolysis. The exact structure of lignin is unknown; however, the main building blocks are syringol, guaiacol, and p-hydroxyphenyl, differentiated from each other by the amount of methoxyl substitution. Overall the older samples produced a higher carbon yield of lignin derivatives with 1,2,4-trimethoxy benzene showing the largest increase in the yield with biomass age. Bark also has a noticeable effect on the composition of phenolic monomers and produces more 4-methyl-2,5-dimethoxybenzaldehyde and 2,6-dimethoxyphenol than both 2EWoB and 7EWoB.

Acids are a major product from the feedstocks and their carbon yields range from 8.4% to 9.4% with 2EWB giving the highest yield. The main compound is acetic acid and is responsible for 2EWB producing a higher total amount of acids. Propanoic acid 2-methyl, methyl ester is the second most abundant compound and its higher yield is observed from 2EWB. The yields of acids are correlated with the level of hemicellulose and cellulose (2EWB > 2EWoB > 7EWoB) as determined spectroscopically in this work and physically in the previous publication. [45]

The group of compounds with aldehyde functional groups are mainly represented by acetaldehyde and furfural for the younger samples, whereas 7EWoB also produces higher amounts of 2-propenal. The total yield for this group of compounds ranges from 4.2% to 5.8%. Ketones are the smallest group of compounds after aldehydes, acids and S-type phenolic monomers that generate yields over 4%. Cyclopentanediones and cyclopentanones are the main ketones along with lower levels of 1-hydroxy-2-propanone. The yields from these feedstocks are similar and show no major difference in composition. The differences in cellulose CrI was observed to only slightly alter the results of pyrolysis. Furan and furfural yields were not drastically different. The main observation from these trials was the formation of D-allose exclusively from 7EwoB, as observed in table 2.8.

Table 2.8. Carbon yield of major GC detectable pyrolysis products.

Library/ID	Feedstock		
	2-year Euc W/Bark	2-year Euc Wo/Bark	7-year Euc Wo/Bark
Yield (C%)			
Light gases			
Carbon dioxide	6.21%	5.92%	7.06%
Carbon Monoxide (TCD)	0.26%	0.28%	1.29%
1-Propene, 2-methyl-	-	-	0.82%

1,3-Cyclopentadiene	0.02%	0.02%	0.02%
Isobutane	0.41%	-	-
Sum	6.89%	6.21%	9.19%
Alcohols			
d-Allose	-	-	1.44%
1,2-Benzenediol	0.22%	-	0.30%
1,2-Benzenediol, 3-methoxy-	0.22%	0.16%	0.23%
3-Amino-1,2-propanediol	-	0.43%	-
3-Methylpenta-1,3-diene-5-ol, (E)-	-	0.10%	-
Sum	0.44%	0.69%	1.98%
Ketones			
Acetone	-	-	0.43%
1,3-Cyclopentanedione	0.15%	-	0.28%
1,2-Cyclopentanedione, 3-methyl-	0.20%	0.39%	0.49%
1-Propanol, 2-methyl-	0.46%	1.41%	-
1-Propene, 2-methyl-	0.35%	0.54%	-
2,3-Butanedione	0.32%	0.11%	0.34%
2-Cyclopenten-1-one, 2-hydroxy-	1.29%	1.16%	1.48%
2-Cyclopenten-1-one, 2-methyl-	0.00%	-	0.19%
2-Cyclopenten-1-one, 5-hydroxy-2,3-dimethyl-	0.13%	0.02%	-
3-(But-3-enyl)-cycloheanone	-	-	0.20%
4-Penten-2-one	0.23%	-	-
2-Propanone, 1-hydroxy-	0.77%	-	0.79%
Sum	3.92%	3.63%	4.19%
Furans			
2(3H)-Furanone, 5-ethyldihydro-	0.35%	-	-
2(5H)-Furanone	1.11%	0.89%	1.26%
3(2H)-Benzofuranone, 2,4-dimethyl-	-	0.13%	-
3-Methyl-benzofuran	-	0.14%	0.11%
3-Furanmethanol	-	0.34%	0.63%
Furan	-	0.19%	-
Furan, 2,5-dihydro-	-	-	0.46%
Furan, 2-methyl-	0.12%	-	0.15%
Sum	1.58%	1.69%	2.61%
Aldehydes			
Acetaldehyde	1.28%	1.26%	1.60%
Furfural	1.29%	1.15%	1.39%
Butanal	-	-	0.54%
2-Propenal	0.47%	0.22%	0.62%
Sum	3.04%	2.63%	4.16%
Acids			
Acetic acid	6.71%	5.47%	4.48%
Acetic acid, hexyl ester	-	0.80%	-
Propanoic acid, 2-methyl-, methyl ester	1.61%	1.31%	1.58%

Sum	8.32%	7.58%	6.06%
Amines			
Aziridine, 2-methyl-3-(1-methylethyl)-1-(2-propenyl)	0.26%	0.28%	-
1,4-Butanediamine, 2,3-dimethoxy -tetramethyl	-	0.09%	0.20%
4-Hydroxy-N-methylpiperidine	-	0.17%	-
Imidazole, 2-hydroxy-4-methyl-	-	0.16%	-
Sum	0.26%	0.70%	0.20%
Phenolic monomers			
H			
Phenol	0.10%	0.10%	0.11%
Phenol, 2-methyl-	0.06%	0.08%	0.07%
Sum	0.16%	0.18%	0.17%
S			
Phenol, 2,6-dimethoxy-	0.90%	0.64%	0.78%
Phenol, 2,6-dimethoxy-4-(2-propenyl)-	1.62%	1.51%	1.70%
Ethanone, 1-(2,4,6-trimethylphenyl)-	-	0.18%	-
Ethanone, 1-(2,6-dihydroxy-4-methoxyphenyl)-	-	-	0.11%
Ethanone, 1-(4-hydroxy-3,5-dimethoxyphenyl)-	0.34%	0.09%	0.06%
Benzaldehyde, 4-hydroxy-3,5-dimethoxy-	0.41%	0.44%	0.46%
3,5-Dimethoxy-4-hydroxycinnamalde	0.29%	-	0.29%
3,5-Dimethoxy-4-hydroxyphenylacetic acid	-	0.41%	-
1,2,3-Trimethoxybenzene	-	-	0.60%
1,2,4-Trimethoxybenzene	-	0.44%	-
4-Methyl-2,5-dimethoxybenzaldehyde	0.98%	0.84%	0.99%
Sum	4.55%	4.56%	5.00%
G			
Phenol, 2-methoxy-	0.51%	0.43%	0.64%
Phenol, 2-methoxy-3-(2-propenyl)-	0.12%	0.14%	-
Phenol, 2-methoxy-4-(1-propenyl)-	0.64%	0.62%	0.74%
Phenol, 2-methoxy-4-(methoxymethyl)-	-	0.08%	-
Phenol, 2-methoxy-4-methyl-	0.25%	0.22%	0.34%
Phenol, 4-(3-hydroxy-1-propenyl)-2-methoxy-	-	-	0.04%
Phenol, 4-ethyl-2-methoxy-	0.10%	0.08%	0.12%
Phenol, 4-methoxy-3-(methoxymethyl)-	0.44%	-	-
Vanillin	0.11%	-	-
Homovanillyl alcohol	-	0.02%	0.02%
Eugenol	-	-	0.19%
Ethanone, 1-(4-hydroxy-3-methoxyphenyl)-	-	-	0.15%
Benzaldehyde, 3-hydroxy-4-methoxy-	-	0.12%	0.14%
4-Hydroxy-2-methoxycinnamaldehyde	-	0.27%	-
2-Methoxy-4-vinylphenol	0.67%	0.48%	0.73%
Sum	2.84%	2.46%	3.11%
Total	31.98%	30.34%	36.65%

2.4.7 TGA Kinetics

Thermo-gravimetric analysis was used to determine the thermal decomposition behavior of 2EWB, 2EWoB, and 7EWoB using non-isothermal conditions. Three model-free methods (KAS, FWO, and Kissinger) were used to determine the kinetic parameters including activation energy and pre-exponential factors according to equations 2.5 – 2.7. [54] Results are presented in Table S1 and Table 2.9. The small differences in biomass chemical compositions (cellulose, hemicellulose, and lignin mass fractions) seem to have only a small effect on the thermal behavior of these samples, likely because the mass fractions are very similar. The ash content and crystallinity of cellulose do however appear to influence not only pyrolysis products as mentioned but also the kinetic parameters. 2EWB which had a higher ash content, also had a higher average activation energy than 2EWoB and 7EWoB, for all the methods. High ash content was previously reported to delay the thermal decomposition of biomass by Carpenter et al. [55] Crystalline cellulose was observed to have a lower decomposition rate than amorphous cellulose as shown by Wang et al. [56] The crystallinity index was found to be higher for 7EWoB and similarly the activation energy is higher than 2EWoB, which has a similar ash content but lower cellulose CrI. The kinetic parameters are within the values reported by other authors for eucalyptus. [24] 2EWoB had the lowest activation energy which is due to the lower ash content and lower CrI. Also, 2EWoB has a higher hemicellulose mass fraction and hemicellulose has been shown to decompose more easily than cellulose. [57]

Table 2.9. Global kinetic parameters for *E. Benthamii* samples.

	Kissinger		
	2EWB	7EWoB	2EWoB
E (kJ mol^{-1})	214.7	174.3	141.8
Ln A (s^{-1})	31.1	23.9	17.8

2.4.8 Pyrolysis/Gasification of lignin model compounds

Lignin model dimers with the β-O-4linkage were used to determine the difference in reactivity of these compounds based on the shift from 0, 2, and 4 methoxyl groups per β-O-4 linkage represent the difference in H, G, and S lignin dimers. The effects of chain end β-O-4 linkages where the C4 position contains a phenolic group can also be differentiated from groups with biphenyl ligands at this position. The main products from pyrolysis at 850°C are shown in Table 2.10 and a full list of compounds can be found in the Chapter 3 Appendix.

The theory of tar formation through a direct combination of aromatic rings is the primary tar forming mechanism investigated for this work. This mechanism is illustrated in Figure 2.9. The methoxy groups are thought to be broken through hemolytic cleavage resulting in radical species, the higher amount of methoxyl groups should lead to a higher probability of condensation reactions resulting in more secondary and tertiary tars. What was observed is that a common compound found in gasification tar,

indene's, were only observed from S type dimers. Additionally, the selectivity of 2-Ring aromatics is higher for S type dimers than G. The selectivity of 2-ring aromatics increases with methoxyl content ranging from 4.4% with H type dimers up to 9.4% with S type dimers.

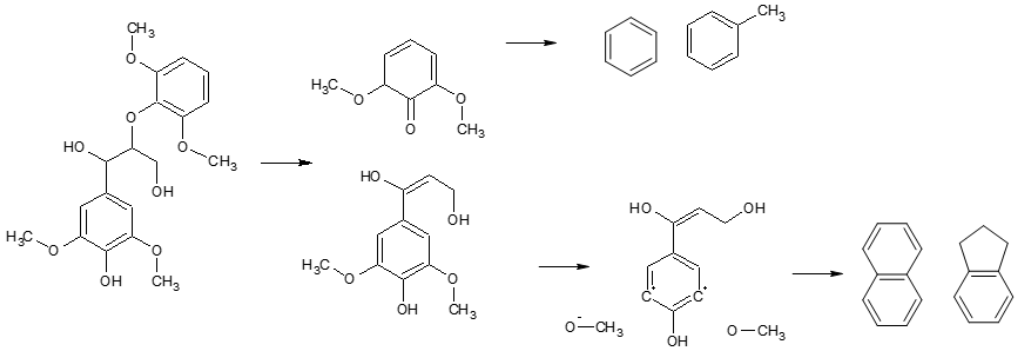

Figure 2.9. Formation of tar compounds from S type β-O-4 phenolic dimers

Secondary effects of the different methoxyl content are highlighted in the selectivity of all major compounds including, phenols, furans, 1-ring aromatics and light gases. H type dimers show the highest selectivity of phenols and 1-ring aromatics, G type dimers produce the most furans, and S type dimers produce more light gases.

The formation of 1-Ring aromatics shows H type dimers have the highest selectivity while S type dimers have a higher selective than G type dimers. After fragmentation of the β-O-4linkage, H dimers will undergo the fewest reactions to stabilize and from1-ring aromatics leading to a more selective pathway. For S type dimers it may be possible for the two radicals left from methoxyl cleavage to self-condense leading to stable, 1-ring aromatics while G dimers are unable to self-condense and therefore likely to undergo further reactions to form stable compounds.

G type dimers show more tertiary tars such as phenanthrene while S dimers give the lowest yield of these tars. Light gasses are also significantly affected by methoxyl content. The higher amount of methoxy groups are contributing to this as they are released however, the highest selectivity for light gasses are larger compounds like 1,4 pentadiene, 1,3 butadiene, and propene

The presence of the phenolic group instead of the biphenyl group is also important as the selectivity of indene's increased from 0.3% to 2.3% with the phenolic group. The higher selectivity of indenes with the phenolic group for S type dimers was followed by a decrease of 1-Ring (44.7% to 37.5%) and 2-Ring (9.4% to 6.9%) aromatics. The main compounds that showed lower selectivity were largely ethylbenzene and toluene for the 1-Ring compounds and ethylene-1,1-diphenyl and methylated naphthalene for the two ring compounds.

Table 2.10. Gasification/Pyrolysis products from lignin model compounds (FID Area %)

Library/ID	Non-phenolic						Phenolic			
	HH		GG		SS		GG		SS	
	Avg.	Stdv.	Avg.	Stdv.	Avg.	Stdv.	Avg.	Stdv.	Avg.	Stdv.
Light gases	8.43	1.11	4.45	0.24	11.43	0.57	9.29	0.31	37.47	1.85
Primary Tar	23.70	2.18	18.50	1.08	8.24	0.90	47.08	1.52	48.78	1.22
Ketones	-	-	-	-	-	-	0.80	0.03	0.98	0.05
Aldehydes	6.32	0.91	1.48	0.09	0.48	0.05	2.90	0.27	2.20	0.21
Phenols	15.97	3.57	12.67	0.48	4.97	0.63	34.21	1.58	37.85	0.40
Alcohols	0.15	0.14	0.55	0.14	-	-	1.33	0.02	1.33	0.49
Furans	1.27	0.15	3.80	0.46	2.78	0.13	7.84	0.43	6.41	0.34
Secondary Tar	60.52	1.68	44.55	1.46	56.06	1.75	26.33	1.38	46.77	1.06
1-Ring	53.22	2.55	35.52	2.04	44.69	2.34	21.22	1.58	37.49	0.33
Indene	-	-	-	-	0.33	0.00	-	-	2.36	0.28
2-Ring	4.43	0.29	6.07	0.10	9.42	0.73	4.85	0.33	6.92	0.52
Tertiary Tar	2.87	0.17	2.96	0.16	1.62	0.03	0.26	0.07	-	-

A full list of compounds can be found in Chapter 3 Appendix

2.5 Conclusions

Gasification performance of short rotation *E. benthamii* was found to be comparable to that of *P. taeda* in terms of syngas yields and profile. Differences were established in the amount of tar produced during gasification and was noticeably lower for *E. benthamii* samples. Tree harvesting age and the presence/absence of bark were determined to be suitable parameters for adjusting the syngas and tar profiles. Older 7EWoB generated higher levels of CH_4 leading to a higher heating value of the syngas compared to both younger samples (2EWoB and 2EWB). Tar profiles showed increased amounts of naphthalene and indene for older samples but a significant decrease in benzene which resulted in the total tar yields being lower for older samples. The presence of bark was found to increase the H_2 yield which leads to a higher H_2: CO gas ratio with the 2EWB sample. Finally, the effect of alteration of fluidized bed H/D ratio in combination with the 2EWB samples on gasification performance indicated an improved conversion of biomass and char to vapors. This lead to higher syngas yields as well as higher tar yields. The H/D ratio also shifted syngas profiles to increase the formation of CH_4 and CO_2 and higher ratios while CO and H_2 yields were higher at low H/D ratios. Spectroscopic characterization, TGA kinetic analysis and

pyrolysis of *E. benthamii* samples were used to further investigate differences in gasification product slates and tar yields. Variations in the cellulose crystallinity and lignin composition of *E. benthamii* were observed with varying the harvesting age and presence/absence of bark, which in turn altered the product slate from fast pyrolysis.7EWoB was found to have a higher cellulose CrI which led to an exclusive formation of d-Allose upon pyrolysis. The higher ash content of 2EWB affected the kinetics of pyrolysis leading to the highest activation energy among the samples studied. Tar formation from lignin model compounds was studied using S, G and H type β-O-4 linkages. Condensation of radical species was the main reaction pathway for the growth of tars. S type dimers produce more 2-ring secondary tar compounds as well as indene tars. G type dimers form primary tars such as furans and also tertiary tars. H type dimers are more selective towards 1-ring compounds like benzene, toluene, and phenols.

References

1. Ajay, K.; Jones, D.; Milford, H. Thermochemical Biomass Gasification: A Review of the Current Status of the Technology. *energies* **2009,** 556-581.

2. Milne, T.; Evans, R.; Abatzoglou, N. Biomass gasifier tars their nature, formation, and conversion. *NREL/TP-570-25357, National Renewable Energy Laboratory: Golden Colorado* **1998**.

3. Heyne, S.; Liliedahl, T.; Marklund, M. Biomass gasification - A synthesis of technical barriers and current research issues for the deployment at large scale. *The Swedish Knowledge Center for Renewable Transportation Fuels: Goteborg, Sweden. 2013.*

4. Carpenter, D.; Bain, R.; Davis, R.; Dutta, A.; Feik, C.; Gaston, K.; Jablonski, W.; Phillips, S.; Nimlos, M. Pilot-Scale Gasification of Corn Stover, Switchgrass, Wheat Straw, and Wood: 1. Parametric Study and Comparison with Literature. *Ind. Eng. Chem. Res.* **2010,** *49*, 1859–1871.

5. Zhiqi, W.; Tao, H.; Jianqing, L.; Jingli, W.; Jianguang, Q.; Guangbo, L.; Dezhi, H.; Zhongyue, Z.; Zhuo, L.; Jinhu, W. Design and operation of a pilot plant for biomass to liquid fuels by integrating gasification, DME synthesis and DME to gasoline. *Fuel* **2016,** ISSN: 00162361; DOI: 10.1016/j.fuel.2016.08.108.

6. Baker, E.; Brown, M.; Moore, R.; Mudge, L.; Elliot, D. Engineering analysis of biomass gasifier product gas cleaning technology. *In PNL-5534; Pacific Northwest Laboratory: Richland, WA, USA, 1986*.

7. Stevens, D. Hot gas conditioning: recent progress with large-scale biomass gasification systems. *In NREL/SR-510-29952; National Renewable Energy Laboratory: Golden, CO, USA, 2001*.

8. Abdoulmoumine, N.; Adhikari, S.; Kulkarni, A.; Chattanathan, S. A review on biomass gasification syngas cleanup. *Applied Energy* **2015,** *155*, 294-307.

9. Kitzler, H.; Pfeifer, C.; Hofbauer, H. Pressurized gasification of woody biomass - Variation of parameters. *Fuel Processing Technology* **2011,** *92,* 908-914.

10. Leclerc, A.; Larachi, F. Allothermal fluidized bed reactor for steam gasification of biomass. *Instrumentation Science and Technology* **2015,** *43,* 390-428.

11. Hosseini, S.; Wahid, M. Hydrogen production from renewable and sustainable energy resources: Promising green energy carrier for clean development. *Renewable and Sustainable Energy Reviews* **2016,** *57,* 850-886.

12. Lapuerta, M.; Hernandez, J.; Pazo, A.; Lopez, J. Gasification and co-gasification of biomass wastes: Effect of the biomass origin and the gasifier operating conditions. *Fuel Processing Technology* **2008,** *89,* 828-837.

13. Lim, M.; Alimuddin, Z. Bubbling fluidized bed biomass gasification-Performances, process findings, and energy analysis. *Renewable Energy* **2008,** *33,* 2339-2343.

14. Myers, B. J.; Theiveyanathan, S.; O'Brien, N. D. O.; Bond, W. J. Growth and water use of Eucalyptus grandis and Pinus radiata plantations irrigated with effluent. *Tree Physiology* **1995,** 211-219.

15. Rencoret, J.; Gutierrez, A.; Nieto, L.; Jimenez-Barbero, J.; Faulds, C.; Kim, H.; Ralph, J.; Martinez, A.; del Rio, J. Lignin Composition and Structure in Young versus Adult Eucalyptus globulus Plants. *Plant Physiol* **2011,** *155,* 667-682.

16. Senelwa, K.; Sims, R. Fuel characteristics of short rotation forest biomass. *Biomass and Bioenergy* **1999,** 127-140.

17. Hanaoka, T.; Inour, S.; Uno, S.; Ogi, T.; Minowa, T. Effect of woody biomass components on air-steam gasification. *Biomass & Bioenergy* **2005,** *28,* 69-76.

18. Wan Ab Karim Ghani, W.; Moghadam, R.; Mohd Salleh, M.; Alias, A. Air Gasification of Agricultural Waste in a Fluidized Bed Gasifier: Hydrogen Production Performance. *Energies* **2009,** *2,* 258-268.

19. Mayerhofer, M.; Fendt, S.; Spliethoff, H.; Gaderer, M. Fluidized bed gasification of biomass-In bed investigation of gas and tar formation. *Fuel* **2014,** 1248-1255.

20. Sluiter, A.; Hames, B.; Ruiz, R.; Scarlata, C.; Sluiter, J.; Templeton, D.; Crocker, D. *Determination of Structural Carbohydrates and Lignin in Biomass;* Technical Report ; NREL: Golden, 2012.

21. Fu, L.; McCallum, S.; Miao, J.; Hart, C.; Tudryn, G.; Zhang, F.; Linhardt, R. Rapid and accurate determination of lignin content of lignocellulosic biomass by solid-state NMR. *Fuel* **2015,** *141,* 39-45.

22. Acquah, G.; Via, B.; Fasina, O.; Eckhardt, L. Rapid quantitative analysis of forest biomass using fourier transform infared spectroscopy and partial least squares regression. *J. Anal. Methods Chem.* **2016,** 10.1155/2016/1839598.

23. Park, S.; Baker, J.; Himmel, M.; Parilla, P.; Johnson, D. Cellulose crystallinity index: measurment techniques and their impact on interperting cellulase performance. *Biotechnology for Biofuels* **2010,** *3* (10).

24. Velden, M.; Baeyens, J.; Brems, A.; Janssens, B.; Dewil, R. Fundimentals, kinetics and endothermicity of the biomass pyrolysis reaction. *Renewable Energy* **2010,** *35,* 232-242.

25. Kongkaew, N.; Pruksakit, W.; Patumsawad , S. Thermogravimetric kinetic analysis of the pyrolysis of rice straw. *Energy Procedia* **2015,** *79,* 633-670.

26. Anca-Couce, A.; Berger, A.; Zobel, N. How to determine consitsent biomass pyrolysis kinetics in a parallel reaction scheme. *Fuel* **2014,** *123,* 230-240.

27. Klein, M.; Virk, P. *Ind. Eng. Chem. Fundam.* **1983,** *22,* 35-45.

28. Jarvis, M.; Daily, J.; Carstensen, H.; Dean, A.; Sharma, S.; Dayton, D.; Robichaud, D.; Nimlos, M. *J. Phys. Chem.* **2011,** *115,* 428-438.

29. Elder, T.; Beste, A. *Energy Fuels* **2014,** *28,* 5229-5235.

30. Choi, Y.; Singh, R.; Zhang, J.; Balasubramanian, G.; Sturgeon, M.; Katahira, R.; Chupka, G.; Beckham, G.; Shanks, B. Pyrolysis reaction network for lignin model compounds: unraveling thermal deconstruction of B-O-4 and a-O-4 compounds. *Green Chem* **2015,** DOI: 10.1039/c5gc02268a.

31. Chu, S.; Subrahmanyam, A.; Hubert, G. The pyrolysis chemistry of a B-O-4 type oligomeric lignin model compound. *Green Chem.* **2013,** *15,* 125.

32. Hosoya, T.; Kawamoto, H.; Saka, S. Role of methoxyl group in char formation from lignin-related compounds. *J. Anal. Appl. Pyrolysis* **2009,** *84,* 79-83.

33. Hosoya, T.; Kawamoto, H.; Saka, S. Pyrolysis gasification reactivity of primary tar and char fractions from cellulose and lignin as studied with closed ampoule reactor. *J. Anal. Appl. Pyrolysis* **2008,** *83,* 71-77.

34. Abdoulmoumine, N.; Kulkarni, A.; Adhikari, S. Effects of Temperature and Equivalence Ratio on Pine Syngas Primary Gases and Contaminants in a Bench-Scale Fluidized Bed Gasifier. *Industrial and Engineering Chemistry Research* **2014,** 5767-5777.

35. Neupane, S.; Adhikari , S.; Wang, Z.; Ragauskas, A.; Pu, Y. Impact of torrefaction on the chemical structure and catalytic fast pyrolysis behavior of heicellulose, lignin, and cellulose. *Green Chem* **2015,** *17,* 2406-2417.

36. van de Kamp, W. L.; de Wild, P. J.; Knoef, H. A. M.; Neeft, J. P. A.; Kiel, J. H. A. Tar measurement in biomass gasification, standardization and supporting R&D. *ECN* **2006,** 06-046.

37. van Paasen, S. V. B.; Kiel, J. H. A. Tar formation in a fluidised-bed gasifier. *ECN-C--04-013, 2014.*

38. Proano-Aviles, J.; Lindstrom, J.; Johnston, P.; Brown, R. Heat and Mass Transfer Effects in a Furnace-Based Micropyrolyzer. *Energy Technol* **2017,** *5,* 189-195.

39. IIsa, K.; French, R.; Orton, K.; Budhi, S.; Mukarakate, C.; Stanton, A.; Yung, M.; Nimlos, M. Catalytic pyrolysis of pine over HZSM-5 with different binders. *Top Catal* **2016,** *59,* 94-108.

40. Xu, M.; Mukarakate, C.; Iisa, K.; Budhi, S.; Menart, M.; Davidson, M.; Robichaud, D.; Nimlos, M.; Trewyn, B.; Richards, R. Deactivation of multilayered MFI nanosheet zeolite during upgrading of biomass pyrolysis vapors. *ACS Sustanable Chem. Eng* **2017,** DOI: 10.1021/acssuschemeng.7b00817.

41. Benkaci-Ali, F.; Baaliouamer, A.; Meklati, B.; Chemat, F. Chemical composition of seed essential oils from Algerian Nigella sativa extraction by microwave and hydrodistillation. *Flavor Fragrance J* **2007,** *22,* 149-153.

42. Jin, W.; Singh, K.; Zondlo, J. Pyrolysis Kinetics of Physical Components of Wood and Wood-Polymers Using Isoconversion Method. *Agriculture* **2013,** *3,* 12-32.

43. Goncalves, B.; Till, D.; Fasina, O.; Tamang, B.; Gallagher, T. Influence of Bark on the Physical and Thermal Decomposition Properties of Short-Rotation Eucalyptus. *Bioenerg. Res.* **2015,** 1414-1423.

44. Yu, H.; Zhang, Z.; Li, Z.; Chen, D. Characteristics of tar formation during cellulose, hemicellulose and lignin gasification. *Fuel* **2014,** 250-256.

45. Cross, P.; Kulkarni, A.; Nam, H.; Adhikari, S.; Fasina, O. Bubbling fluidized bed gasification of short rotation Eucalyptus: Effects of harvesting are and bark. *Biomass and Bioenergy* **2018,** *110,* 98-104.

46. Gilardi, G.; Abis, L.; Cass, A. Carbon-13 CP/MAS solid-state NMR and FT-IR spectroscopy of wood cell wall biodegradation. *Enzyme and Microbial Technology* **1995,** *17.,* 268-275.

47. Mukarakate, c.; Mittal, A.; Ciesielski, P.; Budhi, S.; Thompson, L.; Iisa, K.; Nimlos, M.; Donohoe, B. The influence of crystal allomorph and crystallinity on the products and behavior of cellulose during fast pyrolysis. *ACS Sustainable Chem. Eng.* **2016,** DOI:10.1021/acssuschemeng.6b00812.

48. Higman, C.; Van der Burgt, M. Gasification. *Gulf Professional Publishing* **2008**.

49. Im-orb, K.; Simasatitkul, L.; Arpornwichanop, A. Techno-economic analysis of the biomass gasification and Fischer-Tropsch integrated process with off-gas recirculation. *Energy* **2016,** 483-496.

50. Palma, C. Modeling of tar formation and evolution for biomass gasification A review. *Applied energy* **2013,** *111,* 129-141.

51. Mukarakate, C.; McBrayer, J.; Evans, T.; Budhi, S.; Robichaud, D.; Iisa, K.; Dam, J.; Watson, M.; Baldwin, R.; Nimlos, M. catalytic fast pyrolysis of biomass: the reactions of water and aromatic intermediates produces phenols. *Green Chemistry* **2015,** 4217-4227.

52. Abu El-Rub, Z.; Bramer, E.; Brem, G. Experimental comparison of biomass chars with other catalyst for tar reduction. *Fuel* **2008,** *87,* 2243-2252.

53. Kunii, D.; Levenspiel, O. Fluidization Engineering. *Wiley: New York, 1968.*

54. Mishra, R.; Mohanty, K. Pyrolysis kinetics and thermal behavior of waste sawdust biomass using thermogravimetric analysis. *Bioresource Technology* **2018,** *251*, 63-74.

55. Carpenter , D.; Westover, T.; Czernik, S.; Jablonski, W. Biomass feedstocks for renewable fuel production: a review on the impacts of feedstock and pretreatment on the yield and product distribution of fast pyrolysis bio0oils and vapors. *Green Chem.* **2014,** 10.1039/c3g41631c.

56. Wang, Z.; McDonald, A.; Westerhof, R.; Kersten, S.; Cuba-Torres, C.; Ha, S.; Pecha, B.; Garcia-Perez, M. Effect of cellulose crystallinity on the formation of liquid intermediate and on product distribution during pyrolysis. *Journal of Analytical and Applied Pyrolysis* **2013,** *100*, 56-66.

57. Manya, J.; Velo, E.; Puigjaner, L. Kinetics of biomass pyrolysis: a reformulated three-parallel-reaction model. *Ind. Eng. Chem. Res.* **2003,** *42*, 434-411.

58. Howe, D.; Westover, T.; Carpenter, D.; Santosa, D.; Emerson, R.; Deutch, S.; Starace, A.; Kutnyakov, I.; Lukins, C. Field-to-fuel performance testing of lignocellulosic feedstocks: An integrated study of the fast pyrolysis-hydrotreating pathway. *Energy Fuels* **2015,** *29*, 3188-3197.

59. Bridgwater, A.; Meier, D.; Radlein, D. An overview of fast pyrolysis of biomass. *Organic Geochemistry* **1999,** 1479-1493.

60. Golden, J.; Handfield, R.; Daystar, J.; McConnell, T. An Economic Impact Analysis of the U.S. Biobased Products Industry: A Report to the Congress of the United States of America. A Joint Publication of the Duke Center for Sustainability & Commerce and the Supply Chain Resource Cooperative at North Carolina. **2015**.

61. Dutta, A.; Sahir, A.; Tan, E.; Humbird, D.; Snowden-Swan, L.; Meyer, P.; Ross, J.; Sexton, D.; Yap, R.; Lukas, J. *Process design and economics for the conversion of lignocellulosic biomass to hydrocarbon fuels: Thermochemical research pathways with in situ and ex situ upgrading of fast pyrolysis vapors;* National Renewable Energy Lab (NREL): Golden, CO, 2015.

62. Jones, S.; Meyer, P.; Snowden-Swan, L.; Padmaperuma, A.; Tan, E.; Dutta , A.; Jacobson, J.; Cafferty, K. *Process design and economics for the conversion of lignocellulosic biomass to hydrocarbons fuels: Fast pyrolysis and hydrotrating bio-oil pathway;* National Renewable Energy Laboratory (NREL): Golden, CO, 2013.

63. Eufrade-Junior, H.; Guerra, S.; Sansigolo, C.; Ballarin, A. Management of eucalyptus short-rotation coppice and its outcome on fuel quality. *Renewable energy* **2018,** *121*, 309-314.

64. Dou, C.; Chandler, D.; Resende, F.; Bura, R. Fast pyrolysis of short rotation poplar: An investigation in thermochemical conversion of a realistic feedstock for the biorefinery. *ACS Sustainable Chem. Eng.* **2017,** *5*, 6746-6755.

65. Roman-Leshkov, Y.; Barrett, C.; Liu, Z.; Dumesic, J. *Nature* **2007,** *447*, 982.

Chapter 3 Fast pyrolysis of Prickly pear and Gumweed[3]

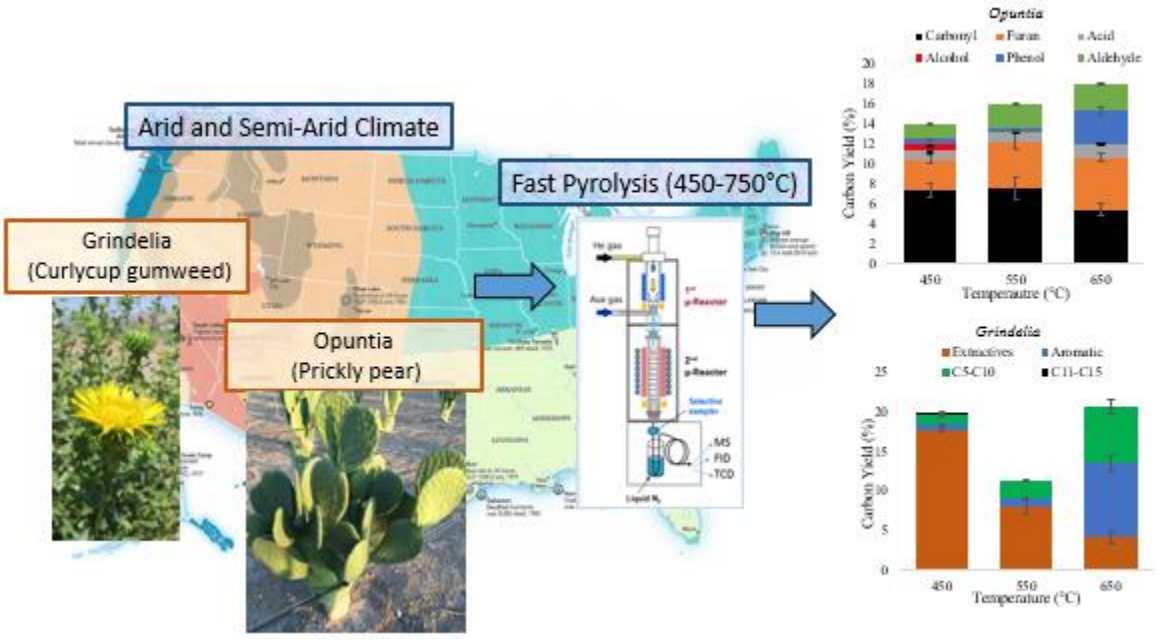

3.1 Abstract

Opuntia ficus-indica (prickly pear) and *Grindelia squarrosa* (gumweed) are two exceptionally drought tolerant plant species capable of growing in arid and semi-arid environments. Additionally, they have unique cell wall structures. Prickly pear contains pectin and high levels of ash (16.1%) that is predominantly Ca and K. Gumweed has high levels of extractives that contain grindelic acid and mono-terpenoids. The objective of this paper was to evaluate how these unique cell wall components alter the pyrolysis performance of prickly pear and gumweed. Using a tandem micro pyrolyzer with GC-MS/FID/TCD, a detailed account of the product slate is given for products generated between 450°C and 650°C. Pyrolysis of prickly pear showed that the high levels of ash increase the amount of organics volatilized and shifted product pools making it possible to generate up to 7.3% carbonyls vs. 3.8% for *Pinus taeda* (loblolly pine) and 10.5% hydrocarbons *vs.* 1.8% for pine depending on reactions conditions. Pyrolysis of gumweed showed that the extractives were volatilized at low temperatures and led to 17.7%

[3] Cross, P.; Mukarakate, C.; Nimlos, M.; Carpenter, D.; Donohoe, B.; Mayer, J.; Cushman, J.; Neupane, B.; Miller, G.; Adhikari, S. Fast pyrolysis of opuntia ficus-indica (prickly pear) and Ggrindelia squarrosa (gumweed). *Energy & Fuels* **2018,** DOI: 10.1021/acs.energyfuels.7b03752.

grindelic acid and mono-terpenoids derivatives in the condensed vapor phase. At high temperatures, the extractives and other biomass components are converted to aromatics and C_5-C_{10} hydrocarbons giving a total yield of 16.6% and also generates large amounts of C_2-C_4 hydrocarbons, 11.3%.

3.2 Introduction

The production of renewable fuels and chemicals from biomass is a key part of the U.S. strategy for reducing dependence on imported petroleum, improving air quality, and supporting rural economies. The large-scale use of non-food biomass as a source of renewable carbon for fuels and chemicals will require the development of dedicated feedstocks co-optimized for growth and efficient conversion (high carbon and hydrogen retention, low catalyst deactivation). The benefits of drought-tolerant plants as feedstocks for biofuels and biochemicals have been identified by other groups [1,2] who stressed that increasing global temperature, drought, and soil-drying conditions caused by global warming will increase competition for agricultural freshwater and cultivated soils. Expanding available biomass resources to include plants with exceptional drought tolerance complements traditional lignocellulosic resources and has the advantage of lower water requirements and the use of arid and semi-arid lands, potentially opening up large areas of the western U.S. to biofuel and biochemical production. The use of marginal lands with low water availability will be a crucial component to the success and ecological sustainability of a future Bioeconomy.

Prickly pear and gumweed were identified as two species of plants that exhibit exceptional drought tolerance and thrive in arid and semi-arid climates. [3,1,4] The annual dry mass yield of prickly pear is 9-15 ton ha^{-1} yr^{-1}, rivaling that of *Panicum virgatum* (switchgrass) (12.9 ton ha^{-1} yr^{-1}). [3] Growth rate and water efficiency of gumweed have shown potential annual dry mass yields of 11.8 ton ha^{-1} yr^{-1} in a semi-arid climate. [5,6] Biochemical routes (pretreatment followed by enzymatic digestion) used for the conversion of these feedstocks have previously been reported. [7,8] Ethanol yields from prickly pear ranged from ~1.4% (w/v) [8] to 2.6% (w/v) [7] with different pretreatment and fermentation conditions being employed. However, to the best of our knowledge, no work has been conducted using the thermochemical route of fast pyrolysis.

Fast pyrolysis was selected as the conversion process because of its high conversion and potential to produce both bio-oil as a biofuel precursor and higher value chemicals. [9,10] The oxygen content in bio-oil from pyrolysis can range up to 62%, averaging 40%, and there can be hundreds of different compounds in the mixture. [9] Some of these oxygenated compounds have a higher economic value than gasoline or diesel and could be sold as co-products to improve the economic viability of the overall processes. [10] Oxygenates that are of high value include simple phenols (phenol \$1–2 kg^{-1} and p-cresol \$2–3 kg^{-1}) [11] and polymer feedstocks with disubstituted functional groups such as C_2-C_6 diols and 2,5-disubstituted furans. [12] Terpenoids are used in the development of sustainable renewable polymers. [13] The other lower value oxygen

compounds can be further upgraded to hydrocarbons through several processes. [14] Strategies to reduce the severity of the upgrading processes can include optimizing reaction conditions and feedstock selection to produce a more favorable product stream that requires less intensive upgrading. [15,16] Elkasabai et al. [17] showed that *Panicum* bio-oil upgraded with a Pt/C catalyst consumed half as much hydrogen as *Eucalyptus benthamii* primarily due to the differences in chemical composition of the biomass leading to the different oxygen content of the bio-oil.

The chemical composition of prickly pear was studied by Yang et al. [18] who performed a wet chemical analysis and also compiled values (mass fraction) from literature [19,20,7] and found that prickly pear cell walls consist of cellulose 6.8-13.1wt%, hemicellulose 9.1-18.5wt%, lignin 7.9-16.0wt%, extractives 17.7-25.0wt%, and ash 16.8-23.7wt% (Ca 10.6wt%, K 8.1wt%, Mg 2.8wt%, Na 0.2wt%). Additionally, Contreras-Padilla et al. determined that crystalline structures existed in prickly pear and contained; calcium carbonate [$CaCO_3$], calcium-magnesium bicarbonate [$CaMg(CO_3)_2$], magnesium oxide [MgO], calcium oxalate monohydrate [$Ca(C_2O_4)*(H_2O)$], potassium peroxydiphosphate [$K_4P_2O_8$], and potassium chloride [KCl]. [21] The extractives isolated from prickly pear using water extraction contain high amounts of pectin. The structural analysis and chemical properties of pectin have been well researched due to its common use in the food industry and the application of its gelling properties. [22,23]

Existing literature on the pyrolysis of pectin may give insight into how the products from pyrolysis of prickly pear will be different from other types of biomass that contain far less pectin. Pyrolysis studies of commercial citrus fruit pectin extract, [24,25] or citrus fruit peels [26,26] that are high in pectin, indicate its decomposition occurs between 150°C and 250°C and due to the structure of these particular pectins produces methanol as a primary product. CO_2 is also an abundant product of pectin pyrolysis and is understood to be formed by cleavage of the carboxylic groups of glucuronic acid. [27] An important characteristic of prickly pear that should affect the product slate is the high level of alkali metal salts and metal oxides. MgO has been shown to significantly increase the yields of carbonyls, specifically cyclopentenones, and aldehydes, and can also increase yields of hydrocarbons while reducing the yield of acids and phenols from poplar. [28] These metal oxides and other major ash-forming elements also affect the secondary conversions to form char at higher temperatures. [29]

The composition (mass fraction) of gumweed was determined by Reza et al. [30] to be 26% cellulose, 18% hemicellulose, 4% lignin, 44% extractives and 8% ash. The unique aspect of gumweed *'s* composition is the extractable hydrocarbons. This fraction of the biomass has generated interest because it has potential as a biofuel with minimal or no downstream processing. [6,4] as well as in the development of sustainable renewable polymers. The extractives of gumweed contain 10-14% extractable hydrocarbons that consist of 52 - 60% diterpene acid grindelic acid. [4,6] Additionally, there are 4.7% monoterpenes such as pinene, limonene, germacrene, elemene and camphene. [6] Work by Neupane et al. [6] showed that these hydrocarbons

can be isolated and upgraded to yield 9.1% bio-fuel that can be blended up to 20% with diesel before viscosity issues become apparent. A review paper by Wilbon et al. discusses the use of terpenes, terpenoids, and rosin as a source of renewable polymers. [13] A goal of the current work is to determine if pyrolysis is a suitable way to convert the whole plant, including the extractable hydrocarbons, into biocrude.

The pyrolysis of feedstocks with high levels of extractives has been shown to generate a two-phase bio-oil with an extractive rich phase that has a lower oxygen content, higher viscosity, and heating value. [31] Extractives are typically made of fatty acids, fatty alcohols, terpenes, resins, and acids which upon pyrolysis will generate a bio-oil with significant differences in oxygen content, polarity, and density as compared to the pyrolysis products of cellulose, hemicellulose and lignin.

The thermochemical conversion of these plants is a novel study that will add to the existing literature by evaluating the potential of these drought-tolerant plants for application as pyrolysis feedstocks. By giving detailed carbon yields on the char and vapors detected at 450-650°C using a tandem micro pyrolyzer GC-MS/FID/TCD the amount and quality of bio-oil, as well as non-condensable gases that are generated with these feedstocks, can be evaluated to determine unique trends and product slates. Ultimately, the goal is to determine if these drought-tolerant feedstocks and their unique cell wall architectures are suitable for fast pyrolysis to generate fuels and chemicals.

3.3 Materials and Methods

Opuntia ficus-indica (prickly pear) cladodes and *Grindelia squarrosa* (gumweed) were obtained from the University of Nevada's research greenhouses and field plots. An excellent study on the cultivation of gumweed is given by Neupane et al. [6] Before being sent to National Renewable Energy Laboratory (NREL), Colorado, USA, Prickly pear cladode samples were freeze-dried at room temperature for three days. Gumweed samples were air dried at ambient temperature for five to seven days. Both feedstocks were dried to be 7-10% moisture content and milled using a hammer mill with 1/8th-inch screen. *Pinus taeda* (loblolly pine) was used as a reference feedstock to compare yields and product molecules.

3.3.1 Biomass Characterization

Proximate and ultimate analyses were conducted to determine the cell wall composition of these feedstocks. Proximate analysis was run using the ASTM D5142 for moisture content (MC), volatile matter (VM), ash content, and fixed carbon (FC). The ultimate analysis was performed to determine the C, H, N, and O composition of the feedstocks.

3.3.2 Micro Pyrolyzer GC-MS/FID/TCD

The same tandem microreactor and calibration methods were used for this section as in Chapter 3. The first chamber was held at 450°C, 550°C or 650°C while the second chamber was held at 350°C

3.4 Results and Discussion

3.4.1 Biomass Characterization

The prickly pear and gumweed samples were characterized by proximate analysis, ultimate analysis and their heating values as indicated in Table 3.1. The proximate analysis showed the proportion of volatile matter (VM), fixed carbon (FC), and ash on a dry basis. The VM for prickly pear and gumweed were both lower than pine;[32] however, more of the organic material is volatilized as shown by the lower fixed carbon for prickly pear and gumweed. Kim et al.[33] reported the FC to be 18.9% and 22.9% for pectin-rich citrus peels and pure pectin, respectively. The main difference between these pectin feedstocks and prickly pear is the higher ash content in prickly pear. The alkali and alkaline earth metal salts present in the ash have been shown to increase the volatilization of FC[34] and are evident in the case of prickly pear where FC is only 4.0%. The high quantity of ash is an important characteristic of prickly pear and is believed to lead to the greater conversion of char and increased volatilization of organics at higher temperatures. Gumweed in the current study has 9.0% higher VM than what was reported by Reza et al.[30] who determined gumweed to have 74.4% VM. The ash in prickly pear and gumweed are significantly higher than pine. The ash content of prickly pear was close to the lower values compiled by Yang et al.[18] which ranged from 16.8% - 23.7%. Reza et al.[30] found the ash content of extracted gumweed to be 7.1 %, which is slightly higher than the current study.

Table 3.1. Proximate and ultimate analyses of prickly pear, gumweed, and pine

	Prickly pear	Gumweed	Pine [32]
Moisture (wt.% a.r.)[a]	7.2± 0.0	7.3 ± 0.1	
Higher heating value[b] (MJ kg^{-1})	14.6 - 15.3	18.6 - 17.7	19.8 – 19.4
Proximate analysis (wt.% d.b.)[b]			
VM	79.9 ± 1.7	83.7 ± 2.0	85.6
Fixed carbon	4.0 ± 1.6	9.6 ± 2.0	14.1
Ash	16.1 ± 0.1	6.7 ± 1.0	0.4
Ultimate analysis (wt.% d.b.)			
C	34.7 ± 0.3	44.9 ± 0.4	47.6
H	5.3 ± 0.1	6.5 ± 0.1	6.8
N	1.0 ± 0.0	1.2 ± 0.0	0.3
O (by difference)	42.9	40.7	44.9

[a] a.r.= as received. d.b.= dry basis.
[b]HHV is calculated using Equations 3.1 and 3.2.

The elemental compositions of carbon, hydrogen, nitrogen, and oxygen were determined through ultimate analysis. The amount of carbon in each sample was used to determine the carbon yield of pyrolysis vapors as previously described. Prickly pear had the lowest amount of carbon (34.7 ± 0.3%) followed by

gumweed (44.9 ± 0.4%) and pine (47.6%). Similarly, the hydrogen content follows the same trend prickly pear < gumweed < pine. These values are within the range of what has been previously reported. [18,30]

$$HHV\ \left(\frac{MJ}{kg}\right) = -1.3675 + 0.3137\ C + 0.7009\ H + 0.0318\ O \quad (3.1)$$

$$HHV\ \left(\frac{MJ}{kg}\right) = 26.601 - 0.304(A) - 0.082\ (VCM) \quad (3.2)$$

The higher heating value of prickly pear, gumweed and, pine was estimated using results of the ultimate analysis combined with Equation (3.1) [32] and another method based on the proximate analysis and Equation (3.2). [35] Due to the lower levels of carbon and hydrogen, the heating value for prickly pear (14.6 – 15.3 MJ kg^{-1}) and gumweed (18.6 - 17.7 MJ kg^{-1}) are less than pine (19.8 - 19.4 MJ kg^{-1}). The HHV as determined by Reza et al. [30] (18.4±0.4 MJ kg^{-1}) is close to the calculated values for gumweed.

3.4.2 Micro Pyrolyzer GC-MS/FID/TCD

PyGC-MS/FID/TCD analysis was carried out to identify and quantify the pyrolysis products of prickly pear and gumweed formed at 450-650°C. The identification of major compounds as well as the retention times, classifications and carbon yields at each temperature are shown in SI (Tables S5.1 and S5.2). There were clear differences depending on temperature and feedstock. Compounds were grouped into several classifications based on phase (liquid or gaseous) at standard temperature and pressure, as well as chemical structure (oxygenates, aromatics, hydrocarbons, extractives), and functional groups (carbonyls, phenols, acids, etc.). The yields of products in these categories are shown in Table 3.2.

Table 3.2. Carbon balance and product pools from pyrolysis of prickly pear, gumweed, and pine

	Prickly pear						Gumweed						Pine	
	450°C		550°C		650°C		450°C		550°C		650°C		550°C	
Non-condensable Gases (C %)	20.6	(2.3)	27.0	(3.4)	34.4	(2.1)	12.9	(1.2)	17.1	(0.7)	31.1	(1.3)	10.8	(2.8)
CO_2	19.6	(2.1)	24.1	(2.6)	25.7	(1.8)	11.9	(1.3)	14.4	(0.2)	17.2	(1.7)	8.4	(2.0)
CO	-		-		2.0	(0.1)	-	-	0.2	(0.2)	2.6	(0.2)	1.2	(0.5)
C_2-C_4	1.0	(0.1)	2.9	(0.8)	6.7	(0.5)	1.0	(0.1)	2.5	(0.4)	11.3	(0.4)	1.2	(0.2)
Condensable Vapors (C %)	17.4	(1.4)	19.2	(2.7)	28.4	(1.8)	35.0	(1.2)	32.4	(0.3)	30.5	(3.6)	24.2	(1.5)
Oxygenates	14.0	(1.2)	15.3	(2.2)	18.0	(0.5)	15.1	(0.7)	17.2	(2.2)	9.8	(1.1)	22.4	(1.7)
Carbonyl	7.3	(0.7)	7.0	(1.1)	5.4	(0.6)	4.2	(0.4)	5.6	(0.1)	2.0	(0.3)	3.8	(0.3)
Furan	3.2	(0.5)	4.7	(0.8)	5.2	(0.4)	1.6	(0.2)	0.8	(0.3)	2.2	(0.1)	4.0	(0.2)
Acid	0.9	(0.1)	0.9	(0.1)	1.4	(0.1)	3.2	(0.1)	3.4	(0.9)	2.0	(0.1)	3.4	(0.7)
Alcohol	0.6	(0.2)	-	-	-	-	-	(0.0)	0.3	(0.4)	-	-	1.9	(0.1)
Phenol	0.6	(0.1)	0.4	-	3.2	-	2.1	(0.5)	2.5	(0.6)	1.4	(0.4)	0.9	(0.3)
Methoxy Phenol	-	-	-	-	-	-	2.6	(0.5)	3.1	(0.5)	-	-	7.5	(1.1)

Aldehyde	1.5	(0.1)	2.4	(0.1)	2.7	(0.1)	0.9	(0.3)	1.4	(0.2)	2.0	(0.6)	0.7	(0.1)
Hydrocarbons	3.4	(0.2)	3.9	(0.6)	10.5	(1.3)	19.9	(0.3)	15.2	(0.7)	20.7	(1.8)	1.8	(0.3)
C_5-C_{10}	2.3	(0.1)	2.7	(0.4)	5.7	(0.5)	1.2	(0.3)	4.3	(0.6)	7.2	(0.8)	0.8	(0.1)
C_{11}-C_{15}	0.3	(0.1)	0.2	(0.1)	1.9	(0.2)	0.2	(0.2)	0.3	(0.1)	-	-	-	-
Aromatics	0.9	(0.1)	1.0	(0.3)	2.8	(0.5)	0.7	(0.1)	1.1	(0.1)	9.4	(1.0)	1.0	(0.3)
Extractives[1]	-	-	-	-	-	-	17.7	(0.2)	9.6	(3.2)	4.1	(0.8)	-	-
Total (C %)	36.0	-	46.3	-	62.8	-	47.9	-	49.3	-	61.6	-	34.9	-
Char (Wt %)	38.0	-	35.8	-	18.4	-	18.5	-	12.2	-	6.0	-	16.0	-

[1]Table S3.2 lists identified extractives.
Standard deviation is given in parenthesis.

3.4.3 Condensable vapors

The yield of GC detectable pyrolysis vapors are shown in Figure 3.1. All compounds presumed to be in the bio-oil fraction and measurable by chromatography are grouped into this category, including oxygenates, aromatics, C_5-C_{10} hydrocarbons and C_{11}-C_{15} hydrocarbons. Additionally, FID chromatograms are given in the SI. For prickly pear, the release of pyrolysis vapors was positively correlated with temperature and reached a maximum yield of 28.4% at 650°C. The yield of pyrolysis vapors for gumweed decreased with temperature and had a maximum value of 35.0% at a lower temperature of 450°C. The yield of condensable pyrolysis vapors for gumweed was higher than what was observed for prickly pear at all temperatures. The yield of pyrolysis vapors for the reference pine at 550°C was 24.2%. The correlation of temperature to the yield of pyrolysis vapors for the different feedstocks is caused by the unique characteristic of each plants cell wall. For prickly pear, partitioning to char drops off significantly at 650°C, along with a large increase in condensable vapors, and slight increase in non-condensable gases. Gumweed produces higher yields at lower temperatures because the extractives are easily volatilized at this temperature and do not need to undergo depolymerization or fragmentation to enter the gas phase. At higher temperatures the larger compounds are broken into small non-condensable gasses.

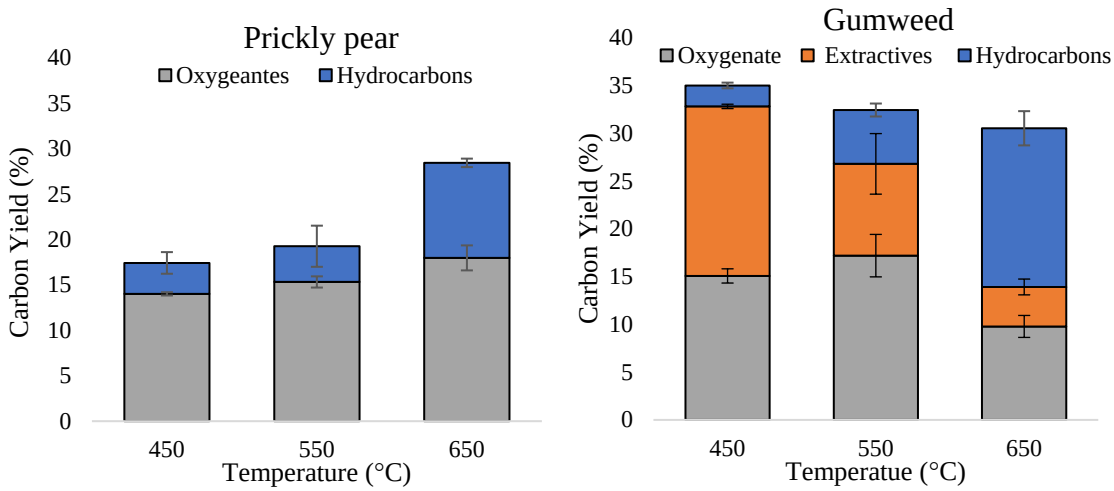

Figure 3.1. Carbon yield of GC detectable oxygenates and hydrocarbons in pyrolysis vapors

Pyrolysis of prickly pear at 650°C showed a much lower yield of char, and also produced higher yields of aromatics, C_5-C_{10} and C_{11}-C_{15} hydrocarbons. At 450°C and 550°C, the char yield is much higher and does not change as significantly, 38.0% to 35.8%, respectively. Kim et al. [33] showed that the char yield of pectin and citrus peels level off around 450°C and 35.0% and stays in this range even up to 700°C. In the current study, char yield drops significantly at 650°C to 18.4% as seen in Figure 3.2. The observed changes in product yields are due to improved heat transfer to biomass samples at high temperatures because the micropyrolyzer suffer from heat and mass transfer limitations especially at low temperatures as previously reported. [36]

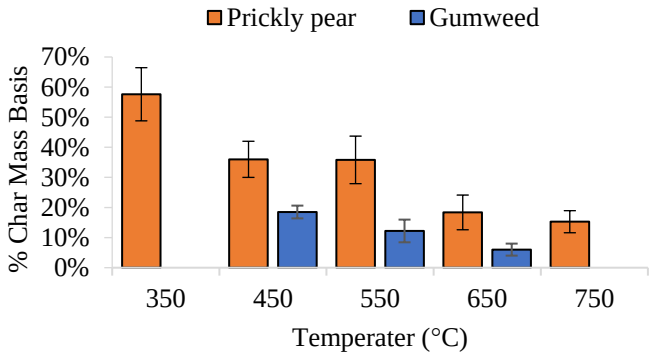

Figure 3.2. Char yields of prickly pear at 350°C - 750°C and gumweed 450°C -650°C

Pyrolysis of gumweed at 450°C showed that volatilization of extractives at this temperature gave the highest yield of condensable GC detectable compounds. At 450°C, the total carbon yield of condensable pyrolysis vapors was 35.0%, this value drops to 32.4% at 550°C and continues to decrease to 30.5% at

650°C. At 650°C the temperature is high enough to convert the extractives and other pyrolysis vapors into smaller, more volatile aromatics which show a large increase in yield between 550°C and 650°C. At 650°C the char yield was 6.0 wt% and although this is lower than the average ash value 6.7±1.0. it is still within the standard deviation.

An abundant group of products for both feedstocks was oxygenates. Oxygenates formed during the pyrolysis of prickly pear do not have a significant change in yield over this temperature range and increase from 14.0% at 450°C to 18.0% at 650°C. Gumweed generated a maximum yield of oxygenates at 550°C, 17.2%, with lower values of 15.1% at 450°C and 9.8% at 650°C. The yield of aromatics reaches a maximum at 650°C for both feedstocks. However, gumweed reaches 9.4% while prickly pear only achieves a 2.8% yield. Both feedstocks have a similar profile for the formation of C_5-C_{10} hydrocarbons, but prickly pear generates significantly more C_{11}-C_{15} hydrocarbons than gumweed at 650°C.

The total product yields from pyrolysis of these feedstocks are promising and surpass that of the biochemical routes used to date. Ethanol production from prickly pear is low <4.0% [1] while the GC detectable bio-oil yield can reach 28% when using pyrolysis. Acetone extraction of gumweed is a viable way to isolate the extractable hydrocarbons and can generate yields of around 12.5%. Pyrolysis of gumweed produced up to 20% hydrocarbons at elevated temperatures and 17.7% extractives at low temperature.

3.4.4 Oxygenates

Oxygenates are smaller, polar molecules, and can be categorized by the oxygen-containing functional groups such as carbonyl, furan, acid, phenol, alcohol, and methoxy phenol. By comparing the yields of these groups, it is possible to distinguish how the different cell wall structures of prickly pear and gumweed lead to the formation of unique product slates.

The yields of oxygenate sub-categories are shown in Figure 3.3. The yield of total oxygenates from prickly pear continues to increase with increasing temperature and can be attributed to the formation of new phenolic and acidic compounds as well as the continued increase of furan compounds and a stable formation of carbonyls. Oxygenates generated during pyrolysis of gumweed reach their maximum at 550°C. This is reflected by the yields of all oxygenates except furans and aldehydes which are higher at 650°C

Carbonyl compounds were the most abundant category for prickly pear and reach a maximum production of 7.3% at 450°C. The carbonyl fraction consisted of mostly acetone, butanones and cyclopentenones which are valuable products; however, aldehydes such as acetaldehyde, furfural, and 2-propenal were 1.5% at 450°C and increased at 650°C reaching 2.7%. These carbonyls can be produced by the decomposition of xylose [37] as well as pectin during pyrolysis. [24] The trend in carbonyl formation from gumweed is dependent on the yields of acetone, acetaldehyde, and 2-propanone-1-hydroxy. The total yield of all carbonyls at 450°C is 4.2%. Ketones, including 2-pentanone and 2-propanone-1-hydroxy, as well as other more complex carbonyls observed only at 550°C, increase the yield to 5.6% at 550°C. Acetone and

acetaldehyde continue to increase in yield at 650°C, but most other carbonyls are not present at this temperature, causing the overall yield to decrease to 2.0%.

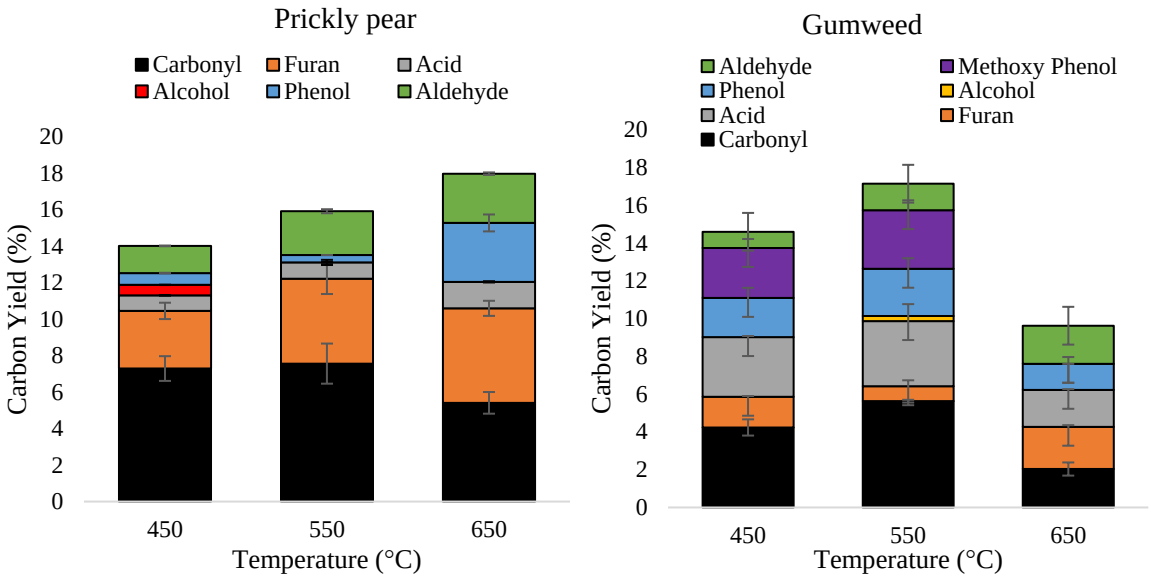

Figure 3.3. Carbon yield of GC detectable oxygenates

Phenolic compounds from prickly pear reached their maximum yield of 3.23% at 650°C. At low temperatures, only 4-methylphenol and 4-butyl phenol are generated in detectable amounts while at higher temperatures phenol, and various methyl phenol and ethylphenol compounds are formed. These can form through different reactions which include the breakdown of xylose and lignin. [38] The phenols from gumweed are mostly made of the pure phenol compound which was mainly formed at 450°C and 550°C. At 650°C 3-methylphenol, 2-5-dimethylphenol and 4-methylphenol were more abundant but a drop in pure phenol formation still lowered the total yield to 1.4%.

The acid fraction from prickly pear mostly contained acetic acid at lower temperatures. At 650°C, the acid fraction reached a maximum value of 1.4%. This trend is due to larger amounts of propanoic acid being present at 650°C. The acids from gumweed where most abundant at 550°C and followed the trend of 3.2% to 3.4% to 2.0%. This behavior was because butanoic acid is only formed at 450°C and 550°C and acetic acid, which is present at all temperatures, decreases significantly at 650°C.

The continued growth of furan compounds from prickly pear caused furans to reach their maximum yield of 5.2% at 650°C. The furans included the basic furan compound as well as more substituted compounds like 2-furancarboxaldehyde-5-methyl, and 2-5-dimethylfuran. These furans are likely from the breakdown of levoglucosan produced by the thermal decomposition of cellulose. [39]

The methoxy phenol compounds from gumweed are formed from the decomposition of lignin. [40] The total yield of methoxy phenols reached a maximum at 550°C of 3.1%. 2-Methoxy-4-vinyl phenol is the most abundant guaiacol derivative and 2-6-dimethoxyphenol is present from the syringyl type lignin. [40]

3.4.5 Hydrocarbons

The hydrocarbons are larger, less polar molecules, and can be categorized as aromatics, C_5-C_{10} hydrocarbons, C_{11}-C_{20} hydrocarbons, and extractives. Yields of hydrocarbons are shown in Figure 3.4. The total yield of hydrocarbons from prickly pear increased with temperature and had the largest total yield at 650°C equal to 10.5%. The extractives produced from gumweed give the hydrocarbons a unique trend, having similar total yields at 450°C and 650°C but at lower temperatures, the extractives are the dominant molecules while at higher temperatures aromatics and C_5-C_{10} hydrocarbons are the most abundant.

Aromatic compounds and C_5-C_{10} hydrocarbons showed the greatest increase in yield between 550°C and 650°C. For prickly pear, this is caused by the more abundant formation of 2-ring aromatics like indene, 1-methyl-1H-indene and 1-ring aromatics such as 1-3-dimethylbenzene at 650°C. At lower temperatures, compounds like benzene, toluene, and ethylbenzene are formed and increase exponentially with temperature and also contribute to the higher yield of aromatics at 650°C. For gumweed, the large increase in the yield of aromatics at 650°C is caused by the formation of 1-ring aromatics such as benzene, p-xylene and, 1-2-3-dimethylbenzene as well as the formation of 2-ring aromatics such as, 2-methylnaphthalene and 2,7-dimethyl naphthalene which are not observed at a lower temperature.

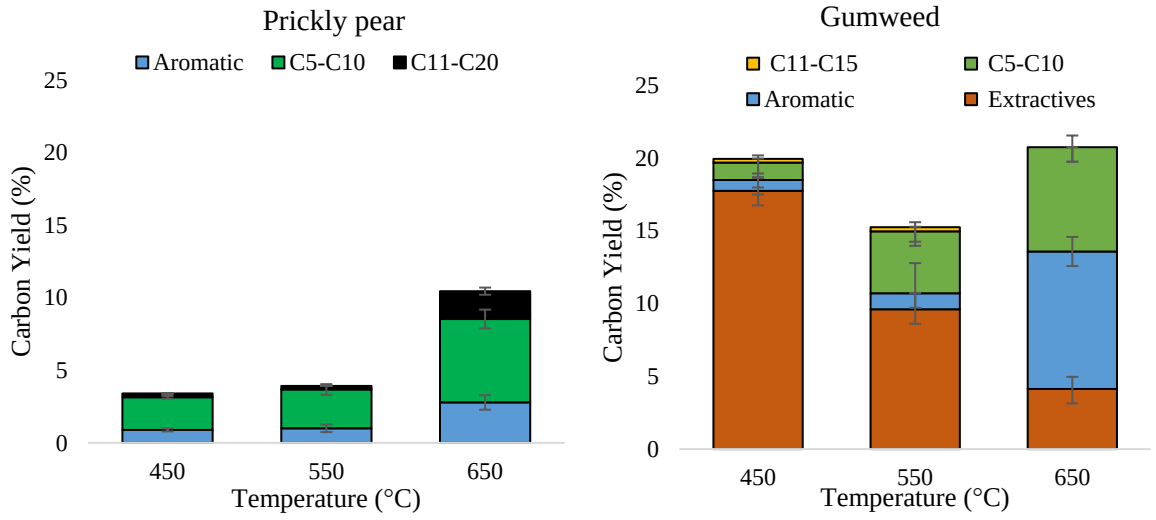

Figure 3.4. Carbon yield of GC detectable hydrocarbons

The increase in yield for the C_5-C_{10} hydrocarbons for prickly pear is due to the continued growth of cyclic alkenes such as 1-3-cyclopentadiene and 1-cyclopentadiene-1-methyl. Formation of longer straight chain alkenes such as 1-heptene and 1-pentene at these higher temperatures was also observed in

small quantities. Similarly, gumweed produced cyclic alkenes typically consisting of 5 carbon rings such as 1-3-Cyclopentadiene-1-methyl. Alkenes of varying length and substituent carbons such as 1-4-Pentadiene, and 2-Pentene-4-methyl were observed as well.

C_{11}-C_{20} hydrocarbons have a very low 0.3% yield for prickly pear and slightly increases to 1.9% at 650°C. This shift is largely due to the presence of decene compounds like 1-pentadecene. The GC-MS/FID/TCD also detected 1-undecene, 1-tridecene, and 1-tetradecene at higher yields for 650°C than for 550°C. The yield of C_{11}-C_{20} hydrocarbons for gumweed is exceedingly low. The hydrocarbon product trends shown for prickly pear are due to improved heat transfer at higher temperatures, leading to increased yields of hydrocarbons. The trends observed for gumweed are due to cracking of vapors from extractives at high temperatures to form aromatics and C_5-C_{10} species.

3.4.6 Non-Condensable Gases

The non-condensable gases included CO_2, CO, and C_2-C_4 hydrocarbons, these are shown in Figure 3.5. These compounds continued to become more prevalent with increasing temperature for both feedstocks. At 650°C when the highest yield of pyrolysis vapors was obtained for prickly pear the non-condensable gases had a 34.4% yield. The non-condensable gases made up a large fraction of the carbon yield even at lower temperatures where the yield was 20.6% even at 450°C. Gumweed produces lower levels of non-condensable gases at all temperatures ranging from 12.9% at 450°C to 31.1% at 650°C.

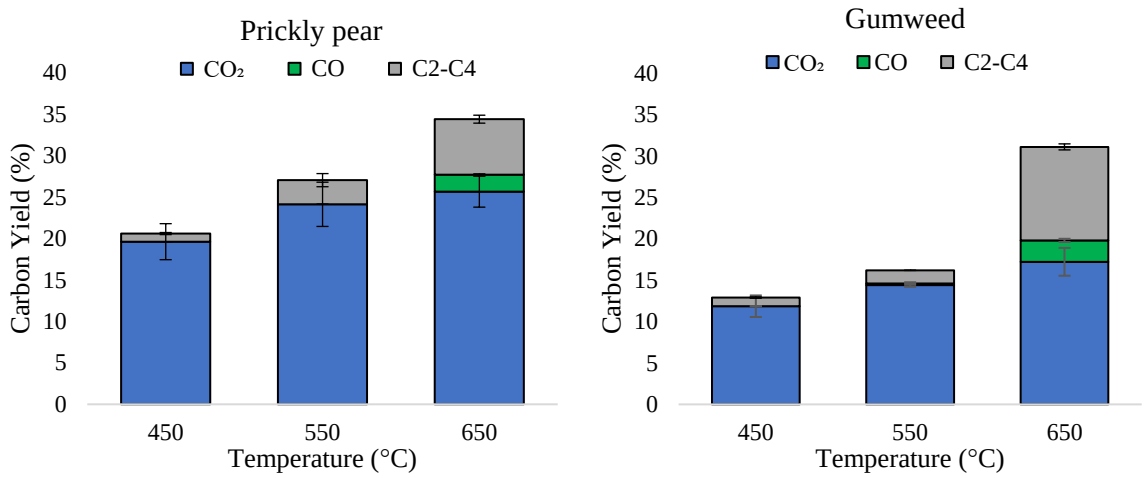

Figure 3.5. The yield of GC detectable non-condensable gases

CO_2 is the dominant product in this category. The simplest mechanism that forms CO_2 is decomposition of carboxyl groups of pectin in prickly pear and carbonyl groups of hemicellulose within the cell wall of both feedstocks. Other routes of forming CO_2 at elevated temperatures are through C-C and C-O scission.[39] More complex routes of forming CO_2 include decarboxylation of β-keto acids which could potentially form after homolytic cleavage of the glycosidic bond and rearrangement if carboxyl groups are

not converted to CO_2 before the glycosidic bond is broken. CO is much less prevalent and is not formed below 550°C but increases significantly between 550°C and 650°C. One reason for the low levels of CO could be the lower levels of cellulose in these feedstocks. [41] The lighter hydrocarbons are predominantly made up of ethene, propene, and 1-propene-2-methyl and increase exponentially with temperature.

3.5 Conclusions

The pyrolysis of drought-tolerant prickly pear and gumweed was conducted on a tandem micro pyrolyzer with GC-MS/FID/TCD to determine if the unique cell wall components of these crops can produce valuable fuels and chemicals from pyrolysis. Additionally, pyrolysis was conducted between 450°C and 650°C to evaluate changes in the product slate with temperature. Prickly pear generated the largest amounts of valuable carbonyls at 450°C (7.3%) along with lower levels of deleterious aldehydes (1.5%) and acids (0.9%). At higher temperatures of 650°C prickly pear generated higher levels of furans (5.2%), aromatics (2.8%) and C_5-C_{10} hydrocarbons (5.7%) and reached the highest yield of pyrolysis vapors 28.4%. Gumweed was able to produce up to 9.4% aromatics and 7.2% C_5-C_{10} hydrocarbons at 650°C giving a total yield of pyrolysis vapors of 30.5%. Interestingly at lower temperatures (450°C), gumweed produced 17.7% of extractives which are larger (C_{20}) compounds that have usually only a single oxygen atom. Based on these results, it is determined that prickly pear is a valuable feedstock based on its potential to produce higher yields of valuable carbonyl chemicals at low temperatures and shift the product pool to favor hydrocarbons at higher temperatures. Gumweed has significant potential because of the high yield of extractives and hydrocarbons. The aromatics and hydrocarbons could be used for drop-in fuel blendstocks. The oxygenates could either by upgraded using hydrotreating to produce hydrocarbon fuels or they could be used as value-added products that could improve the economics of the biorefinery. For instance, the phenols and furans could be used as precursors for preparing polymers, such as polycarbonates or phenol/formaldehyde resins. Future work should include TG and DGTA studies to understand more about the thermochemistry of these substrates and catalytic upgrading schemes to further increase the value of these feedstocks.

References

1. Cushman, J.; Davis, S.; Yang, X.; Borland, A. Development and use of bioenergy feedstocks for semi-arid. *Journal of Experimental Botany* doi:10.1093/jxb/erv087.

2. Yang, X. A roadmap for research on crassulacean acid metabolism (CAM) to enhance sustainable food and bioenergy production in a hotter, drier world. *New Phytologist* **2015,** *207,* 491-504.

3. Mason, M.; Glover, K.; Smith, A.; Willis, K.; Woods, J.; Thompson, I. The potential of CAM crops as a globally significant bioenergy resource: moving from 'fuel or food' to 'fuel and more food'. *energy Environ. Sci.* **2015**.

4. McLaughlin, S.; Kingsolver, B.; Hoffman, J. Biocrude Production in Arid Lands. *Economic Botany* **1983,** 150-158.

5. Hoffmann, J.; McLaughlin, S. Grindelia camporum: Potential Cash Crop for the Arid Southwest. *Economic Botany* **1986,** 162-169.

6. Neupane, B.; Shintani, D.; Lin, H.; Coronella, C.; Miller, G. Grindelia squarrosa: A Potential Arid Lands Biofuel Plant. *ACS Sustainable Chem. Eng.* **2017,** 995−1001.

7. Kuloyo, O. Ethanol production by yeast fermentation of Opuntia ficus-indica biomass hydrolysate. *University of Free State* **2012**.

8. Retamal, N.; Duran, J.; Fernandez, J. Ethanol production by fermentation of fruits and cladodes of prickly pear cactus (Opuntia ficus-indica (L.) Miller). *Journal of the science of Food and Agriculture* **1987,** *40,* 213-218.

9. Bridgwater, A.; Meier, D.; Radlein, D. An overview of fast pyrolysis of biomass. *Organic Geochemistry* **1999,** 1479-1493.

10. Golden, J.; Handfield, R.; Daystar, J.; McConnell, T. An Economic Impact Analysis of the U.S. Biobased Products Industry: A Report to the Congress of the United States of America. A Joint Publication of the Duke Center for Sustainability & Commerce and the Supply Chain Resource Cooperative at North Carolina. **2015**.

11. Iisa, K.; Robichaud, D.; Watson, M.; Dam, J.; Dutta, A.; Mukarakate, C.; Kim, S.; Nimlos, M.; Baldwin, R. Improving biomass pyrolysis economics by integrating vapor and liquid phase upgrading. *Green chemistry* **2017,** 10.1039/C7GC02947K.

12. Vispute, T.; Zhang, H.; Sanna, A.; Xiao, R.; Huber, G. Renewable chemical commodity feedstocks from integrated catalytic processing of pyrolysis oils. *Science* **2010,** *330,* 1222-1227.

13. Wilbon, P.; Chu, F.; Tang, C. Progress in renewable polymers from natural terpenes, terpenoids, and rosin. *Macromolecular Rapid Communications* **2012,** *34,* 8-37.

14. Xiu, S.; Shahbazi, A. Bio-oil production and upgrading research: Areview. *Renewable and Sustainable Energy Reviews* **2012,** 4406-4414.

15. Butler, E.; Devlin, G.; Meier, D.; McDonnell, K. A review of recent laboratory research and commercial developments in fast pyrolysis and upgrading. *Renewable and Sustainable Energy Reviews* **2011,** *4186* (15), 4171.

16. Howe, T.; Westover, D.; Carpenter, D.; Santosa, D.; Emerson, R.; Deutch; Starace, A.; Kutnyakov, I.; Lukins, C. Field to Fuel Performance Testing of Lignocellulosic Feedstocks: An Integrated Study of the Fast Pyrolysis-Hydrotreating Pathway. *Energy Fuels* **2015,** 3188-3197.

17. Elkasabi, A.; Mullen, C.; Pighinelli, A.; Boateng, A. Hydrodeoxygenation of fast-pyrolysis bio-oils from various feedstocks using carbon-supported catalysts. *Fuel Processing Technology* **2014,** *123*, 11–18.

18. Yang, L.; Lu, M.; Carl, S.; Mayer, J.; Cushman, J.; Tian, E.; Lin, H. Biomass characterization of Agave and Opuntia as potential biofuel feedstocks. *Biomass and Bioenergy* **2015,** 43-53.

19. Mciteka, H. Fermentation characteristics and nutritional value of Opuntia ficus-indica var. fusicaulis cladode silage. *University of Free State* **2008**.

20. Ginestra, G.; Parker, M.; Bennett, R.; Robertson, J.; Mandalari, G.; Narbad, A. Anatomical, chemical, and biochemical characterization of cladodes from prickly pear [Opuntia ficus-indica (L.) Mill]. *J. Agr. Food Chem.* **2009,** 10323-10330.

21. Contreras-Padilla, M.; Rivera-Munoz, E.; Gutierrez-Cortez, E.; Lopez, A.; Rodriguez-Garcia, M. Characterization of crystalline structures in Opunita ficus-indica. *J Biol Phys* **2015,** *41*, 99-112.

22. Ca´rdenas, A.; Goycoolea, F.; Rinaudo, M. On the gelling behavior of 'nopal' (Opuntia ficus indica) low methoxyl pectin. *Carbohydrate Polymers* **2008,** *73*, 212-222.

23. Grant, T.; Morris, R.; Rees, A.; Smith, C.; Thom, D. Biological interactions between polysaccharides and divalent cations: The egg-box model. *FEBS Letters* **1973,** *32*, 195-198.

24. Ge, S.; Xu, Y.; Tian, Z.; She, S.; Huang, L.; Zhang, Z.; Hu, Y.; Weng, J.; Cao, M.; Sheng, L. Pyrolysis study of pectin by tunable synchrotron vacuum ultraviolet photoionization mass spectrometry. *J. Them. Anal. Calorim* **2015,** 1399-1405.

25. Aburto, J.; Moran, M.; Galano, A.; Torres-Garcia, E. Non-isothermal pyrolysis of pectin: A thermochemical and kinetic approach. *Journal of Analytical and Applied Pyrolysis* **2015,** 94-104.

26. Kim, Y.-M.; Jaw, J.; Lee, H.; Han, T.; Lee, H.; Park, S.; Kim, S.; Watanabe, C.; Park, Y.-K. Ex-situ catalytic pyrolysis of citrus fruit peels over mesoporous MFI and AL-MCM-41. *Energy Conversion and Management* **2016,** 277-289.

27. Ohhishi, A.; Takagi, E.; Kato, K. Thermal decomposition of pectic substances. *Carbohydr Res* **1978,** 281-288.

28. Lu, Q.; Zhang, Z.; Dong, C.; Zhu, X. Catalytic Upgrading of Biomass Fast Pyrolysis Vapors with Nano Metal Oxides: An Analytical Py-GC/MS Study. *Energies* **2010,** *11*, 1805-1820.

29. Bridgewater, A. Review of fast pyrolysis of biomass and product upgrading. *Biomass and Bioenergy* **2012,** *38*, 68-94.

30. Reza, M.; Yang, X.; Coronella, C.; Lin, H.; Hathwaik, U.; Shintani, D.; Neupane, B.; Miller, G. Hydrothermal Carbonization (HTC) and Pelletization of Two Arid Land Plants Bagasse for energy Densification. *ACS Sustainable Chem. Eng.* **2016,** 1106-1114.

31. Oasmaa, A.; Kuoppala, E.; Gust, S.; Solantausta, Y. Fast Pyrolysis of Forestry Residue. 1. Effect of Extractives on Phase Separation of Pyrolysis Liquids. *Energy & Fuels* **2003,** *17*.

32. Sheng, C.; Azevedo, J. Estimating the higher heating value of biomass fuels from basic analysis data. *Biomass and Bioenergy* **2005,** *28,* 449-507.

33. Kim, Y.-M.; Lee, H.; Kim, S.; Watanabe, C.; Park, Y.-K. Non-isothermal pyrolysis of citrus unshiu peel. *Bioenerg. Res* **2015,** 431-439.

34. Darvell, L.; Hrycko, P.; Jones, J.; Nowakowski, D.; Pourkashanian, M.; Williams, A. Impact of minerals and alkali metals on willow combustion properties. *World Renewable Energy Congress* **2005,** 584-589.

35. Capareda, S. *Introduction to Biomass Energy Conversions;* CRC Press: Boca Raton, 2012.

36. Proano-Aviles, J.; Lindstrom, J.; Johnston, P.; Brown, R. Heat and Mass Transfer Effects in a Furnace-Based Micropyrolyzer. *Energy Technol* **2017,** *5,* 189-185.

37. Stefanidis, S.; Kalogiannis, K.; Iliopoulou, E.; Michailof, C.; Pilavachi, P.; Lappas, A. A study of lignocellulosic biomass pyrolysis via the pyrolysis of cellulose, hemicellulose, and lignin. *Journal of Analytical and Applied Pyrolysis* **2014,** 143-150.

38. Lv, G.; Wu, S. Analytical pyrolysis studies of corn stalk and its three main components by TG-MS and Py-GC/MS. *Journal of Analytical and Applied Pyrolysis* **2012,** *97,* 11-19.

39. Patwardhan, P. Understanding the product distribution from biomass fast pyrolysis. In *Doctoral Dissertation;* Iowa State University: Ames, Iowa, 2010.

40. Liu, Q.; Wang, S.; Zheng, Y.; Luo, Z.; Cen, K. Mechanism study of wood lignin pyrolysis by using TG–FTIR analysis. *J. Anal. Appl. Pyrolysis* **2008,** *82,* 170-177.

41. Yang, H.; Yan, R.; Chen, H.; Lee, D.; Zheng, C. Characteristics of hemicellulose, cellulose and lignin pyrolysis. *Fuel* **2007,** *86,* 1781-1788.

Chapter 4 Catalytic fast pyrolysis of drought-tolerant biomass: Optimal catalyst configuration and evaluation of deactivation patterns

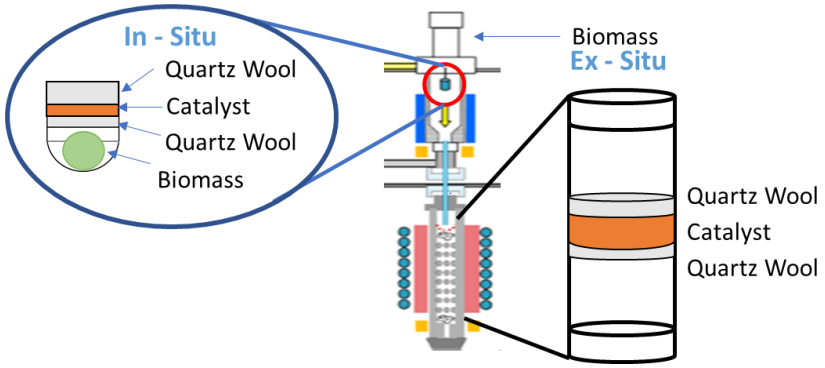

4.1 Abstract

Opuntia ficus-indica (prickly pear) and *Grindelia squarrosa* (gumweed) are two types of biomass that possess unique cell wall architectures tailored for prolific growth in arid and semi-arid climates. The adaptation of these plants to harsh climes has generated cell wall architectures composed of complex matrices that hold different compositions of lignocellulosic biopolymers (cellulose, hemicellulose, and lignin) while additionally utilizing alternative carbohydrates and resins to thrive in these climates. Most notably these plants have developed much lower levels of lignin. This characteristic alone can lead to improved zeolite lifetime and limit the deactivation of zeolites through coke forming lignin condensation reactions. Additionally, the unique carbohydrates and resins have been found to be more efficiently converted to hydrocarbons and generate their own slate of oxygenates not yet observed in the catalytic fast pyrolysis of biomass. Prickly pear holds higher levels of pectin carbohydrates, as well as alkali and alkaline earth metal salts that have proven to shift the products to favor more volatilization of organic compounds and generate unique and valuable, oxygenates such as cyclopentanones. Gumweed forms a resin on the plants surface that contains larger monomeric compounds including terpenes and terpenoids as well as diterpenes. The CFP of these compounds was found to produce higher yields of aromatics than the cell wall of pine, switchgrass or corn Stover. These compounds also generate their own slate of unique oxygenates not yet observed in catalytic fast pyrolysis.

Using a tandem micro pyrolyzer with GCMS-FID-TCD, a detailed account of the product slate is given for products obtained from in-situ and ex-situ catalytic fast pyrolysis with ZSM-5 at 550°C. Additionally, the deactivation of the zeolite catalyst during ex-situ pyrolysis was studied. Pyrolysis of prickly pear with in-situ HZSM-5 resulted in 17.3% aromatics, 11.9% alkenes, gumweed produced 28.8% aromatics and 12.4% alkene. Ex-situ catalytic fast pyrolysis of prickly pear resulted in 8.4% aromatics, 14.8% alkenes at a catalyst to biomass ratio of 10:1. After catalyst deactivation experiments the aromatic yield was 3.9%, the alkenes were 10.1% at a catalyst to biomass ratio of 1:2. Ex-situ catalytic fast pyrolysis of gumweed resulted in 14.8% aromatics, 32.5% alkenes and after catalyst deactivation experiments the aromatic yield was 3.6%, the alkenes were 13.1%.

4.2 Introduction

The production of renewable fuels and chemicals from biomass is a key part of the U.S. strategy for reducing dependence on imported petroleum, improving air quality, and supporting rural economies. The large-scale use of non-food biomass as a source of renewable carbon for fuels and chemicals will require the development of dedicated feedstocks co-optimized for growth and efficient conversion (high carbon and hydrogen retention, low catalyst deactivation). The benefits of drought-tolerant plants as feedstocks for biofuels and biochemicals have been identified by other groups [1,2] who stressed that increasing global temperature, drought, and soil-drying conditions caused by global warming will increase competition for agricultural freshwater and cultivated soils. Expanding available biomass resources to include plants with exceptional drought tolerance complements traditional lignocellulosic resources and has the advantage of lower water requirements and the use of arid and semi-arid lands, potentially opening up large areas of the western U.S. to biofuel and biochemical production. The use of marginal lands with low water availability will be a crucial component to the success and ecological sustainability of a future Bioeconomy.

These drought-tolerant feedstocks were previously studied using non-catalytic pyrolysis [3] and showed that the high levels of ash in prickly pear increase the amount of organics volatilized and shifted product pools making it possible to generate up to 7.3% carbonyls and 10.5% hydrocarbons depending on reactions conditions. Pyrolysis of gumweed showed that the extractives were volatilized at low temperatures and led to 17.7% grindelic acid and mono-terpenoids derivatives in the condensed vapor phase. At high temperatures, the extractives and other biomass components are converted to aromatics and C_5-C_{10} hydrocarbons giving a total yield of 16.6% and also generates large amounts of C_2-C_4 hydrocarbons, 11.3%. These feedstocks also produced high levels of CO_2, 24.1% from prickly pear and 14.4% from gumweed. Additionally, low yields of lignin derivatives were observed for these feedstocks. Parascanu et

al. [4] performed slow pyrolysis of prickly pear and gasification of the resulting char. Similar results were observed in regard to higher char and CO_2 yields.

Vapor phase upgrading of biomass pyrolysis compounds using zeolite catalyst has been shown to be an effective method of reducing the oxygen content of the pyrolysis vapors and generating hydrocarbons and valuable chemicals. [5, 6] Zeolites, most notably ZSM-5 deoxygenate pyrolysis vapors through dehydration, decarbonylation, and decarboxylation. [7] The formation of aromatics and olefins with ZSM-5 is through two competing catalytic cycles. The olefins cycles consist of methylation and cracking reactions to produce olefins that are C3+ in length and the aromatics cycle consist of methylation and dealkylation of polymethylbenzenes to form aromatics and C2 olefins. [8] The critical technical issues with ZSM-5 catalyst is the low yield and deactivation through coke formation. [9] The yield of pyrolysis oil and the amount of coke deposition can be improved by altering the catalyst through impregnation with various metals, changing the acidity of the catalyst by altering the silicon to aluminum ration (SAR), changing the pore size and structure and shifting catalyst placement of in-situ or ex-situ. [10] The lifetime and productivity of ZSM-5 catalyst is also determined by pyrolysis vapor composition which depends on the feedstock used, the temperature of pyrolysis and residence time of pyrolysis vapors. [3, 11] The current model that is used to predict the behavior of ZSM-5 is the hydrogen to carbon effective ration (H/C_{eff}). This ratio has been shown to predict the yields of aromatics, olefins and coke for ZSM-5 CFP. [12] The model is based on the theory that ZSM-5 utilizes a hydrocarbon pool to generate products and depending on the amount of available hydrogen the products shift from olefins to aromatics to coke as the amount of hydrogen decreases. [12] The non-catalytic pyrolysis of prickly pear and gumweed generated vapors with higher H/C_{eff} values of 0.9 for prickly pear and 1.0 for gumweed compared to 0.78 for pine. [3]

Catalyst place is an important parameter that can shift the amount of condensable vapors, deoxygenation of pyrolysis vapors and formation of hydrocarbons. [13, 14] The in-situ configuration places the catalyst in the same apparatus as the biomass while ex-situ configurations will use a separate reactor to house the catalyst. The main differences of in-situ vs ex-situ CFP is the temperature of the catalyst and the vapor residence time. In-situ CFP has a lower catalyst temperature as the biomass/catalyst mixture ramps from room temperature and also has a longer vapor residence time as the vapors pass directly over the catalyst bed and are not diluted by the He carrier gas. Wang et al. used a micro scale Py-GCMS reactor and found the lower temperature and longer residence time leads to more aromatics (26.1% vs 18.9%) in the product stream for in-situ CFP while ex-situ produces more olefins (17.4% vs 5.4%). [13] Iisa et al. determined the organic liquid carbon yield to be slightly higher with in-situ catalyst, 25% compared with 21% for ex-sit for a bench scale reactor with pine. [14]

Producing a desirable product slate in combination with catalyst longevity are the main hurdles to progressing this technology. Ex-situ catalyst deactivation studies using microscale Py-GCMS reactors are

a valuable tool to understand how the product slate shifts while the ZSM-5 catalyst deactivates. [15] Deactivation studies have found the yields of furans, phenols and cresols to peak when the catalyst is partially deactivated [10, 16, 9] for pine feedstocks where lignin derivatives are abundant. Phenols and cresols are valuable products (phenol \$1–2 kg^{-1} and p-cresol \$2–3 kg^{-1}) [17] and in this regard a partially deactivated catalyst is beneficial. However, continued coke formation leads to a decreased yield of these valuable intermediates as well as other hydrocarbons. Coke yields typically range from 10-20 wt% of biomass. [7] Wang et al. [13] found the coke mass yield from hybrid poplar to be 18.6% when using a microscale reactor. Iisa et al. [14] determined the coke yield of pine to be 7.9% for a larger bench scale reactor with pine feedstock. Higher coke yields in PyGC reactors is attributed to the slower heat transfer rates. [18] Other factors that influence coke formation are lignin condensation reactions, [19] co-reactants such as O_2, CO, and CO_2 [20] and H/C_{eff} ratio. [12] Prickly pear and gumweed are unique feedstocks in that they have low lignin levels, and produce higher amounts of CO_2 and the approximated H/C_{eff} value is higher than that of pine. Coke yields are determined by analyzing the mass loss of the catalyst as the coke is oxidized after pyrolysis experiments are complete. ZSM-5 coke has been broadly categorized as soft coke, which will desorb between 200-400°C and has of an effect on catalyst activity and selectivity. Hard coke desorbs above 400°C and is more detrimental to catalyst performance. Hard coke requires combustion with oxygen to be fully removed which can also deactivate the catalyst during regeneration. [21]

The objective of the current work is to evaluate vapor phase upgrading of prickly pear and gumweed pyrolysis vapors using a tandem microreactor with ZSM-5 (SAR 30). A comparison of in-situ and ex-situ catalyst placements is conducted to understand how differences in catalyst temperature and vapor residence/contact time effect product yields. Additionally, the tandem microreactor used in this work allows for an ex-situ catalyst deactivation study where a 1:2 catalyst to biomass weight ratio can be achieved to understand the sequential shift in products and the overall coke formation.

4.3 Materials and Methods

4.3.1 Feedstock and Catalyst

Opuntia ficus-indica (prickly pear) cladodes and *Grindelia squarrosa* (gumweed) were grown at the University of Nevada's research greenhouses and field plots. Cultivation, preprocessing (drying and milling), and characterization (proximate and ultimate analysis) of these feedstocks can be found in previous publications by Neupane et al. [22] and Cross et al. [3] In short, both feedstocks were dried to be 7-10% moisture content and milled using a hammer mill with 1/8th inch screen. *Pinus taeda* (loblolly pine) was used as a reference feedstock to compare yields and product molecules produced from in-situ ZSM-5. The ZSM-5 zeolite catalyst was obtained from Nexceris and had a particle size of 300-500 μm, the silica-to-alumina ratio (SAR) of 30 and used Al_2O_3 (boehmite, 10 wt. % binder) as a binder.

4.3.2 Micro Pyrolyzer GC-MS/FID/TCD

The same tandem microreactor and calibration methods were used for this section as in Chapter 3. The first chamber was held at 550°C and the second chamber was held at 500°C

4.3.3 Experimental Procedure

In-situ catalytic fast pyrolysis experiments were replicated three times, biomass samples of 0.5 mg were mixed with 5mg of HZSM-5 and loaded into small deactivated stainless-steel cups and charged into the 1st pyrolysis chamber maintained at a set point of 550°C. During ex-situ catalytic fast pyrolysis experiments, 5mg HZSM-5 was loaded into the 2nd reactor chamber and maintained at 550°C, then 0.5mg of biomass were charged into the 1st reactor chamber and the vapors were passed over the catalyst bed in the 2nd chamber. Once pyrolysis was completed the cups were ejected from the 1st reactor and another biomass sample was injected. This was repeated 20 times until the catalyst to biomass ratio was 1:2 (C1: B2).

4.4 Results and Discussion

The effect of ZSM-5 catalyst placement on the pyrolysis vapors produced from prickly pear and gumweed were evaluated in this work. Additionally, the deactivation process was studied for these feedstocks and evaluated changes in the product slates as well as coke analysis with TGA. A comparison of fresh in-situ and ex-situ catalyst and non-catalytic pyrolysis vapors are presented in Table 4.1. Here, the total amount of detected vapors is given as both carbon yield and total FID area, these values are also given for total oxygenates, hydrocarbons, C2-C4 gases, CO and CO_2. The composition of GC detectable vapors was much higher in aromatics and olefins with the ZSM-5 catalyst when compared to the non-catalytic experiments at 550°C reported previously. The ZSM-5 catalyst efficiently deoxygenated the pyrolysis vapors in this study and is believed to have done so primarily through dehydration reactions and the formation of H_2O. [6] The use of ZSM-5 catalyst also increased the yields of CO through decarbonylation reactions which effectively reduced the levels of carbonyl oxygenates. Interestingly, CO_2 yields showed little change between catalytic and non-catalytic experiments for these drought-tolerant feedstocks. These drought-tolerant feedstocks produced significant amounts of CO_2 from non-catalytic pyrolysis and suggest that most carboxyl groups are thermally decomposed which was supported by the low level of these compounds in non-catalytic pyrolysis. H_2O was not accounted for in this study, however, it is well documented that vapor upgrading with ZSM-5 rejects oxygen from biomass pyrolysis vapors through the formation of reaction water. [23]

Table 4.1. Carbon yield and FID area (10^6) for prickly pear, gumweed and pine for the different catalyst placements, in-situ and ex-situ and non-catalytic pyrolysis1

.	Prickly pear			Gumweed			Pine	
	In-situ	Ex-situ	Non-catalytic	In-situ	Ex-situ	Non-catalytic	In-situ	Non-catalytic
CO_2	24.2	21.4	24.1	14.3	15.1	14.4	8.8	8.4
CO	2.0	1.2	-	1.9	2.1	0.2	4.7	1.2
Gasses	12.2	10.2	2.9	13.8	16.2	2.4	9.1	1.2
Oxygenates	2.4	8.6	15.3	-	9.5	17.2	4.2	22.4
Hydrocarbons	17.5	16.7	3.9	31.6	30.9	15.2	28.0	1.8
Total C %	58.4	58.2	46.3	61.5	73.8	49.3	54.7	34.9
CO_2 (MS)	107.5	98.6	107.2	89.3	92.8	90.0	70.1	69.3
CO (TCD)	26.2	20.3	5.2	29.2	31.4	13.3	61.4	24.0
Gasses[2]	323.1	255.4	75.6	442.6	542.9	56.3	318.0	49.0
Oxygenates	24.9	109.7	123.0	-	181.6	167.8	37.4	329.7
Hydrocarbons	352.1	312.9	40.1	848.9	876.8	65.3	787.9	39.7
Total FID area 10^{6*}	699.9	678.0	351.1	1,291.5	1,601.3	677.5	1,143.3	418.4

[1]non-catalytic pyrolysis data taken from Cross et al. [3]
[2]Gasses include C_2-C_4 hydrocarbons
[*]CO_2 and CO are calculated from MS and TCD area, respectively
In situ vs Ex Situ Catalyst Placement

The effect of in-situ catalyst placement was compared to ex-situ placement for these drought-tolerant feedstocks. The catalyst to biomass ratio was 10:1 (5mg catalyst, 0.5mg biomass) and the reaction temperature was 550°C. A comparison with pine using in situ catalyst placement is also given to serve as a reference. The total yield of detectable pyrolysis vapors can be broken down into two categories condensable vapors and non-condensable gases. Condensable vapors included oxygenates and hydrocarbons that are large enough to condense as STP. Non-condensable gasses included CO, CO2 and C2-C4 hydrocarbons. Zeolite catalyst typically result in low yields of condensable vapors. [6] Yields for condensable vapors and non-condensable gasses were similar for both drought tolerant feedstocks, however, GC-MS-FID is limited in its ability to generate high carbon balances for biomass pyrolysis. Prickly pear generated a carbon yield of 19.9 - 25.3% (in-situ vs ex-situ) GC detectable condensable vapors and 38.4 - 32.8% non-condensable gases. Gumweed generated a carbon yield of 31.6% - 40.4% GC detectable condensable vapors and 30.0% - 33.4% non-condensable gases. Gamliel et. al., [24] found switchgrass to produce lower amounts of non-condensable gases and higher amounts of liquids for an in-situ catalyst which is not observed for these drought-tolerant feedstocks. This inconsistency could be caused by the lower total carbon yield for in-situ catalyst caused by the limitation of GC to produce high carbon balances or it may also be due to higher coke yields on in-situ catalyst leading to the lower total carbon yields. [24]

The distribution of specific aromatics and olefins can be seen in Figure 4.1 and illustrates the effect of catalyst placement on individual product pools for these drought-tolerant feedstocks. The identified

aromatics and olefins match well with the calibration compounds used and therefore results are given as carbon yield. Aromatics and light olefins are the largest product pools for both feedstocks but catalyst placement shifts the selectivity of these product pools. In situ catalyst generates the highest yields of aromatics regardless of feedstock. The carbon yield of aromatics was 17.3% for prickly pear, 30.3% for gumweed and 27.4% for pine. The most abundant 1-ring aromatics included toluene, xylene, and benzene. Gamliel et al. [24] found the yields of toluene (4 C%) and xylene (4 C%) were the highest for the 1-ring aromatics for in situ CFP of switchgrass. Similar results were determined in this report for pine, 4.6% toluene and 4.6% xylenes. Gumweed produced over 6% for toluene, 4.5% xylene and 3.0% benzene. Prickly pear produced 4.4% toluene and less than 3% benzene and xylene. Polymethyl aromatics and alkyl aromatics were also observed for these feedstocks. Polymethylbenzenes were in similar abundance for the three feedstocks (2.3%-2.9%) however polymethylnaphthalenes and were higher with gumweed (6.7%). Larger polycyclic aromatics (PCA) including polymethyl anthracenes, polymethyl phenanthrene, and polymethyl fluorene were present for pine with a combined carbon yield of 3.2%. It is thought that the polymerization of pyrolysis vapors to larger polycyclic aromatics leads to coke formation. [9] This polymerization is clearly observed for pine but the larger PCA compounds were less abundant for drought-tolerant feedstocks, 0.1% for prickly pear and 0.9% for gumweed with in-situ configuration. The ex-situ catalyst configuration leads to a more homogeneous temperature and longer contact/residence time shifting the yields of aromatics and olefins. [13] With these factors the growth of aromatics is not as prominent and the total yields reach 11.9% for prickly pear, and 23.4% for gumweed. Interestingly, alkylbenzenes such as benzene-(1-methyl-1-butenyl) have a higher yield with ex-situ catalyst. With this configuration 7.3% alkylbenzenes were produced from gumweed making them the second most abundant class of aromatics considering both configurations. For prickly pear, alkylbenzenes are 2.1% which is similar to the yields of toluene and naphthalene’s.

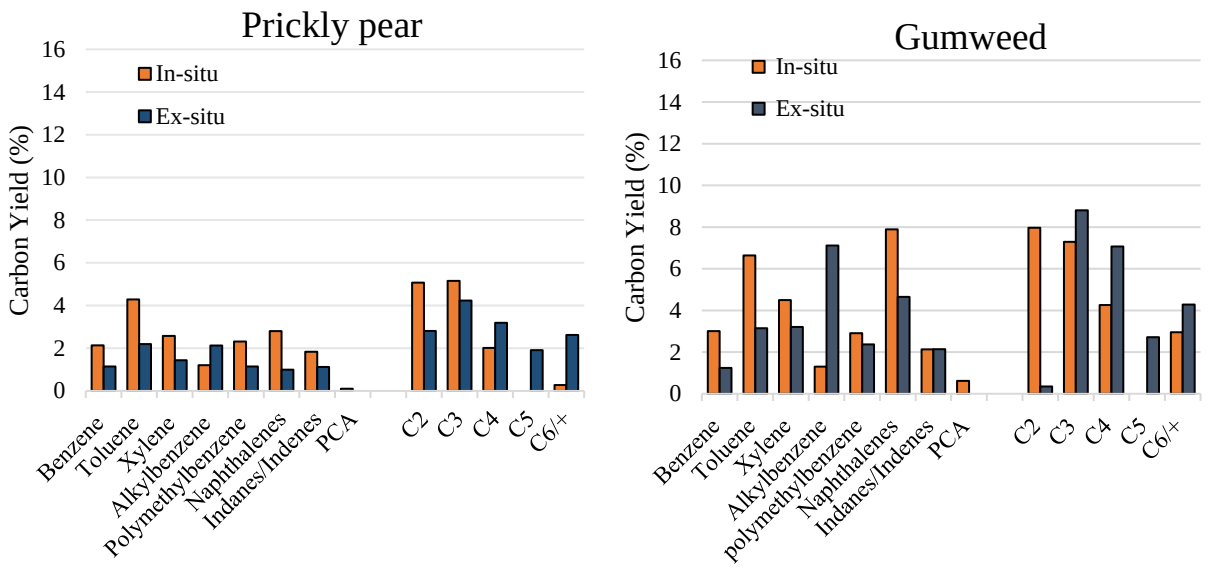

Figure 4.1. Total carbon yields of GC detectable hydrocarbons for prickly pear, gumweed and pine.

Ex situ catalyst generated more olefins (C2-C4 and C5-C6+) where total carbon yields were 14.7% for prickly pear, and 23.2% for gumweed. This increase in olefins is from a higher abundance of branched olefins such as 2-Butene-2-methyl compared to straight olefins like 1-butene and ethene which have similar carbon yields for in-situ and ex-situ. Additionally, cyclic alkenes have a higher carbon yield for ex-situ catalyst placement. Wang et al. [13] found the olefins to be 7.7% with hybrid poplar and ex-situ catalyst and the selectivity of olefins to favor C2 and C3 formation. For prickly pear, C4 (3.2%) and C3 (4.2%) straight chain olefins were the most abundant while gumweed produced large amounts of C3 (8.8%) and C4 (7.1%) and although the yields of C5 (2.7%) and C6 (2.3%) were lower they are still relatively high. The findings that these drought-tolerant feedstocks produce higher levels of C5+ olefins are significant. There were elevated amounts of these larger olefins in the non-catalyzed pyrolysis vapors which may be shifting the products pools of ZSM-5. Ilias et al. [25] found that co-feeding propene with dimethyl ether over ZSM-5 can increase the propagation of the olefins cycle while co-feeding toluene can increase the aromatics-cycle. This may have been caused by the different H/C_{eff} value for propene (2.0) and toluene (1.1). Zhang et al. [12] found that increasing H/C_{eff} will increase the ratio of olefins to aromatics. Using the supplementary information from a previous publication the H/C_{eff} values of the non-catalytic pyrolysis vapors were estimated to be 0.9 for prickly pear, 1.0 for gumweed and 0.78 for Pinus. This is one possible explanation for the higher C5+ olefins yield for these feedstocks.

The carbon yields and FID area (10^6) of detectable oxygenates are shown in Table 4.2. The total yield of oxygenates was dependent on catalyst placement and feedstock with prickly pear generating carbon yields of 2.4% oxygenates with in situ catalyst and pine generated 4.2%. Interestingly, a very low yield of

oxygenates (>1.0%) was observed from gumweed with the in-situ catalyst which suggests that smaller oxygenates were converted to hydrocarbons and oxygen was rejected through the formation of non-condensable gases and the larger oxygenates were converted to coke or condensed inside the reactor. Only carbonyls which included acetone and acetaldehyde were detected for in situ catalyst placement with prickly pear. Pine also generated these carbonyls but additionally, furans and methoxy phenols were detected. The higher abundance of cellulose and lignin in pine leads to higher yields of furans and methoxyphenols and the inhomogeneous catalyst temperature may prevent these small oxygenates from being completely deoxygenated. [14] Carbon yields of oxygenates with ex situ catalyst were higher than in situ and were 8.6% for prickly pear and 9.5% with gumweed. Higher yields of oxygenates with ex-situ catalyst has been observed by Wan et. al. [13] Oxygenates from prickly pear with ex-situ catalyst were acetone and acetaldehyde, similar to in-situ, but also showed furans acids and alcohols. Aldehydes, acids, and ketones are common oxygenates see in product streams from ZSM-5. [13] Similarly, oxygenates from gumweed included acetone, acetaldehydes and furans plus a mixture of oxygenated benzene and naphthalene like compounds with alcohol and carbonyl functional groups. These are believed to be produced from the terpenoids and diterpenoids present in gumweed. The lower residence/contact time may have led to the formation of these compounds while with the in-situ configuration they are converted to either smaller hydrocarbons or coke.

Table 4.2. Carbon yield and FID area (10^6) of total oxygenates and product pools for prickly pear, gumweed and pine for the different catalyst placements, in-situ and ex-situ and non-catalytic pyrolysis[1]

	Prickly pear			Gumweed			Pine	
	In-situ	Ex-situ	Non-catalytic	In-situ	Ex-situ	Non-catalytic	In-situ	Non-catalytic
Oxygenates (C%)	2.4	10.0	15.3	>1.0	9.5	25.7	4.2	22.4
Carbonyl	2.4	5.9	7.6	*	4.6	5.6	1.3	3.8
Furan	-	0.9	4.7	-	1.4	0.8	2.5	4.0
Methoxyphenol	-	-	-	*	-	3.1	0.4	7.5
Acid	-	0.8	0.9	-	-	2.8	-	3.4
Phenol	-	-	0.4	-	-	2.5	-	0.9
Alcohol	-	0.7	-	-	1.2	0.5	-	1.9
Oxygenates (FID 10^6)	24.9	109.7	149.1	>10.0	181.6	366.1	37.4	329.7
Carbonyl	24.9	68.2	61.6	*	93.5	90.8	29.0	82.3
Furan	-	8.8	26.6	-	44.2	6.7	7.4	36.0
Methoxy/phenol	-	-	-	*	-	34.4	1.0	127.4
Acid	-	8.1	11.9	-	-	59.7	-	50.8
Phenol			1.3	-	-	26.1	-	14.7
Alcohol	-	2.9	-	-	15.0	2.7	-	18.5

[1]non-catalytic pyrolysis data taken from Cross et al. [3]

* These compounds are seen in MS, however, FID areas were not detected.

4.4.1 Ex Situ Catalyst Deactivation

The deactivation of ex-situ catalyst was also studied for these drought-tolerant feedstocks. ZSM-5 was placed in the second reaction chamber and 20 biomass samples were sequentially pyrolyzed and the upgraded vapors analyzed with the GC-MS-FID-TCD system. Each pyrolysis run is referred to by the catalyst to biomass weight ratio, C1: B0.1 being the first sample and C1: B2 being the last. Deactivation was interpreted as a decrease in overall yield indicating that the catalyst is not as active and cannot convert pyrolysis vapors into smaller GC detectable compounds. [9, 10, 16] Deactivation is also represented by a decrease in hydrocarbon yields with an accompanying increase in oxygenates, signaling that the dehydration, decarboxylation, decarbonylation, cracking, oligomerization, and aromatization reactions that convert oxygenates into hydrocarbons are not as prevalent. [16, 9]

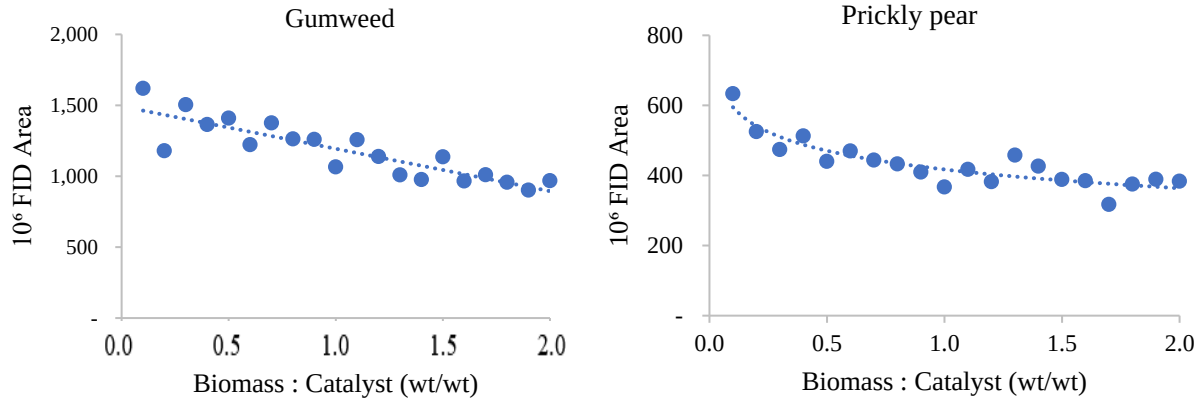

Figure 4.2. FID integration areas for gumweed and prickly pear during ex-situ catalyst deactivation of ZSM-5 (SAR-30). Final catalyst to biomass ratio was 1:2 after 20 sequential pulses of 0.5mg biomass over 5mg of catalyst.

Deactivation of the ex-situ ZSM-5 resulted in lower FID area counts Figure 4.2, and total carbon yields of GC detectable compounds. The effect of 20 biomass pulses on ZSM-5 activity can be seen in the carbon yield for prickly pear which dropped from 62.3% at C1: B0.1 to 41.0% at C1: B2. The deactivated ZSM-5 resulted in a similar total carbon yield compared with the non-catalytic pyrolysis (46.3%) for prickly pear. Although the total carbon yields from prickly pear for the deactivated ZSM-5 vapors and non-catalytic vapors may be similar the distribution of product pools is different. C_2-C_8 hydrocarbons are still far more prevalent with the deactivated ZSM-5 at 12.1% (Figure 4.3) while non-catalytic pyrolysis generated 5.6%. The amount of GC detectable oxygenates was 6.6% with the deactivated catalyst compared to 15.3% for non-catalytic pyrolysis and showed higher yields of phenols (1.1%) and alcohols (1.4%). For gumweed, the total carbon yields varied from 73.8% at C1: B0.1 to 58.6% at C1: B2. At 20 biomass pulses, gumweed still generates a higher total yield of GC detectable compounds compared with the non-catalytic pyrolysis.

Like prickly pear, gumweed also produces much higher yields of C_2-C_{10} hydrocarbons (13.1%) with the deactivated ZSM-5 compared with non-catalytic pyrolysis. The extractives and oxygenates from gumweed returned to 26.2% compared with 27.0%.

The first 5 biomass pulses result in the most rapid deactivation of ZSM-5 for the prickly pear feedstock. The aromatic hydrocarbons and smaller, straight olefins including ethene, propene, and butene show the largest decrease in yield during these initial biomass pulses. With the ex-situ catalyst placement, the formation of these compounds is already less prominent, and the rapid deactivation illustrates the challenges with producing these compounds. However, deactivation is less apparent for the remaining biomass pulses and the yield of single ring aromatics such as alkylbenzenes and polymethyl benzene appear to stabilize. Additionally, methylated olefins such as 2-pentene-3-methyl and cyclic-alkenes like 1,3-cyclohexadiene show little decrease in carbon yield. Polycyclic aromatics including polymethylnaphthalenes are significantly affected however and may not be generated at higher levels of ZSM-5 deactivations. The oxygenates reflect the stabilization of the 1-ring aromatics and larger olefins and do not return to the levels of non-catalytic pyrolysis. Acetic acid levels stay constant throughout the experiments, acetaldehyde is trending upwards at a slow rate, furan is also constant while furan-2-methyl increase very slightly. 2-Cyclopenten-1-one was observed in the non-catalytic pyrolysis vapors and breaks through early in the deactivation process, however other carbonyls such as butanone that was observed for non-catalytic pyrolysis were not detected after 20 biomass pulses indicating the ZSM-5 is still partially active. Phenol is also observed from when the catalyst is partially deactivated and is first seen at a catalyst to biomass ratio of 1:1.4. The decarbonylation reactions are confirmed by the elevated CO levels while the CO_2 levels are similar to the non-catalytic pyrolysis signaling that thermal decarboxylation is prominent for prickly pear.

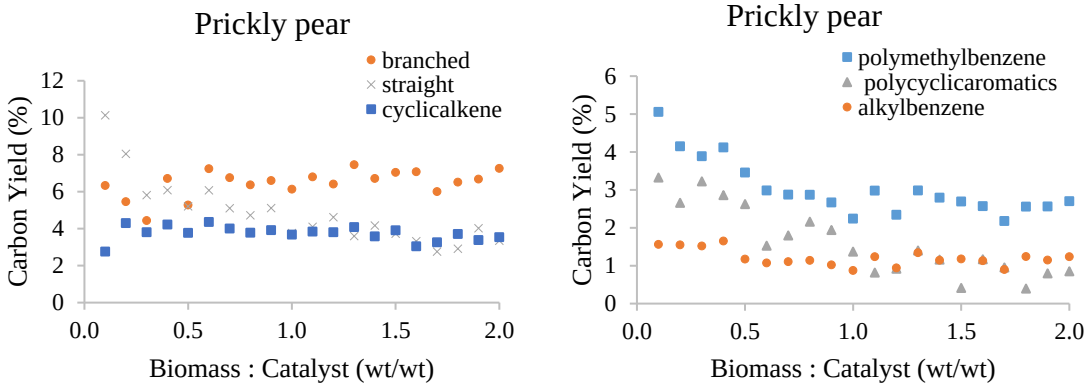

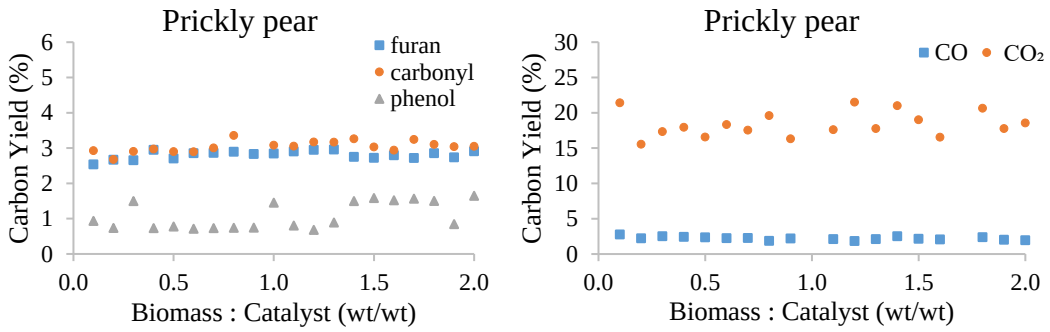

Figure 4.3. Carbon yield of major compounds and compound groupings for prickly pear with 5mg ex-situ ZSM-5 (SAR 30) catalyst deactivated over 20, 0.5mg, biomass pulses.

Ex-situ upgrading of the gumweed pyrolysis vapors generates a large amount of GC detectable compounds with the total FID area more than doubling that of prickly pear. Many of the hydrocarbons and smaller oxygenates can be appropriately matched to one of the calibration compounds and therefore carbon yields can be determined. However, over the course of the ZSM-5 deactivation, many oxygenated species with multiple functional groups and larger C10+ structures were observed. Calibration compounds were initially used to calculate an estimated total carbon yield but the total FID area for these compounds is also given to show how their abundance correlates with the catalyst deactivation (Figure 4.4). These compounds are believed to be derived from the diterpenoids present in the resin of gumweed.[26] Grindelic acid is most abundant of these compounds in the resin however it is not observed in the pyrolysis vapors. For the first biomass pulse, the most abundant of these compounds is 3,3,5,6-tetramethyl-1-indanone. The methylated carbon ring and carbonyl structure are present in many of the other complex vapors. The original structures of gumweed resin identified by Bohlmann et al.[26] contain some alkyl substituents and carbonyl functional groups, however, none were observed to have polymethylation. These palymitoylated compounds are observed throughout all 20 biomass pulses. Other common structures observed that are unique to this feedstock are multi carbon ring compounds with amine and pyridine groups.

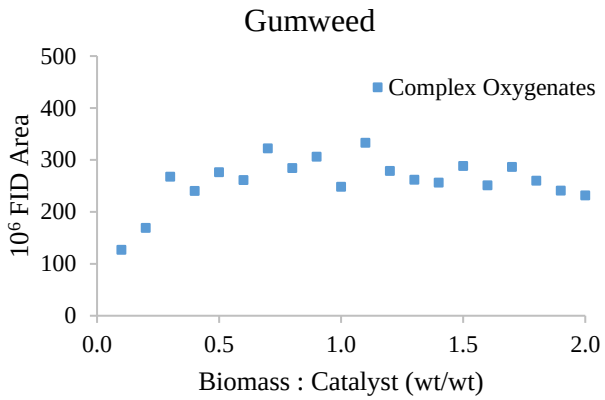

Figure 4.4. FID area counts for complex oxygenates from gumweed with 5mg ex-situ ZSM-5 (SAR 30) catalyst during deactivation over 20, 0.5mg, biomass pulses.

The hydrocarbon species that were most abundant with the fresh ex-situ catalyst are the most affected by the ZSM-5 deactivation. These included smaller straight olefins and polymethylbenzenes as well as toluene and xylene. Most of these compounds showed rapid deactivation after the first biomass pulse. However, by the 5th biomass pulse, these compounds were in similar abundance to other hydrocarbons and their carbon yields decreased at a similar rate. The smaller oxygenates consisted of mostly carbonyl compounds like acetone and acetaldehyde. Once the catalyst is partially deactivated other ketone compounds like 1-butanone are observed. The total yield of carbonyls does not return to the same level as the non-catalytic pyrolysis and this is reflected in the elevated CO levels throughout the deactivation experiments.

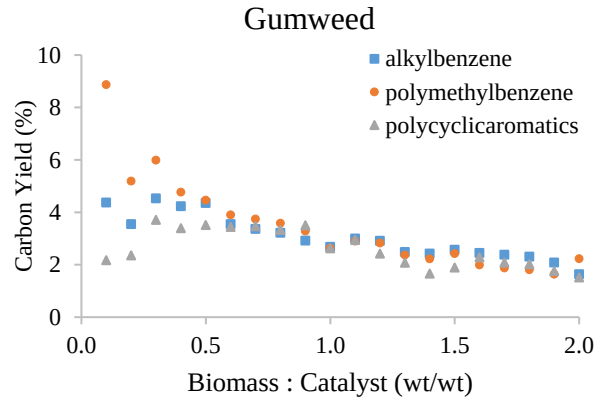

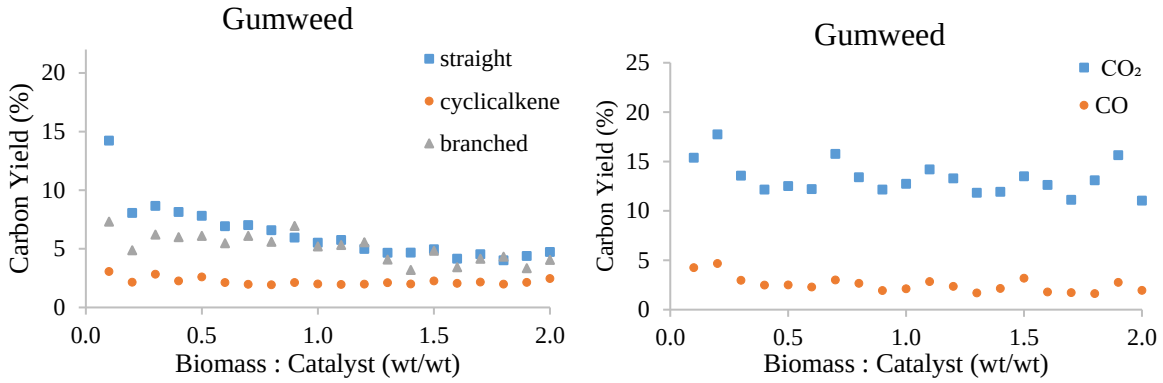

Figure 4.5. Carbon yield of major compounds and compound groupings for gumweed with 5mg ex-situ ZSM-5 (SAR 30) catalyst deactivation over 20, 0.5mg, biomass pulses.

4.4.2 Thermogravimetric Analysis Catalyst Coke

The amount of coke on the deactivated ex situ ZSM-5 catalysts was determined by TGA (Figure 4.6). The total weight loss amounted to 7.1% for both prickly pear and gumweed. The coke burn off data for the deactivated ZSM 5 catalyst are very similar during the low-temperature region (20-150 °C) where 3.1% mass loss occurs. The weight loss in this range is due to desorption of water within the zeolite pores. Within the temperatures range of 150 - 250°C the mass loss is due to additional water loss as well as light organic species sometimes referred to as soft coke.[7] The mass loss in this region is greater for prickly pear which was 2.2% compared with 1.9% for gumweed suggesting that more soft coke was formed. Above 250°C and continuing up to the final temperature of 780°C is where most of the carbonaceous coke or hard coke is removed.[7] It was observed that there is a greater mass loss in this region for the gumweed, 2.1%, compared with 1.9% from prickly pear indicating that more hard coke was formed from these vapors.

Mukarakate et al.[9] showed that the coke from pine started to burn off at 250°C, based on this the total mass fraction of coke was 18%. There are several factors contributing to the lower coke yields of these drought-tolerant feedstocks. The high levels of CO_2 in the non-catalytic pyrolysis vapors may be helping to remove coke by converting it to CO.[20] Another contributing factor is the higher H/C_{eff} for the identified pyrolysis vapors of prickly pear and gumweed.[12]

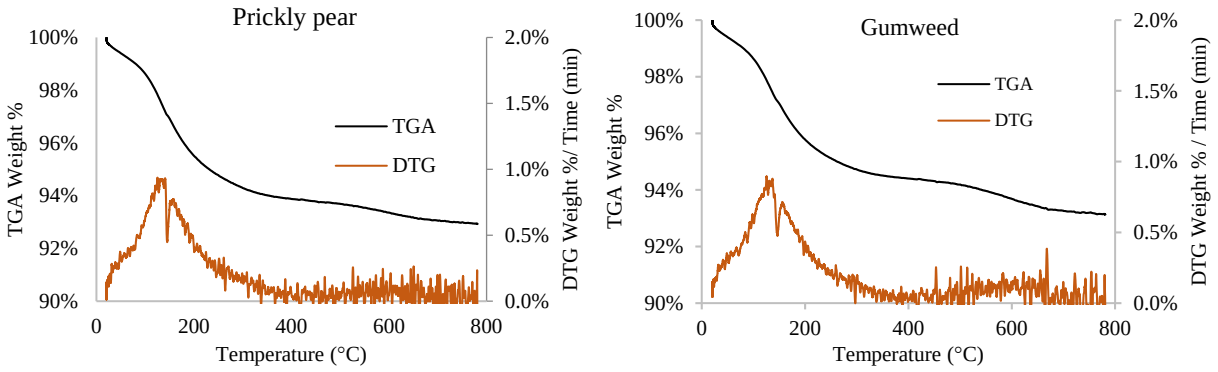

Figure 4.6. TGA coke analysis for ex-situ ZSM-5 (SAR 30) at 1:2 catalyst to biomass weight ratio.

4.5 Conclusion

The objective of the current work was to evaluate vapor phase upgrading of *Opuntia ficus-indica* (prickly pear) cladodes and *Grindelia squarrosa* (gumweed) pyrolysis vapors using a tandem microreactor with ZSM-5 (SAR 30). Pyrolysis vapors from prickly pear were effectively deoxygenated and converted to aromatics and olefins with slightly lower yields than that of pine. The higher H/C_{eff} values lead to lower yields of aromatics even for the in-situ configuration and therefore ex-situ catalyst used to produce larger C3+ olefins is recommended. The ex-situ deactivation and coke formation were observed to be less severe for prickly pear than other feedstocks and is attributed to the higher H/C_{eff} values and elevated CO_2 yields of non-catalytic pyrolysis vapors. Gumweed produced high levels of aromatics, moistly naphthalene's and toluene with in-situ catalyst placement. Ex-situ catalyst can be used to produce high levels of olefins and potentially valuable oxygenates such as 3,3,5,6-tetramethyl-1-indanone. Ex-situ deactivation showed that these oxygenates can be produced even at a catalyst to biomass ratio of 1:2 while yields of light olefins and aromatics decreased.

References

1. Cushman, J.; Davis, S.; Yang, X.; Borland, A. Development and use of bioenergy feedstocks for semi-arid. *Journal of Experimental Botany* doi:10.1093/jxb/erv087.

2. Yang, X. A roadmap for research on crassulacean acid metabolism (CAM) to enhance sustainable food and bioenergy production in a hotter, drier world. *New Phytologist* **2015,** *207,* 491-504.

3. Cross, P.; Mukarakate, C.; Nimlos, M.; Carpenter, D.; Donohoe, B.; Mayer, J.; Cushman, J.; Neupane, B.; Miller, G.; Adhikari, S. Fast pyrolysis of Opuntia ficus-indica (prickly pear) and Grindelia squarrosa (gumweed). *Energy & Fuels* **2018,** DOI: 10.1021/acs.energyfuels.7b03752.

4. Parascanu, M.; Sandoval-Salas, F.; Soreanu, G.; Valverde, J.; Sanchez-Silva, L. Valorization of Mexican biomass through pyrolysis, combustion and gasification processes. *Renewable and Sustainable Energy Reviews* **2017,** *71,* 509-522.

5. Mortensen, P.; Grunwaldt, J.; Jensen, P.; Kundsen, K.; Jensen, A. A review of catalytic upgrading of bio-oil to engine fuels. *Applied Catalyst A: General* **2011,** *407,* 1-19.

6. Dickerson, T.; Soria, J. Catalytic Fast Pyrolysis: A Review. *Energies* **2013,** *6,* 514-538.

7. Mukarakate, C.; Zhang, X.; Stanton, A.; Robichaud, D.; Ciesielski, P.; Malhotra, K.; Donohoe, B.; Gjersing, E.; Evans, R.; Heroux, D.; Richards, R.; Iisa, K.; Nimlos, M. Real-time monitoring of the deactivation of HZSM-5 during upgrading of pine pyrolysis vapors. *Green Chem.* **2013,** DOI: 10.1039/c3gc42065e.

8. Bjorgen, M.; Svelle, S.; Joensen, F.; Nerlov, J.; Kolboe, S.; Bonino, F.; Palumbo, L.; Bordiga, S.; Olsbye, U. Conversion of methanol to hydrocarbons over zeolite H-ZSM-5: on the origin of the olefins species. *J. Catal.* **2007,** *249,* 195-207.

9. Mukarakate, C.; Zhang; Stanton, A.; Robichaud, D.; Ciesielski, P.; Malhotra, K.; Donohoe, B.; Gjersing, E.; Evans, R.; Heroux, D.; Richards, R.; Iisa, K.; Nimlos, M. Real-time monitoring of the deactivation of HZSM-5 during upgrading of pine pyrolysis vapors. *Green Chemistry* **2013,** DOI: 10.1039/c3gc42065e.

10. Xu, M.; Mukarakate, C.; Robichaud, D.; Nimlos, M.; Richards, R.; Trewyn, B. Elucidating Zeolite Deactivation Mechanisms During Biomass Catalytic Fast Pyrolysis from Model Reactions and Zeolite Syntheses. *Top Catal* **2015,** DOI 10.1007/s11244-DOI 10.1015-0507-5.

11. Howe, T.; Westover, D.; Carpenter, D.; Santosa, D.; Emerson, R.; Deutch, R.; Starace, A.; Kutnyakov, L.; Lukins, C. Field to fuel performance testing of lignocellulosic feedstocks: an integrated study of the fast pyrolysis-hydrotreating pathway. *Energy Fuels* **2015,** 3188-3197.

12. Zhang, H.; Cheng, Y.; Vispute, T.; Xiao, R.; Huber, G. Catalytic conversion of biomass-derived feedstocks into olefins and aromatics with ZSM-5: the hydrogen to carbon effective ratio. *Energy Environ. Sci* **2011,** 2297–2307.

13. Wang, K.; Johnston, P.; Brown, R. Comparison of in-situ and ex-situ catalytic pyrolysis in a micro-reactor system. *Bioresource Technology* **2014,** *173,* 124-131.

14. Iisa , K.; French, R.; Orton, K.; Yung, M.; Johnson, D.; Dam, J.; Watson, M.; Nimlos, M. In situ and ex-situ catalytic pyrolysis of pine in a bench-scale fluidized bed reactor system. *Energy Fuels* **2016,** *30,* 2144-2157.

15. Wan, S.; Waters, C.; Stevens, A.; Gumidyala, A.; Jentoft, R.; Lobban, L.; Resasco, D.; Mallinson, R.; Crossley, S. Decoupling HZSM-5 catalyst activity from deactivation during upgrading of pyrolysis oil vapors. *ChemSusChem* **2015,** *8,* 552-559.

16. Xu, M.; Mukarakate, C.; Iisa, K.; Budhi, S.; Menart, M.; Davidson, M.; Robichaud, D.; Nimlos, M.; Trewyn, B.; Richards, R. Deactivation of Multilayered MFI Nanosheet Zelote during Upgrading of Biomass Pyrolysis Vapors. *ACS Sustainable Chem. Eng* **2017,** *5,* 5477-5484.

17. Iisa, K.; Robichaud, D.; Watson, M.; Dam, J.; Dutta, A.; Mukarakate, C.; Kim, S.; Nimlos, M.; Baldwin, R. Improving biomass pyrolysis economics by integrating vapor and liquid phase upgrading. *Green chemistry* **2017,** 10.1039/C7GC02947K.

18. Torri, C.; Reinikainen, M.; Lindfors, C.; Fabbri, D.; Oasmaa, A.; Kuoppala, E. Investigation on catalytic pyrolysis of pine sawdust: catalyst screening by Py-GC-MIP-AED`. *J. Anal. Appl. Pyrolysis* **2010,** *88,* 7-13.

19. Mengze, X.; Mukarakate, C.; Robichaud, D.; Nimlos, M.; Richards, R.; Trewyn, B. Elucidating zeolite deactivation mechanisms during biomass catalytic fast pyrolysis from model reactions and zeolite syntheses. *Top Catal* **2016,** *59,* 73-85.

20. Liu, Z.; Nutt, M.; Iglesia, E. The effects of CO2, CO and H2 co-reactants on methane reactions catalyzed by Mo/H-ZSM-5. *Catalysis Letters* **2002,** *81,* 271-279.

21. Gou, M.; Cai, J.; Song, W.; Liu, Z.; Ren, Y.; Pan, B.; Niu, Q. Coking and deactivation behavior of ZSM-5 during the isomerization of styrene oxide to phenylacetaldehyde. *Catalyst Communications* **2017,** *98,* 116-120.

22. Neupane, B.; Shintani, D.; Lin, H.; Coronella, C.; Miller, G. Grindelia squarrosa: A Potential Arid Lands Biofuel Plant. *ACS Sustainable Chem. Eng.* **2017,** 995−1001.

23. Nguyen, S.; Zabeti, M.; Lefferts, L.; Brem, G.; Seshan, K. Catalytic upgrading of biomass pyrolysis vapors using faujasite zeolite catalyst. *Biomass and Bioenergy* **2013,** *48,* 100-110.

24. Gamliel, D.; Du, S.; Bollas, G.; Valla, J. Investigation of in situ and ex-situ catalytic pyrolysis of miscanthus x giganteus using PyGC-MS microsystem and comparison with a bench-scale spouted reactor. *Bioresource Technology* **2015,** *191,* 187-196.

25. Ilias, S.; Aditya, B. Tuning the selectivity of methanol-to-hydrocarbons conversion on H-ZSM-5 by co-processing olefins or aromatic compounds. *Journal of Catalysis* **2012,** *290,* 186-192.

26. Bohlmann, F.; Ahmed, M.; Borthakur, N.; Wallmeyer, M.; Jakupovic, J.; King, R.; Robinson, H. Diterpenes related to grindelic acid and further constituents from grindelia species. *Phytochemistry* **1982,** *21,* 167-172.

Chapter 5 Pyrolysis of organosolv and ionic liquid extracted lignin

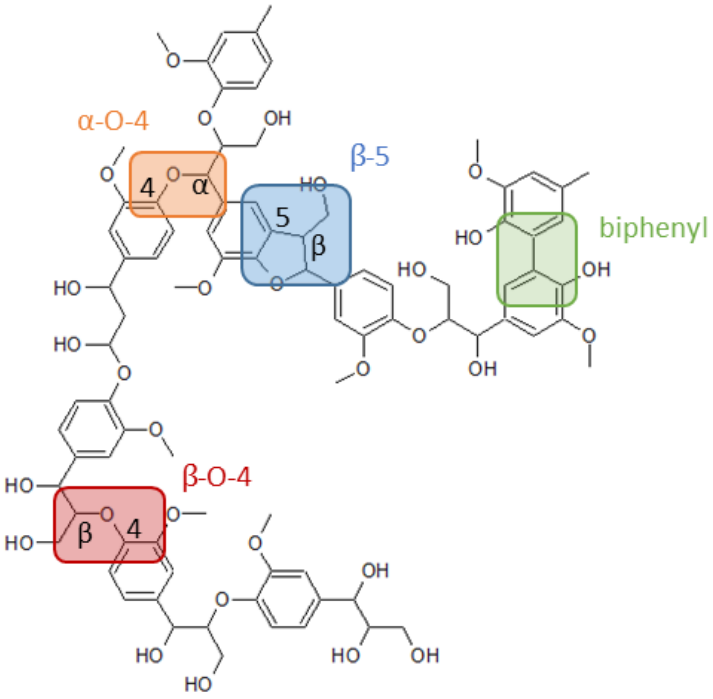

5.1 Abstract

Thermochemical pyrolysis of isolated lignin provides a route for generating high value, phenolic-based specialty chemicals. The source and isolation technique used to obtain lignin can alter the fragmentation and depolymerization pathways of lignin during pyrolysis, hence altering the overall conversion and specific product slate. Therefore, in this work three types of woody biomass; Douglas fir, eucalyptus, and poplar were used to generate lignin through two different pretreatment methods, ethanol organosolv (EOL) and ionic liquid ionosolv (IL). Lignin structures were revealed using ^{13}C-^{1}H HSQC and ^{31}P NMR, ATR-FTIR, and GPC methods. Full product analysis of the pyrolysis slate is given for EOL and IL lignin as well as the whole biomass with a bench scale horizontal reactor-MBMS, and a tandem microreactor-GCMS-FID-TCD.

5.2 Introduction

With a sustained interest in the production of biofuels and specialty chemicals from renewable resources such as biomass, the importance of lignin as a source of aromatic and phenolic reagents is growing. Lignin makes up 23-33% of softwood biomass and 16-25% in hardwoods. [1] The exact nature of lignin including its molecular weight, elemental composition, chemical linkages, reactivity and overall macromolecular structure is highly variant and can be difficult to determine. Controlled isolation of lignin could be used to tailor the macromolecular structure of lignin and remove carbohydrates. [2, 3] Subsequent pyrolysis of isolated lignin can further depolymerize it into monomeric phenolic compounds. Additionally, by removing carbohydrate derivatives from the mixture, a relatively pure feedstock of phenolic compounds can be obtained.[4-6, 1]

Lignin is a crosslinked phenylpropane polymer that can range from 17,200 Mw (g mol^{-1}) to 53,850 Mw (g mol^{-1}). [7] There are three main types of lignin monomers that include 4-hydroxy-3-methoxyphenylpropane (guaiacol), 3,5-dimethoxy-4-hydroxyphenylpropane (syringyl), and 4-hydroxyphenylpropane (p-hydroxyphenyl). These monomers are polymerized to form β -O-4, α-O-4, β-β, β-5, and 5-5 linkages. [8] Lignin and carbohydrates are connected through various covalent linkages that make the isolation of any single compound difficult. The three-main lignin-carbohydrate linkages are phenol glycoside (PhGlc), γ-ester (Est), and benzyl ether (BE). [9] Selective bond cleavage and lignin isolation can be carried out through a number of processes with ionic liquids and ethanol organosolv being some of the environmentally-friendly technologies. [2]

The use of ionic liquids for biomass pretreatment has gained interest because of its low volatility, ability to be recycled, and is generally considered a green solvent. Ionic liquids are described as salts that are liquid at room temperature. [10] Lignin has been shown to be dissolved in ionic liquids that contain a 1,3-dialkylimidazolium cation, however, the solubilization of lignin benefits from an a moderate to strong hydrogen-bonding anion such as trifluoromethanesulfonate (triflate, [OTf]-), methyl sulfate ([$MeSO_4$]-), hydrogen sulfate ([HSO_4]-), chloride, bromide and acetate anions. [2] The imidazolium cation was shown to be a good choice of cation for lignin dissolution by using dispersion corrected density functional theory, which showed the cation interacting with lignin phenyl rings via the aromatic rings. [11] Muhammad et al. [1] showed that isolating lignin from bamboo with 1-3-butyl-methylimidazolium chloride [Bmim][Cl] and 1-butyl-3-methylimidazolium acetate [Bmim][OAc] followed by fast pyrolysis can reduce the yields of deleterious aldehydes and ketones that are responsible for the aging of bio-oil, and at the same time can produce the desired phenols, furans, alcohols and hydrocarbons. Lei et al. [6] used [Bmim][Cl] to alter the already isolated alkali lignin and found that the yield of phenolic compounds from pyrolysis increased 11 times over the yields of non-treated alkali lignin. The change in pyrolysis behavior was attributed to a decrease in the hydrogen bonds of lignin after the treatment of [Bmim][Cl] as determined through FTIR.

Organosolv utilizes an organic solvent and an acid catalyst to dissolve lignin from biomass. Commonly used solvents for this process are methanol, ethanol, acetic, formic, and sulfuric acids. Other chemicals that are useful in this process are phenols, amines, glycols, nitrobenzene, dioxane, dimethyl sulphoxide, sulpholane, and liquid carbon dioxide [12]. The primary mechanism of organosolv involves: (i) disrupting the internal bonds of lignin through hydrolysis as well as the lignin-hemicellulose bonds such as ether and 4-O-methyl-D-glucuronic acid ester bonds; (ii) breaking the glycosidic bonds of hemicellulose through hydrolysis; and (iii) degradation of monosaccharides catalyzed by acidic reagents. [3] Liu et al. [5] performed pyrolysis at temperatures ranging from 400°C to 800°C and determined that the highest selectivity of phenols was produced in the temperature range of 500°C-600°C. Additionally, it was shown that higher amounts of β-β' linkages in the lignin structure led to lower yields of S-type lignin and higher yields of G-type lignin. This was attributed to the higher thermal stability of β-β' linkages enabling more demethoxylation reactions to occur before the linkage broke and the compound volatilized.

The target of this work is to assess the relevance of lignin isolation technique and lignin source on the chemical structure and pyrolysis behavior. A detailed structural analysis of the isolated lignin is given using ^{13}C-^{1}H hetero singular quantum coherence nuclear magnetic resonance (HSQC-NMR), ^{31}P nuclear magnetic resonance, ATR-FTIR, gel permeation chromatography (GPC) and elemental analysis to illustrate differences in the lignin structure that arise due to the extraction technique and the woody biomass source. Pyrolysis behavior is characterized by Py-GC/MS/FID/TCD and a bench scale horizontal reactor with molecular beam mass spectrometry (MBMS).

5.3 Materials and Methods

5.3.1 Lignin Extraction

Douglas fir, eucalyptus, and poplar were obtained from Forestry Products LLC (WA). Samples were ground into wood flour with a particle size < 200 μm and dried to a moisture content of 7-10% dry basis before IL and EOL extraction.

For EOL extraction, biomass samples were treated with 1.1 wt.% H_2SO_4 and 65.0 v% ethanol, loaded into a sealed reactor and heated to 170°C for 60 min. The solid fraction was filtered off and washed 3 times with 300 mL aqueous ethanol at the same concentration as the cooking liquor at 60°C to further extract lignin. Spent liquor and ethanol washes were diluted with water to precipitate lignin which was then filtered and further washed with water, dried and kept as the ethanol organosolv lignin fraction. [13-15]

For IL extraction, 1-Butyl-3-methylimidazolium hydrogen sulfide [Bmim][HSO_4] was purchased from Sigma Aldrich and used as received. IL and water were first mixed in a 50mL culture tube so that water was 20% of the total volume. 1.0g biomass was then added for every 10mL of solution. The mixture was incubated in an oven at 120°C for 4 hours. The samples were then cooled to room temperature and

mixed with 2X volume of methanol and left for 2 hours. The pulp was filtered off using Whatman 541 filter papers. To remove the methanol from the supernatant, it was stored at 75°C overnight. To precipitate the lignin, 150mL water was added for every 5mL of the original liquor. This mixture was then heated to 70°C and held at that temperature for 30min. The precipitate was filtered and washed thrice with 10 mL of distilled water at 70°C. The recovered lignin was then dried for several days. [16]

5.3.2 Lignin Structural Characterization

^{13}C and two-dimensional ^{13}C-^{1}H HSQC spectra were acquired with a Bruker Avance 500 MHz spectrometer. The lignin samples were placed into a 4 mL vial and dissolved in deuterated dimethyl sulfoxide (DMSO-d6). The ^{13}C spectra were carried out at 300 ^{o}K using a 90° pulse with a minimum of 12288 scans accumulated for each sample. The central solvent peak for DMSO (δc= 39.5 ppm) was used as an internal reference for the chemical shift calibration. Two-dimensional ^{13}C-^{1}H heteronuclear single quantum coherence (HSQC) spectra were acquired in a Bruker Avance HD 500-MHz spectrometer with a z-gradient triple resonance Cryo-probe. The samples were dissolved in 0.6 mL dimethylsulfoxide (DMSO)-d6 and a Bruker standard pulse sequence ('hsqcetgpsi2') was used to record the spectra. [17, 18] The spectral widths were 10 ppm in F2 (1H) dimension with 2048 time of domain and 210 ppm in F1 (13C) dimension with 256 time of domain, respectively. The number of transients was 96 with a recycle delay of 1.5-s and the $^{1}J_{CH}$ of 145 Hz. The central DMSO solvent peaks (δ_H/δ_C=2.49/39.5 ppm) were used for chemical shift calibration. Volume integration of cross peaks in HSQC spectra was carried out using Bruker's TopSpin 3.5pl7 software. [19, 9, 20]

Samples for ^{31}P-NMR consisted of a stock solution of 1.54mL pyridine, 0.96mL chloroform-d to make a stock solution #1. Added to this was 12.5mg NHND (internal standard) and 27.13mg $Cr(acac)_3$. Lignin was first sieved to smaller particle size and then 25 mg of it was added to 0.65mL of stock solution. 0.1mL TMDP was added to this mixture and then vortexed for 2min. The solution was then transferred to an NMR tube and ^{31}P-NMR spectra were acquired with a 90° pulse angle, 0.98 s acquisition time, 25 s pulse delay, and 128 transients at room temperature. [21, 22]

FTIR analysis of the whole biomass and isolated lignin was conducted on a Perkin Elmer Spectrum model 400 (Perkin Elmer Co., Waltham, MA). Spectrums were recorded after 32 scans from 4000 cm^{-1} to 650 cm^{-1}, advanced ATR correction and automatic bassline correction were applied for processing of the spectrums. [23]

The weight-average molecular weight (M_w) and the number-average molecular weight (M_n) of lignin samples were analyzed by gel permeation chromatography (GPC). Each sample was derivatized with acetic anhydride/pyridine mixture (1:1, v/v) at room temperature for 24 hr. Acetylated lignin samples were recovered by rotary evaporation, dissolved in THF and filtered by PTFE membrane filter (size in μm) for GPC analysis. The GPC analysis was conducted using SECurity GPC 1200 System (Agilent Technologies

Inc., Santa Clara, CA) equipped with Agilent UV detector and three Waters Styragel columns (HR1, HR4 and HR5, Waters Corporation, Milford, MA). The analysis was operated with 1 mL/min flow rate, THF as mobile phase and UV absorbance at 270 nm. Each analysis was conducted in duplicate. The molecular weights were calculated by Polymer Standards Service WinGPC Unit software with 14 polystyrene standards (0.58×10^3 to 5.38×10^5 g/mol).

5.3.3 Pyrolysis

5.3.3.1 Tandem micro pyrolyzer-GCMS/FID/TCD

The same tandem microreactor and calibration methods were used for this section as in Chapter 3. The first chamber was held at 500°C and the second chamber was held at 380°C

5.3.3.2 Horizontal Reactor – MBMS

The horizontal reactor is a bench scale system used in pyrolyzing samples of 30mg at a temperature of 550°C with a second reaction chamber that was held at 550°C. MBMS is capable of analyzing the entire product slate of pyrolysis vapors and the adiabatic cooling of MBMS and low ionization energy (22.5 eV) limits fragmentation which simplifies the spectrum of pyrolysis products. MBMS is not able to distinguish ions of the same mass and therefore complimentary analysis with GC-MS gives an excellent description of the product slate. Several studies have given excellent descriptions of the MBMS system and gave ample detail on the theories and operations of the system. [28]

5.4 Results and Discussion

5.4.1 Lignin Structural characterization

^{13}C-^{1}H HSQC of isolated lignin show three regions representing aliphatic, side-chain, and aromatic ^{13}C-^{1}H correlations. Side-chain and aromatic regions cross-signals were identified by comparing with literature [29]. For monolignol compositions of S, G, H quantitation, the S2/6, G2, H2/6 in aromatic regions were integrated. In the aliphatic oxygenated region, the Cα/Hα correlations signals were used for contour integration for inter-unit linkages estimation. The relative abundance of inter-unit linkage was calculated with respect to the total aromatic rings and results are presented in Table 5.1. The EOL lignin has depleted all the interunit linkages except with a trace amount of resinol type linkages that remained there. The IL lignin retains a large abundance of β-O-4 ether linkages in addition to the phenylcoumaran and resinol linkages. In addition, the IL lignin has a higher S/G ratio than the EOL lignin.

Table 5.1. Relative abundance (%) for lignin subunits and inter-unit linkages.

Lignin subunits	Douglas Fir IL	Douglas Fir EOL	Eucalyptus IL	Eucalyptus EOL	Poplar IL	Poplar EOL
S total	-	-	65.8	48.2	75.8	33.5
S’	-	-	6.4	4.1	4.3	1.7

S condensed	-	-	23.1	31.7	-	-
G total	55.25	66.2	35.8	51.7	29.6	39.5
G condensed	-	-	11.6	11.6	-	-
H	-	-	-	-	1.1	0.6
S/G ratio	-	-	1.8	0.9	2.6	0.8
Interunit linkages (%)						
β-O-4	13.2	-	19.4	-	14	-
β-5	3.2	-	2.8	-	2.1	-
β-β	2.7	0.44	7.5	1	3.6	0.7

Note. Compositions are expressed as a fraction of S+G+H.
S: syringyl unit; S': oxidized syringyl units
G: guaiacyl unit
H: p-hydroxyphenyl unit
β-O-4: β-aryl ether
β-5: phenylcoumaran
β-β: resinol

The quantitative analysis of hydroxyl structures including aliphatic alcohols, phenolic C5-substituted-OH, Guaiacyl-OH, p-hydroxy-OH, and carboxylic acid groups in ethanol organosolv and [C_4C_1im] [HSO_4] ionic liquid lignin was based on the technique using TMDP for phosphitylation. [22] The resulting NMR spectrums are presented in Figure 5.1. The concentration of each hydroxyl group was calculated based on the internal standard, endo-N-hydroxy-5-norbornene-2,3dicarboximide (NHND). Integration results are presented in Table 5.2. Interpretation of the ^{31}P NMR spectra is based on literature. [30, 22, 31]

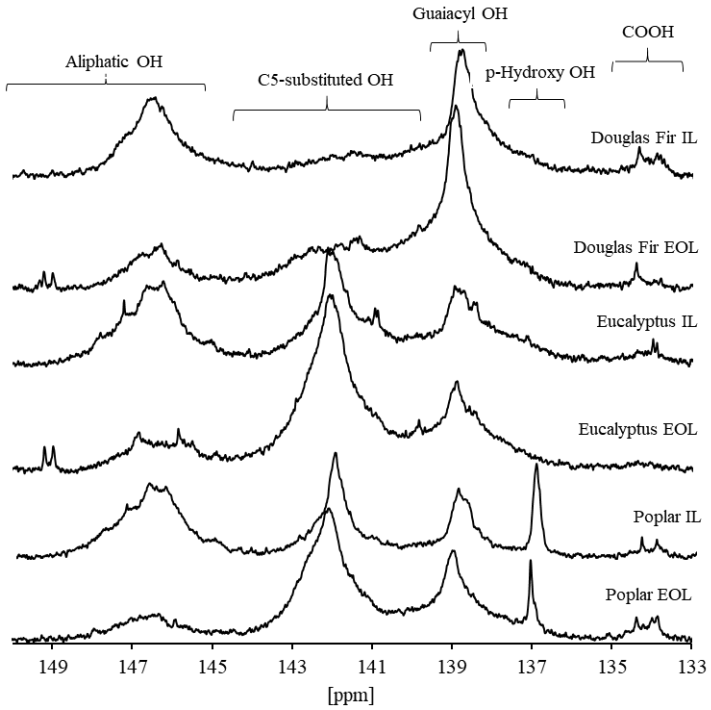

Figure 5.1. ^{31}P NMR spectrum of different hydroxyl groups in EOL and IL lignin's

The most abundant hydroxyl group was found to be aliphatic alcohols of IL lignin. A survey of literature conducted by Pu et al. [22] found values for these groups to range from 0.33 – 7.30 mmol g^{-1} with values depending on biomass type and the extraction method. These can be the side chain hydroxyl groups of lignin or carbohydrates. Lower amounts of these hydroxyl groups are present in EOL lignin because of the acid catalyzed elimination reactions being more dominant in EOL extraction. The amount of C5 substituted phenols was higher for the EOL extracted lignin and indicates the higher extent of condensation reactions. The C5-substituted groups included syringyl lignin and according to Balakshin et al. [31] these groups should not be separately quantified as this can lead to a large overestimation. Literature values ranged from 0.34 - 1.80 mmol g^{-1} for the C5-substituted groups. [32] Results of the current work are out of this range, with eucalyptus and poplar having higher values, whereas Douglas fir having lower values of the C-5 substituted groups. Guaiacyl groups are only slight higher in EOL for Douglas fir and poplar while eucalyptus showed lower amounts of guaiacol from EOL compared with IL. This is because of the shoulder on the IL lignin. P-hydroxyphenyl may be present in all the samples but is very distinguishable in poplar samples. The different composition of S/G/H type lignin for the respective hardwood and softwood species is well aligned with literature values.

Table 5.2. ^{31}P NMR analysis of different hydroxyl groups in EOL and IL lignin's

		Phenolic OH, mmol g^{-1}			
	Aliphatic OH, mmol g^{-1}	C5 substituted	Guaiacyl	p-hydroxyphenyl	COOH, mmol g^{-1}
Douglas Fir IL	2.12	0.16	1.70		0.21
Douglas Fir EOL	0.64	0.41	1.83		0.06
Eucalyptus IL	2.48	1.99	0.68		0.19
Eucalyptus EOL	0.61	2.61	0.43		0.08
Poplar IL	2.01	1.08	0.54	0.34	0.13
Poplar EOL	0.47	1.93	0.64	0.15	0.19

ATR-FTIR of the six lignin samples reveals ample information about the structures and also confirms some of the observations from NMR. FTIR is also able to characterize whole biomass and identify alterations caused by extraction procedures. There is a noticeable difference between IL and EOL spectrum at the 1709-1738 cm^{-1} peak that correlates with the unconjugated C=O vibration. This peak is more prominent in the EOL lignin and can be caused by the presence of xylose but could also be a result of the β-O-4 cleavage, which can produce a C=O bond at the β position in lignin phenolic structures. The aromatic in-plane deformation of S units can be seen at 1125 cm^{-1} for eucalyptus and poplar and is absent from the Douglas fir samples in the case of EOL. The condensed guaiacol signals are present for EOL samples from 1270-1335 cm^{-1}. In this region of the spectrum, there is a much broader signal indicating multiple overlapping signals as opposed to the better resolved signals from IL lignin. Additionally, the C-H deformation in secondary alcohols and aliphatic ethers at ~1090 cm^{-1} is weaker in the EOL spectrum, which indicates that the side chain region has been compromised and is condensed. These observations can be confirmed with the NMR results. IL lignin spectrum closely resembles that of the alkaline lignin, milled wood lignin and cellulolytic enzyme lignin produced by Yuan et al. [20] Ethanol organosolv extraction of Loblolly pine (softwood) was studied by Mahadevan et al. [23] and its FTIR spectrum is nearly identical to that of Douglas fir reported in this work indicating similar structures after the EOL extraction.

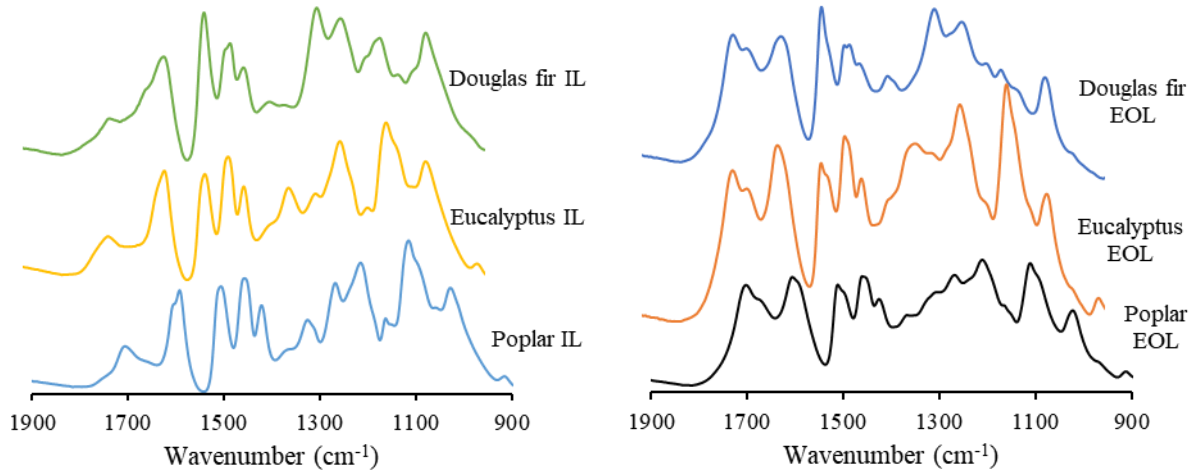

Figure 5.2. ATR-FTIR spectrum of IL and EOL lignin.

5.4.2 Pyrolysis

5.4.2.1 Tandem micro pyrolyzer-GCMS/FID/TCD

Microscale pyrolysis experiments were conducted on a Py-GC/MS/FID/TCD system to quantify differences in product distributions depending on lignin source and isolation technique. Quantification of GC detectable compounds is given in Table 5.3. The quantified products included light gases, mostly CO and CO_2, phenolic monomers, acids, aldehydes, alcohols, furans, and ketones. The sum of all identified products accounted for 20-30% of the carbon yield. The major compounds were linked to the results of MBMS and confirm the observed molecular species.

The largest group of compounds in the pyrolysis products was identified as the light gases. The light gases accounted for 4.2-10.4 % of the carbon in the product, with whole biomass and IL lignin giving higher yields than EOL lignin. For IL lignin the light gasses consisted of CO, CO_2, and isobutene. EOL lignin produced more species of hydrocarbons with lower individual yields. The trends in CO_2 yields are well aligned with the amount of carboxylic acids in the lignin structures as determined by ^{31}P NMR, indicating higher levels for IL lignin.

Monomeric liquid products accounted for 10-25 % of the product carbon, with higher yields obtained from whole biomass pyrolysis, which can be explained by the volatility of carbohydrates. Liquid yields for isolated lignin were low and only 8-10 % of the product carbon. This is typical for lignin as the C-C bonds are not readily cleaved during pyrolysis, and hence the char yield ranged from 45.8 - 52.8 wt.% compared to 13.9 – 18.8 wt. % for whole biomass. The identified liquid products from isolated lignin are primarily made of phenolic monomers with either S, G or H methoxyl substitution and various ligands at

the C4 position. The highest yield of a single compound was 3.4 % for phenol from IL extracted poplar. Poplar biomass and EOL lignin also gave higher yields of phenols compared with eucalyptus and Douglas fir indicating that the source of biomass is responsible for this trend.

The total carbon yield of phenolic monomers is highly dependent on the biomass species and the lignin extraction method. For the whole biomass, poplar generated the highest carbon yield of phenolic monomers followed by Douglas fir and lastly eucalypts; all ranging from 4.8 to 7.5 %. Poplar produces large amounts of all the three types of lignin derivatives, 1.7% H, 3.0 % G and 2.9 % S, as shown in table 5.3. Eucalyptus does not produce any H type phenolic monomers and Douglas fir does not produce any S type phenolic monomers regardless of the extraction method. With the EOL lignin the trend in total carbon yield of phenolic monomers follows that of the whole biomass, poplar > Douglas fir > eucalyptus, with yields ranging from 3.7% to 2.3%. The total yield is lower with EOL lignin due to the lack of β-O-4 linkages as determined by HSQC. With IL lignin, the yield of phenolic monomers does not follow the same trend as whole biomass and EOL. With IL lignin eucalyptus produces more phenolic monomers than Douglas fir. This is mainly caused by an increase in the G type monomers from eucalyptus. With the IL lignin the yield of G monomers is 3.8% for eucalyptus, which is higher than what is observed from whole biomass (2.4 %) or EOL (1.8 %). The G derivatives that showed the most increase in yield with eucalyptus IL are 4-ethyl-guaiacol, guaiacol and 2-Methoxy-4-vinyl phenol. There is also a large increase in the amount of syringyl from eucalyptus IL. This means that the IL extraction method is altering the structure of the lignin in a such way that makes the aforementioned G and S lignin monomers more easily volatilized. By isolating lignin with the β-O-4 linkages intact, this may be caused by the reduction in Mw compared with that of the raw EOL lignin characterized in this work. GPC analysis of lignin by other researchers has shown that the Mw of natural lignin is closer to 5000 Da, which may partially explain why IL lignin from hardwoods can produce higher carbon yields of phenolic monomers than whole biomass. Volatilization occurs during the primary reaction phase between 200-400°C. During this stage the biomass polymer constituents depolymerize primarily through homolysis of ether bonds. At terminal ends of the lignin macromolecules homolysis can result in evaporation and the radical intermediates can be stabilized through hydrogen donation in the gas phase. Within the lignin macromolecule, homolysis does not result in evaporation and therefore the stabilization of radicals is more likely to occur through carbon-carbon bond formation.

The remaining portion of the liquid products from pyrolysis of IL and EOL lignin is a diverse mix of compounds. Interestingly furans show an increase in yield with EOL lignin. It is thought that furans are formed from the degradation of carbohydrates during the extraction process. Furan yields were higher with hardwood species and varied from 2.0% with eucalyptus up to 2.3% from poplar. Acetaldehyde is a common product from all feedstocks and was between 1.6% and 2.2% for whole biomass and 0.2% to 0.6%

from lignin from EOL. The yield of ketones is mainly from acetone, which is only detected in the case of lignin samples and gave higher yields from EOL.

Table 5.3. Tandem Microreactor Pyrolysis products from lignin's

		Poplar			Douglas Fir			Eucalyptus		
Library/ID	m/z	BM	EOL	IL	BM	EOL	IL	BM	EOL	IL
Yield (C%)										
Light gases										
Ethene	28	-	0.6	-	-	0.4	-	-	0.4	-
Ethane	30	-	0.5	-	-	0.4	-	-	0.2	-
Butane	58	-	-	0.7	-	-	0.9	-	-	0.6
Propene	42	-	0.4	-	-	0.3	-	-	0.2	-
1-Propene, 2-methyl-	56	-	-	2.7	-	-	1.0	-	-	2.2
CO	28	0.8	1.7	1.8	0.6	1.1	1.1	0.6	1.7	0.7
CO_2	44	6.6	3.1	5.2	6.1	2.1	2.9	6.3	3.3	4.6
Sum		7.4	6.4	10.4	6.7	4.2	5.8	6.8	5.7	8.2
Liquid products		23.7	10.9	11.7	15.0	8.9	5.4	24.1	8.6	8.8
Phenolic monomers										
Vanillin	152	0.2	-	0.3	0.4	0.1	0.3	-	-	0.2
Phenol, 4-methyl-	108	-	-	-	0.2	0.1	-	-	-	-
Phenol, 4-methoxy-3-(methoxymethyl)-	168	0.3	-	0.4	-	-	-	0.4	-	0.5
Phenol, 4-hydroxyacetyl-2-methoxy-	154	-	-	-	-	0.2	0.1	-	0.1	-
Phenol, 4-ethyl-2-methoxy-	152	-	-	0.6	0.2	0.2	0.3	-	0.1	0.7
Phenol, 2-methyl-	108	0.2	0.1	0.2	-	0.1	0.2	-	-	0.1
Phenol, 2-methoxy-4-methyl-	138	0.2	0.6	-	1.2	0.7	1.1	-	0.4	-
Phenol, 2-methoxy-4-(1-propenyl)-	164	0.7	0.1	0.2	1.2	0.1	0.2	0.5	-	0.2
Phenol, 2-methoxy-	124	0.8	0.5	1.3	1.0	0.5	1.4	0.7	0.4	1.0
4-Methoxy-2-methyl-1-(methylthio)benzene	168	-	0.4	-	-	-	-	-	0.4	-
2-Methoxy-5-methylphenol	138	-	-	0.9	-	-	-	0.2	-	0.4
2-Methoxy-4-vinylphenol	150	0.6	0.2	0.7	1.0	0.3	0.8	0.6	0.2	0.9
Benzeneacetic acid, 4-hydroxy-3-methoxy-	182	-	-	-	-	0.1	-	-	0.1	-
Phenol, 2,6-dimethoxy-4-(2-propenyl)-	194	1.1	-	-	-	-	-	1.2	-	0.4
Phenol, 2,6-dimethoxy-	154	0.7	0.4	1.7	-	-	-	0.8	0.5	1.8
Phenol, 2,4-dimethyl-	122	-	-	-	-	0.1	0.1	-	-	0.0
Benzaldehyde, 4-hydroxy-3,5-dimethoxy-	182	0.4	-	0.2	-	-	-	0.4	-	-
4-Methyl-2,5-dimethoxybenzaldehyde	180	0.7	0.1	-	-	-	-	-	-	-
Phenol	94	1.5	1.1	3.4	0.2	0.1	0.3	-	-	-
Eugenol	164	0.2	-	-	0.3	-	0.1	-	-	-
Sum		7.5	3.7	9.9	6.2	2.7	4.8	4.8	2.3	6.2
Furans										
Furan, 2-methyl-	82	-	0.7	-	-	0.5	-	-	0.7	-
Furan, 2-ethyl-5-methyl-	110	-	0.1	-	-	-	-	-	-	-
Furan, 2,5-dimethyl-	96	-	0.5	-	-	0.3	-	-	0.3	-
Furan	68	0.3	0.8	0.1	-	-	-	0.3	0.7	-

2-Furancarboxaldehyde, 5-methyl-	110	-	0.2	-	0.4	0.0	-	-	0.2	-
2-Furancarboxaldehyde, 5-(hydroxymethyl)-	126	-	-	-	0.5	-	-	-	-	-
Sum		0.3	2.3	0.1	0.8	0.8	-	0.3	2.0	-
Aldehydes / Acids / Alcohols										
Acetaldehyde	44	2.2	0.6	0.4	1.6	0.5	0.2	1.9	0.6	0.3
Furfural	96	1.9	-	0.2	1.4	-	-	1.9	-	-
2-Propenal	56	1.8	-	-	1.1	-	-	1.1	-	-
Acetic acid	60	4.5	-	0.2	1.4	-	-	7.1	-	1.2
Pentanoic acid, 4-oxo-, ethyl ester	144	0.8	-	-	-	0.5	-	1.6	0.3	-
Formic acid, ethyl ester	74	-	0.8	-	-	1.1	-	-	-	-
Ethanol	46	-	2.6	-	-	2.6	-	-	2.5	-
1,2-Benzenediol, 4-methyl-	124	-	-	-	0.2	-	0.2	-	-	-
1,2-Benzenediol, 3-methoxy-	140	0.3	-	0.7	-	-	-	0.3	-	0.9
1,2-Benzenediol	110	0.3	-	-	-	-	-	0.3	-	-
d-Allose	180	-	-	-	-	-	-	0.4	-	-
Sum		11.7	4.0	1.4	5.7	4.8	0.5	14.6	5.7	2.4
Ketones										
Acetone	58	-	0.9	0.3	-	0.6	0.2	-	0.9	0.2
2-Propanone, 1-hydroxy-	74	1.0	-	-	0.6	-	-	0.9	-	-
2(5H)-Furanone	84	0.8	-	-	0.2	-	-	1.2	-	-
2-Cyclopenten-1-one, 2-hydroxy-3-methyl-	112	0.6	-	-	0.5	-	-	-	-	-
2-Cyclopenten-1-one, 2-hydroxy-	98.0	1.5	-	-	1.0	-	-	1.5	-	-
2,3-Butanedione	86.0	-	-	-	0.5	-	-	0.6	-	-
Ethanone, 1-(2,4,6-trimethylphenyl)-	162.0	0.4	-	-	-	-	-	0.4	-	
Sum		4.3	0.9	0.3	2.7	0.6	4.1	4.5	0.9	0.2
Total Carbon Yield (%)		31.0	17.3	22.1	22.1	13.1	15.3	30.9	16.6	16.9

5.4.2.2 Horizontal Reactor – MBMS

The bench-scale horizontal reactor-MBMS was used to observe the entire product slate for these lignin samples. Whole biomass was also run to highlight the effect of isolation technique on the outcome of pyrolysis. Initially, a general mass balance based around char yields was obtained for this system. Lignin samples produced 45.8 - 52.8 wt.% char with no major differences between extraction technique or biomass source. light gas yields ranged from 4.2-10.4 C% and therefore the total liquid yield is not drastically different for these lignin samples regardless of extraction technique of biomass source. However, as shown by the MBMS spectrum in Figure 5.3 the isolation technique has a drastic effect on the product slate and intensity of certain ion signals. The m/z signals for biomass and IL ranged up to 200 m/z and the largest compounds detected are believed to be monomeric lignin derivatives such as 2-Methoxy-4-vinyl phenol which has an m/z of 150. For EOL m/z signals were detected up to 400 m/z which can represent lignin dimers and trimers.

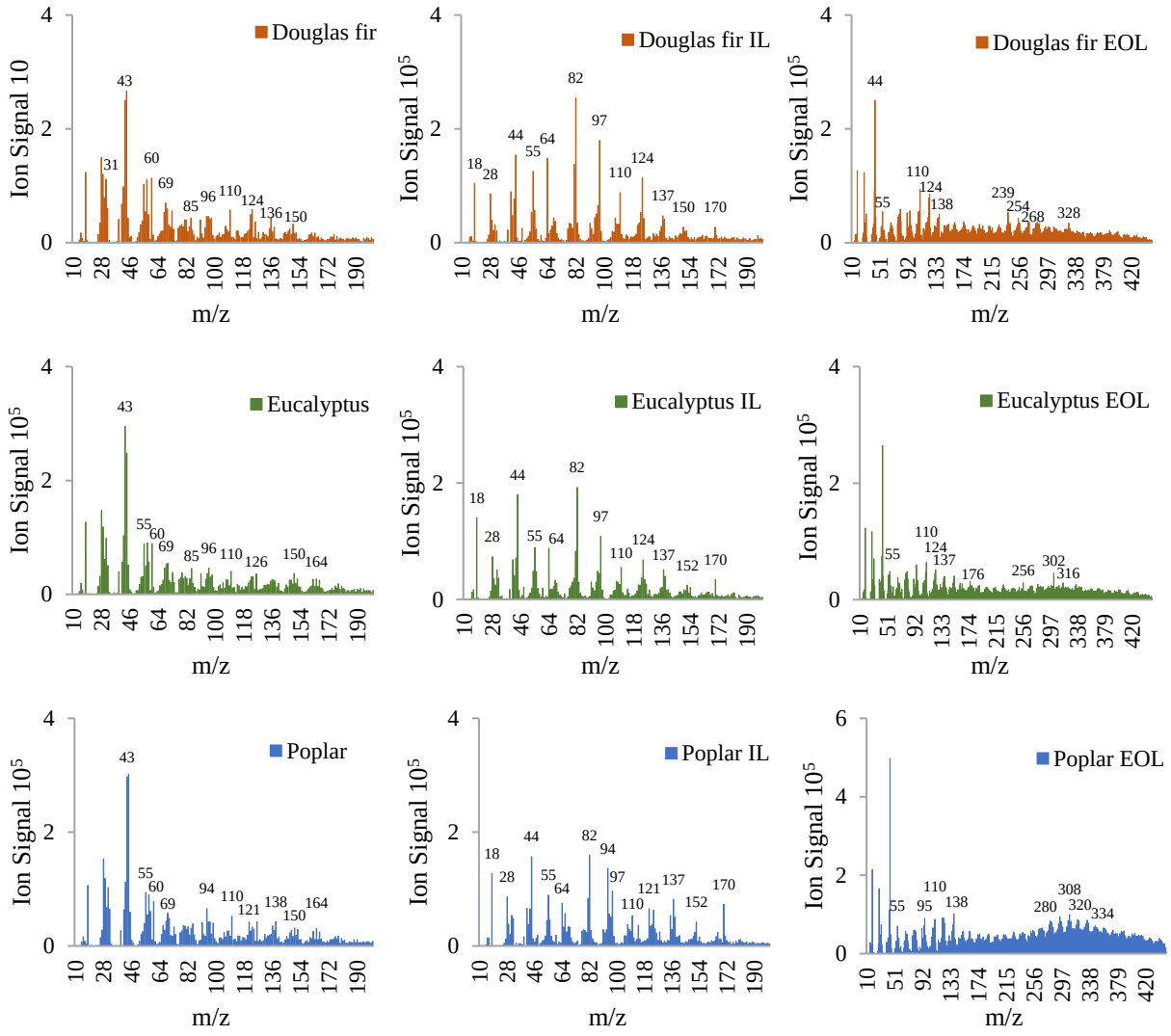

Figure 5.3. MBMS spectrum of whole biomass and isolated lignin's.

5.5 Conclusion

EOL and IL lignin were characterized to determine the role of isolation techniques and lignin source on the outcome of pyrolysis. IL had a greater proportion of β-O-4, β-β and resinol linkages leading to more controlled fragmentation and higher yields of desired monomeric phenols. The highest carbon yield of pure phenol was obtained with IL extraction of poplar and generated 3.4 %. The EOL lignin produced high molecular weight fragments upon pyrolysis and gave lower yields of desired phenolic compounds with a greater diversity of fragments. The char yields and gas yields were similar indicating that the total condensable phase was within 5% for all lignin. This similarity was believed to be related to the similar mass fraction of oxygen in the isolated lignin as determined by elemental analysis. Due to the preservation of the β-O-4 linkage and higher yield of desired monomeric phenols, using [Bmim][HSO_4] is the better pathway for isolating lignin with this application. Lower temperature pyrolysis process can be used to

further enhance the selectivity of bond cleavage with these lignin types and potentially result in a higher selective of phenolic compounds.

References

1. Muhammad, N.; Omar, W.; Man, Z.; Bustam, M.; Rafiq, S.; Uemura, Y. Effect of ionic liquid treatment on pyrolysis products from bamboo. Ind. Eng.Chem. Res. 2012, 51, 2280-2289.

2. Brandt, A.; Gräsvik, J.; Hallett, J.; Welton, T. Deconstruction of lignocellulosic biomass with ionic liquids. Green Chem 2013, 15, 550.

3. Sannigrahi, P.; Ragauskas, A.; Miller, S. Lignin structural modification resulting from ethanol organosolv treatment of loblolly pine. Energy Fuels 2010, 24, 683-689.

4. Guo, X.; Wang, S. Mechanism research on fast pyrolysis of organosolv lignin by pyrolyzer coupled with gas chromatography and mass spectrometry. J. Renewable Sustainable Energy 2015, doi: 10.1063/1.4916633.

5. Liu, C.; Hu, J.; Zhang, H.; Xiao, R. Thermal conversion of lignin to phenols: Relevance between chemical structure and pyrolysis behavior. Fuel 2016, 182, 864-870.

6. Lei, Z.; Hu, Z.; Shui, H.; Ren, S.; Wang, Z.; Kang, S.; Pan, C. Pyrolysis of lignin following ionic liquid pretreatment at low temperature. Fuel Processing Technology 2015, 138, 612-615.

7. Tolbert, A.; Akinosho, H.; Khunsupat, R. Characterization, and analysis of the molecular weight of lignin for biorefining studies. Biofuels, Bioprod. Bioref. 2014, DOI: 10.1002/bbb.

8. Huang, S.; Mahmood, N.; Tymchyshyn, M.; Yuan, Z.; Xu, C. Reductive depolymerization of kraft lignin for chemical and fuels using formic acid as an in-situ hydrogen source. Bioresource Technol. 2014, 171, 95-102.

9. Yuan, T.; Sun, S.; Xu, F.; Sun, R. Characterization of lignin structures and lignin-carbohydrate complex (LCC) linkages by quantitative 13C and 2D HSQC NMR spectroscopy. J. Agric. Food Chem. 2011, 59, 10604-10614.

10. Sun, N.; Rahman, M.; Qin, Y.; Maxim, M.; Rodriguez, H.; Rogers, R. Complete dissolution and partial delignification of wood in the ionic liquid 1-ethyl-3-methylimidazolium acetate. Green Chem. 2009, 11, 646-655.

11. Janesko, B. Phys, Chem. Che. Phys. 2011, 13, 11393.

12. Zhao, X.; Cheng, K.; Liu, D. Organosolv pretreatment of lignocellulosic biomass for enzymatic hydrolysis. Appl Microbiol Biotechnol 2009, 82 (2009), 815-827.

13. Pan, X.; Kadla, J.; Ehara, K.; Gilkes, N.; Saddler, J. Organosolc ethanol lignin from hybrid poplar as radical scavenger: relationship between lignin structure, extraction conditions, and antioxidant activity. journal of Agricultural and Food Chemistry 2006, 5806-5813.

14. Pan, X.; Gilkes, N.; Kadla, J.; Pye, K.; Saka, S.; Gregg, D.; Ehara, K.; Xie, D.; Lam, D.; Saddler, J. Bioconversion of hybrid Poplar to Ethanol and Co-Products using Organosolv Fractionation Process: Optimization of Process Yields. Wiley InterScience 2006.

15. Zhao, X.; Cheng, K.; Liu, D. Organosolv pretreatment of lignocellulosic biomass for enzymatic hydrolysis. Appl Microbiol Biotechnol 2009, 815-827.

16. Brandt, A.; Ray, M.; To, T.; Leak, D.; Murphy, R.; Welton, T. Ionic liquid pretreatment of lignocellulosic biomass with ionic liquid–water mixtures. Green Chem 2011, 13, 2489–2499.

17. Pu, Y.; Chen, F.; Ziebell, A.; Davison, B.; Ragauskas, A. NMR characterization of C3H and HCT down-regulated alfalfa lignin. BioEnergy Research 2, 198-208.

18. Samuel, R.; Pu, Y.; Jiang, N.; Fu, C.; Wang, Z.; Ragauskas, A. Structural characterization of lignin in wild-type versus COMT down-regulated switchgrass. Front, Energy Res. 2014, 1, 1-9.

19. Ewellyn, A. A Comprehensive Approach for Quantitative Lignin Characterization by NMR Spectroscopy. J. Agric. Food Chem. 2004, 1850−1860.

20. Yuan, T.; Sun, S.; Xu, F.; Sun, R. Structural characterization of lignin from triploid of Populus tomentosa Carr. J. Agric. Food Chem. 2011, 59, 6605-6615.

21. Gang Hu, C. C. Y. P. R. S. a. A. J. R. Structural Characterization of Switchgrass Lignin after Ethanol Organosolv Pretreatment. Energy Fuels 2012, 740-745.

22. Pu, Y.; Cao, S.; Ragauskas, A. Application of quantitative 31P NMR in biomass lignin and biofuel precursors characterization. energy Environ. Sci. 2011, 4, 3154-3166.

23. Mahadevan, R.; Adhikari, S.; Shakya, R.; Wang, K.; Dayton, D.; Li, M.; Pu, Y.; Ragauskas, A. Effect of torrecation temperature on lignin macromolecule and product distribution from HZSM-5 catalytic pyrolysis. Journal of Analytical and Applied Pyrolysis 2016, 122, 95-105.

24. Proano-Aviles, J.; Lindstrom, J.; Johnston, P.; Brown, R. Heat and Mass Transfer Effects in a Furnace-Based Micropyrolyzer. Energy Technol 2017, 5, 189-185.

25. Iisa, K.; French, R.; Orton, K.; Budhi, S.; Mukarakate, C.; Stanton, A.; Yung, M.; Nimlos, M. Catalytic pyrolysis of pine over HZSM-5 with different binders. Top Catal 2016, 59, 94-108.

26. Xu, M.; Mukarakate, C.; Iisa, K.; Budhi, S.; Menart, M.; Davidson, M.; Robichaud, D.; Nimlos, M.; Trewyn, B.; Richards, R. Deactivation of Multilayered MFI Nanosheet Zelote during Upgrading of Biomass Pyrolysis Vapors. ACS Sustainable Chem. Eng 2017, 5, 5477-5484.

27. Benkaci–Ali, F.; Baaliouamer, A.; Meklati, B.; Chemat, F. Chemical composition of seed essential oils from Algerian Nigella sativa extracted by microwave and hydrodistillation. Flavour Fragr. J. 2007, 22, 148-153.

28. Mukarakate, C.; Watson, M.; Dam, J.; Baucherel, X.; Budhi, S.; Yung M; Ben, H.; Iisa K; Baldwin, R.; Nimlos, M. Upgrading biomass pyrolysis vapors over B-zeolites: the role of silica-to-alumina ratio. Green Chem. 2014, DOI: 10.1039/c4gc01425a.

29. Rencoret, J.; Marques, G.; Gutierrez, A.; Lbarra, D.; Li, J.; Gellerstedt, G.; Santos, I.; Jimenez-Barbero, J.; Martinez, A.; del Rio, J. Structural characterization of milled wood lignins from different eucalypt species. Holzforschung 2008, 62, 514-526.

30. Constant, S.; Wienk, H.; Frissen, A.; Peinder, P.; Boelens, R.; van Es, D.; Grisel, R.; Weckhuysen, B.; Huijgen, W.; Gosselink, R.; Bruijnincx, P. New insights into the structure and composition of technical lignins: a comparative characterization study. Green Chem. 2016, DOI: 10.1039/c5gc03043a.

31. Balakshin, M.; Capanema, E. On the quantification of lignin hydroxyl groups with 31P and 13C NMR spectroscopy. J. Wood Chem. Technol. 2015, 35, 220-237.

32. Yunqiao, P.; Cao, S.; Ragauskas, A. Application of quantitative 31P NMR in biomass lignin and biofuel precursors characterization. Energy Environ. Sci. 2011, 4, 3154.

Chapter 6 Summary and Future Direction

6.1 Summary

This dissertation addressed the thermochemical conversion of advanced feedstocks to generate fuels and specialty chemicals. Feedstocks were selected to not only intensify yields, expand available land for biofuels, but also improve chemical makeup to facilitate more efficient conversion. Eucalyptus *benthamii* was manipulated through selective growth cycles and presence/absence of bark to give a more favorable chemical composition. By selecting older trees a higher CH_4 concentration and lower tar content can be achieved from gasification. By gasifying the whole tree including bark the H_2: CO ratio was increased.

Gasification tars forming through radical condensation of lignin derivatives were evaluated for S, G, and H type β-O-4and biphenyl model compounds. It was concluded that S type dimers produce more indenes and naphthalenes than G type model compounds which favor phenanthrenes and furans. H type dimers produce the most benzene, toluene, and phenols.

Spectroscopic characterization and pyrolysis of Eucalyptus *benthamii* were able to show that the higher CrI index for older samples leads to more D-allose and lower furfural. The lignin products were also affected by the harvesting age and bark. Samples with bark produced more S type phenolic monomers than the older and younger samples without bark.

Non-catalytic fast pyrolysis of prickly pear and gumweed at temperatures ranging from 450°C-650°C showed that the alternative carbohydrates and resins significantly influence the pyrolysis products. Prickly pear generated more cyclopentanones and also the high ash content leads to a thermal lag in the decomposition leading to higher liquid yields at elevated temperatures. The resins of gumweed produce higher yields at low temperature and the product slate has larger hydrocarbons stable for diesel fuels.

Vapor phase upgrading during catalytic fast pyrolysis of drought-tolerant plants showed improvements in catalyst lifetime and product yields over pine. Prickly pear deactivates the catalyst more slowly than other feedstocks. This was attributed to the lower lignin content of this plant. Gumweed generated higher yields of aromatics than other feedstocks however the catalyst deactivates at a comparable rate to other feedstocks.

Technical lignin were isolated using two extraction techniques the ethanol organosolv and ionic liquid ionosolv. The biomass source affect the type and amount of phenolic monomers produced as well as the extraction method. Ionic liquid extraction of poplar was found to generate higher yields of pure phenols than other samples tested. Additionally, the overall selectivity of phenolic monomers is improved when lignin is extracted with ionic liquids compared with whole or EOL lignins.

6.2 Limitations of the Dissertation and Future Direction

This research has made contributions to the understanding of how the chemical makeup of plants can alter the results of thermochemical conversion for both gasification and pyrolysis. However, further research is available to continue the advancement of these areas.

1) Gasification tar formation can be further studied by developing reactors that are able to continually feed powered samples such as cellulose and lignin. This would allow for direct measurement of tar formation from model compounds in real time.

2) Although ZSM-5 is an effective catalyst for upgrading oxygenated vapors the formation of CO limits the total carbon yield that can be obtained. Removing oxygen through dehydration reactions that form H_2O could be accomplished with an H_2 reactive atmosphere and molybdenum catalyst or a platinum on titanium catalyst.

3) Drought tolerant feedstocks may be further improved by vapor phase upgrading with catalyst other than ZSM-5. The unique product slate may have the ability to deoxygenate through dehydration reactions with a catalyst such as molybdenum carbide or platinum on titanium.

4) Mild isolation processes of lignin can improve the selectivity of lignin pyrolysis and generate cleaner product slates. Therefore, optimizing the yield of lignin through extraction is important and completely recovering the IL from lignin.

5) Fast pyrolysis of biomass releases aerosols, it is thought that this may be the way that ash metals are transported to catalyst surfaces. However, the rate at which biomass is heated and therefore the rate at which volatiles are produced is less severe for lower heating rates. Therefore, this mechanism of transport may be tested by measuring the amount of ash in char that has been produced through pyrolysis at different heating rates.

Supporting Information

Chapter 2

Table S2.1 Major products from gasification/pyrolysis of lignin model compounds

Library/ID	Non-phenolic						Phenolic			
	HH		GG		SS		GG		SS	
	Avg	Stdv	Avg	Stdv	Avg	Stdv	Avg	Stdv	Avg	Stdv
Light gases										
Ethane	-	-	-	-	-	-	-	-	-	-
Ethene	2.20	0.82	-	-	-	-	-	-	-	-
Propene	0.93	0.31	-	-	3.02	0.07	2.31	0.22	7.50	0.30
1,2-Propadiene	-	-	-	-	-	-	0.29	0.01	3.33	0.08
1-Propene, 2-methyl-	-	-	-	-	0.34	0.01	0.21	0.01	0.41	0.02
1-Buten-3-yne	-	-	0.49	0.02	-	-	0.73	0.02	2.65	0.05
1,3-Butadiene			2.15	0.23	2.46	0.50	-	-	9.15	1.75
1,3-Cyclohexadiene	-	-	-	-	-	-	0.86	0.09	-	-
1,3-Cyclopentadiene	-	-	1.47	0.07	-	-	2.87	0.15	6.80	0.07
1,3-Cyclopentadiene, 1-methyl-	-	-	-	-	-	-	0.65	0.06	2.11	0.02
1,3-Cyclopentadiene, 5-methyl-	-	-	-	-	-	-	-	-	2.73	0.02
1,4-Pentadiene	-	-	0.34	0.04	0.74	0.24	1.37	0.12	2.77	0.50
1,3,5,7-Cyclooctatetraene	5.30	0.68	-	-	4.88	0.09	-	-	-	-
Sum Light Gases	8.43	1.11	4.45	0.24	11.43	0.57	9.29	0.31	37.47	1.85
Primary Tar	23.70	2.18	18.50	1.08	8.24	0.90	47.08	1.52	48.78	1.22
Ketone										
2-Cyclopenten-1-one	-	-	-	-	-	-	0.80	0.03	0.50	0.05

2-Cyclopenten-1-one, 2-methyl-	-	-	-	-	-	-	-	-	0.48	0.01
Sum Ketones	-	-	-	-	-	-	0.80	0.03	0.98	0.05
Aldehyde										
Acetaldehyde	-	-	-	-	0.22	0.03	-	-	0.83	0.06
Benzaldehyde	6.32	0.91	1.48	0.09	0.26	0.04	1.56	0.20	-	-
Benzaldehyde, 2-hydroxy-	-	-	-	-	-	-	1.34	0.18	-	-
Benzaldehyde, 3-methoxy-	-	-	-	-	-	-	-	-	1.37	0.19
Sum Aldehydes	6.32	0.91	1.48	0.09	0.48	0.05	2.90	0.27	2.20	0.21
Phenols										
Phenol	15.17	3.50	11.48	0.46	3.55	0.60	18.40	1.39	6.96	0.21
Phenol, 2-(2-propenyl)-	-	-	-	-	-	-	-	-	1.93	0.21
Phenol, 2-(phenylmethyl)-			0.49	0.10	-	-	-	-	-	-
Phenol, 2,3,5,6-tetramethyl-	-	-	-	-	-	-	-	-	1.10	0.02
Phenol, 2,4-dimethyl-	-	-	-	-	0.50	0.13	1.34	0.13	2.69	0.10
Phenol, 2-ethyl-	-	-	-	-	0.72	0.12	1.64	0.23	3.12	0.09
Phenol, 2-ethyl-5-methyl-	-	-	-	-	-	-	-	-	1.86	0.01
Phenol, 2-ethyl-6-methyl-	-	-	-	-	0.21	0.03	-	-	-	-
Phenol, 2-methyl-	-	-	-	-	-	-	10.80	0.69	16.07	0.12
Phenol, 3-methyl-	-	-	-	-	-	-	2.04	0.18	4.14	0.20
Phenol, 4-(phenylmethyl)-	-	-	0.69	0.11	-	-	-	-	-	-
Phenol, 4-methyl-	0.79	0.70	-	-	-	-	-	-	-	-
Sum Phenols	15.97	3.57	12.67	0.48	4.97	0.63	34.21	1.58	37.85	0.40
Alcohol										
1H-Indenol	0.15	0.14	0.55	0.14	-	-	-	-	-	-
1-Naphthalenol	-	-	-	-	-	-	0.33	0.01	1.33	0.49
1-Naphthalenol, 2-methyl-	-	-	-	-	-	-	0.35	0.00		

2-Naphthalenol	-	-	-	-	-	-	0.65	0.01	-	-
Sum Alcohols	0.15	0.14	0.55	0.14	-	-	1.33	0.02	1.33	0.49
Furan										
Dibenzofuran	-	-	0.55	0.09	0.27	0.03	0.67	0.02	-	-
Dibenzofuran, 4-methyl-	-	-	-	-	0.24	0.00	0.30	0.00	-	-
Benzofuran	1.27	0.15	2.61	0.44	-	-	3.99	0.39	-	-
Benzofuran, 2,3-dihydro-	-	-	-	-	-	-	0.60	0.04	0.62	0.03
Benzofuran, 2-ethenyl-	-	-	0.41	0.09	0.27	0.00	0.90	0.17	-	-
Benzofuran, 2-methyl-	-	-	0.24	0.02	1.68	0.13	1.05	0.00	0.78	0.00
Benzofuran, 7-methyl-	-	-	-	-	0.32	0.03	0.32	0.02	5.01	0.04
2,2'-Bifuran	-	-	-	-	-	-	-	-	3.01	0.34
Sum Furans	1.27	0.15	3.80	0.46	2.78	0.13	7.84	0.43	6.41	0.34
Secondary Tar	60.52	1.68	44.55	1.46	56.06	1.75	26.33	1.38	46.77	1.06
1-Ring										
Benzene	22.51	2.24	10.55	0.95	12.32	0.89	11.43	1.44	14.26	0.13
Benzene, (1,1-dimethyl-2-propenyl)-	-	-	-	-	-	-	-	-	1.32	0.02
Benzene, (1-methyl-2-cyclopropen-1-yl)-	-	-	-	-	0.52	0.05	-	-	-	-
Benzene, (ethenyloxy)-	1.32	0.25	-	-	-	-	-	-	-	-
Benzene, 1,2-dimethyl-	-	-	-	-	-	-	-	-	1.14	0.01
Benzene, 1,3-dimethyl-	-	-	-	-	1.00	0.09	-	-	-	-
Benzene, 1-ethenyl-3-methyl-	-	-	0.27	0.00	0.26	0.03	0.37	0.04	-	-
Benzene, 1-ethyl-2-methyl-	-	-	-	-	-	-	0.14	0.02	-	-
Benzene, 1-methoxy-4-(1-propenyl)-	-	-	-	-	-	-	-	-	1.47	0.12
Benzene, 1-propynyl-	0.80	0.07	-	-	3.51	1.11	-	-	-	-
Benzene, 2-propenyl-	-	-	-	-	-	-	-	-	0.46	0.00
p-Xylene	-	-	-	-	0.76	0.26	1.22	0.00	1.70	0.05

Styrene	-	-	-	-	-	-	2.14	0.18	3.07	0.10
Toluene	26.39	1.17	18.32	1.40	20.10	1.82	5.15	0.63	10.24	0.22
Ethylbenzene	1.73	0.17	5.07	1.13	4.79	0.27	0.77	0.08	1.98	0.05
(E)-Stilbene	0.47	0.02	-	-	0.83	0.12	-	-	-	-
.alpha.-Methylstyrene	-	-	-	-	0.60	0.02	-	-	1.34	0.13
Benzocycloheptatriene	-	-	0.80	0.10	-	-	-	-	-	-
Phenylethyne	-	-	0.51	0.03	-	-	-	-	-	-
1-Phenyl-1-butene	-	-	-	-	-	-	-	-	0.51	0.01
Sum 1-Ring	53.22	2.55	35.52	2.04	44.69	2.34	21.22	1.58	37.49	0.33
Indenes										
Indene	-	-	-	-	-	-	-	-	-	-
1H-Indene, 1,3-dimethyl-	-	-	-	-	-	-	-	-	0.37	0.03
1H-Indene, 1-ethenyl-2,3-dihydro-	-	-	-	-	-	-	-	-	0.47	0.06
1H-Indene, 2,3-dihydro-4,7-dimethyl-	-	-	-	-	0.33	0.00	-	-	-	-
2-Methylindene	-	-	-	-	-	-	-	-	1.51	0.27
Sum Indenes	-	-	-	-	0.33	0.00	-	-	2.36	0.28
2-Ring										
Azulene	0.59	0.06	1.77	0.02	-	-	1.65	0.18	-	-
Naphthalene	-	-	-	-	2.93	0.16	-	-	2.18	0.04
Naphthalene, 1,2-dihydro-	-	-	0.90	0.06	0.95	0.10	1.16	0.26	-	-
Naphthalene, 1,2-dimethyl-	-	-	-	-	-	-	-	-	1.21	0.22
Naphthalene, 1-ethyl-	-	-	-	-	0.53	0.06	-	-	-	-
Naphthalene, 2-ethenyl-	-	-	0.52	0.03	1.25	0.11	0.26	0.08	0.59	0.05
Naphthalene, 2-methyl-	-	-	0.61	0.03	2.37	0.69	1.04	0.08	2.14	0.47
Biphenyl	-	-	0.83	0.05	-	-	0.34	0.03	0.38	0.04
Biphenylene	-	-	0.34	0.02	0.37	0.01	0.22	0.01	0.43	0.01

Diphenylmethane	1.46	0.24	-	-	0.59	0.06	-	-	-	-
Ethylene, 1,1-diphenyl-	0.15	0.02	-	-	0.43	0.07	0.18	0.03	-	-
1,1'-Biphenyl, 4-methyl-	0.52	0.06	-	-	-	-	-	-	-	-
1,2-Diphenylethylene	1.72	0.13	1.11	0.05	-	-	-	-	-	-
Sum 2-Ring	4.43	0.29	6.07	0.10	9.42	0.73	4.85	0.33	6.92	0.52
Tertiary Tar										
Phenanthrene	-	-	1.46	0.08	-	-	-	-	-	-
Fluorene	0.61	0.03	0.72	0.14	0.47	0.03	0.26	0.07	-	-
Anthracene	1.82	0.16	-	-	0.89	0.01	-	-	-	-
Anthracene, 1-methyl-	-	-	0.21	0.02	0.25	0.00	-	-	-	-
Anthrone	0.44	0.03	0.57	0.01	-	-	-	-	-	-
Sum Tertiary Tar	2.87	0.17	2.96	0.16	1.62	0.03	0.26	0.07	-	-
Total Area Percent	87.09	-	66.02	-	65.91	-	73.67	-	95.54	-

Table S.2.2 Thermal decomposition of E. Benthamii samples determined by TGA

Feedstock	Heating rate (°C min^{-1})	Maximum decompn rate (mg min^{-1})	Temperature at max decompn rate (°C)	Char content (% dry)
2EWB		-0.20	393.2	1.9%
2EWoB	10	-0.22	392.6	1.1%
7EWoB		-0.25	393.3	1.0%
2EWB		-0.29	406.8	4.0%
2EWoB	15	-0.31	403.8	3.5%
7EWoB		-0.25	402.0	3.8%
2EWB		-0.91	428.8	15.9%
2EWoB	50	-0.96	429.0	12.7%
7EWoB		-0.97	431.1	13.6%
2EWB		-1.85	434.2	15.7%
2EWoB	100	-1.89	437.3	16.9%
7EWoB		-1.89	436.2	16.2%

	Flynn-Wall-Qzawa	

	Ea (kJ mol^{-1})					
Conversion	2EWB	r2	7EWoB	r2	2EWoB	r2
0.1	67.3	0.999	65.9	0.987	59.9	0.997
0.2	82.0	0.996	79.0	0.989	71.5	0.998
0.3	104.5	0.989	98.5	0.994	86.4	0.997
0.4	126.6	0.999	102.2	0.998	92.6	0.997
0.5	129.4	1.000	98.7	0.989	99.2	0.998
0.6	140.5	0.996	109.3	0.999	108.0	0.998
0.7	185.2	0.898	212.2	0.897	208.7	0.990
Average	119.4		109.4		103.8	

	Kissinger–Akahira–Sunose					
	Ea (kJ mol^{-1})					
Conversion	2EWB	r2	7EWoB	r2	2EWoB	r2
0.1	67.9	0.999	50.2	0.986	46.7	0.997
0.2	83.1	0.995	60.4	0.988	55.6	0.998
0.3	106.5	0.988	76.5	0.994	67.1	0.997
0.4	129.4	0.999	80.0	0.998	72.5	0.997
0.5	132.1	1.000	79.6	0.988	78.2	0.998
0.6	143.7	0.996	86.7	0.999	85.3	0.998
0.7	190.5	0.899	205.5	0.893	201.3	0.990
Average	121.9		91.3		86.7	

Chapter 3

Table S3.1 Carbon yield (%), retention time, and classification of pyrolysis vapors determined by GC-MS/FID/TCD for prickly pear during fast pyrolysis at temperatures ranging from 450°C to 550°C

R.T.	Compound Name	MS Quality	Classification 1	Classification 2	Temperature					
					450°C		550°C		650°C	
					Avg.	Stdv.	Avg.	Stdv.	Avg.	Stdv.
1.53	Ethene	78	Alkene	C2	0.3	0.0	0.7	0.1	2.4	0.2
2.14	Carbon dioxide	4	CO2	CO2	19.6	2.2	24.4	2.7	25.7	1.9
2.19	Propene	89.73	Alkene	C3	0.4	0.0	1.2	0.2	1.9	0.1
2.24	1,2-Propadiene	91	Alkene	C3	0.0	0.0	0.1	0.0	0.5	0.0
2.33	Acetaldehyde	90	Oxygenate	Aldehyde	0.9	0.0	1.1	0.1	1.2	0.0
2.37	1,3-Butadiene	81	Alkene	C4	0.2	0.0	0.2	0.0	0.8	0.0
2.39	1-Propene, 2-methyl-	76	Alkene	C4	0.2	0.0	0.6	0.0	0.9	0.1
2.70	2-Propenal	64	Oxygenate	Aldehyde	0.0	0.0	0.8	0.0	0.9	0.0
2.73	Acetone	80	Oxygenate	Carbonyl	1.2	0.0	1.4	0.1	1.5	0.1
2.80	1-pentene		Alkene	C5	0.0	0.0	0.1	0.0	0.3	0.0
2.83	Furan	90	Oxygenate	Furan	1.4	0.0	1.1	0.4	0.8	0.0
2.92	1,3-Butadiene, 2-methyl-	93	Alkene	C5	0.1	0.0	0.3	0.1	0.4	0.0
3.05	3-Buten-2-one	78	Oxygenate	Carbonyl	0.6	0.0	0.4	0.0	0.0	0.0
3.18	1,3-Cyclopentadiene	94.79	Alkene	C5	0.2	0.0	0.3	0.0	0.5	0.0
3.59	2,3-Butanedione	95.07	Oxygenate	Carbonyl	0.7	0.0	0.8	0.0	0.8	0.0
3.74	2-Butanone	95.36	Oxygenate	Carbonyl	0.7	0.0	0.7	0.0	0.7	0.0
3.87	1-Hexene	95	Alkene	C6	0.3	0.0	0.3	0.0	0.4	0.0
4.00	Furan, 2-methyl-	91	Oxygenate	Furan	0.6	0.0	1.3	0.6	2.0	0.0
4.02	Carbon Monoxide (TCD)	TCD	CO	CO	0.0	0.0	1.2	2.5	2.0	0.1
4.47	Acetic acid	90	Oxygenate	Acid	0.9	0.0	0.9	0.1	0.8	0.0
4.78	1,3-Cyclopentadiene, 1-methyl-	91	Alkene	C6	0.5	0.0	0.8	0.0	1.1	0.1
5.12	Benzene	81.89	Aromatic	1-Ring	0.2	0.0	0.4	0.0	0.5	0.1

5.81	1-heptene	95	Alkene	C7	0.0	0.0	0.1	0.0	0.3	0.0
5.97	Furan, 2,5-dimethyl-	85.24	Oxygenate	Furan	0.6	0.0	1.0	0.3	1.2	0.0
6.09	Propanoic acid	46	Oxygenate	Acid	0.0	0.0	0.2	0.0	0.6	0.0
6.84	Toluene	91.1	Aromatic	1-Ring	0.2	0.0	0.4	0.1	0.6	0.1
6.95	Cyclopentanone	68.87	Oxygenate	Carbonyl	0.6	0.0	0.6	0.0	0.6	0.0
7.49	2-Cyclopenten-1-one	90	Oxygenate	Carbonyl	0.4	0.3	0.6	0.0	0.7	0.0
7.54	Furfural	64	Oxygenate	Aldehyde	0.6	0.1	0.8	0.0	0.9	0.4
8.10	Benzene, 1,3-dimethyl-	95	Aromatic	1-Ring	0.0	0.0	0.2	0.0	0.3	0.1
8.35	2-Cyclopenten-1-one, 2-methyl-	85.78	Oxygenate	Carbonyl	0.6	0.0	1.1	0.1	0.7	0.0
8.93	2-Furancarboxaldehyde, 5-methyl-	76	Oxygenate	Furan	0.4	0.4	1.0	0.4	1.1	0.4
9.18	Phenol	91	Oxygenate	Phenol	0.0	0.0	0.3	0.0	0.7	0.1
9.75	Indene	77.28	Aromatic	1-Ring	0.0	0.0	0.1	0.0	0.3	0.1
9.78	Phenol, 2-methyl-	44	Oxygenate	Phenol	0.0	0.0	0.3	0.0	0.6	0.3
9.96	Phenol, 3-methyl-	74	Oxygenate	Phenol	0.0	0.0	0.2	0.0	0.8	0.1
10.54	Phenol, 2,4-dimethyl-	46	Oxygenate	Phenol	0.0	0.0	0.2	0.0	0.4	0.3
10.61	1H-Indene, 1-methyl-	42	Aromatic	1-Ring	0.0	0.0	0.2	0.1	0.6	0.0
10.63	6-Hepten-2-one, 7-phenyl-	68	Oxygenate	Carbonyl	0.6	0.0	0.0	0.0	0.0	0.0
10.67	2,5-Cyclohexadiene-1,4-dione, 2,5-dimethyl-	58	Oxygenate	Carbonyl	0.6	0.0	0.0	0.0	0.0	0.0
10.69	Phenol, 4-ethyl-	56.07	Oxygenate	Phenol	-	-	0.2	0.0	0.6	0.0
12.90	1-Pentadecene	95	Alkene	C15	0.3	0.0	0.4	0.0	0.7	0.1

Table S3.2. FID Area %, and retention time of pyrolysis vapors determined by GC-MS/FID/TCD for prickly pear during fast pyrolysis at temperatures ranging from 450°C to 650°C

R.T.	Compound Name	Temperature					
		450°C		550°C		650°C	
		Avg.	Stdv.	Avg.	Stdv.	Avg.	Stdv.
1.53	Ethene	1.99	0.12	5.40	1.71	10.47	0.24
2.14	Carbon dioxide	35.95	2.54	29.51	0.20	18.89	1.94
2.19	Propene	3.07	0.11	6.71	0.81	8.16	0.39
2.24	1,2-Propadiene	-	-	-	-	1.07	0.10
2.33	Acetaldehyde	4.09	0.44	5.02	0.43	3.59	0.26
2.37	1,3-Butadiene	2.75	0.04	-	-	3.52	0.22
2.39	1-Propene, 2-methyl-	3.48	0.12	5.01	1.06	4.45	0.21
2.70	2-Propenal	-	-	1.64	0.04	1.97	0.08
2.73	Acetone	8.56	0.30	7.72	0.15	5.48	0.26
2.80	1-pentene	-	-	-	-	0.80	0.02
2.83	Furan	4.25	0.30	2.26	0.32	1.43	0.07
2.92	1,3-Butadiene, 2-methyl-	0.48	0.14	0.92	0.23	1.48	0.13
3.05	3-Buten-2-one	0.61	0.17	0.27	0.11	-	-
3.18	1,3-Cyclopentadiene	0.80	0.04	1.24	0.04	1.67	0.02
3.59	2,3-Butanedione	1.41	0.16	2.13	0.17	1.48	0.08
3.74	2-Butanone	1.41	0.11	1.81	0.15	1.06	0.04
3.87	1-Hexene	0.38	0.01	0.44	0.02	0.74	0.04
4.00	Furan, 2-methyl-	1.03	0.09	0.78	0.19	0.95	0.04
4.02	Carbon Monoxide (TCD)	2.01	0.20	1.49	1.29	4.49	0.56
4.47	Acetic acid	4.08	0.21	3.22	1.09	1.63	0.12
4.78	1,3-Cyclopentadiene, 1-methyl-	0.54	0.04	1.13	0.19	1.60	0.21
5.12	Benzene	1.02	0.30	1.39	0.23	1.78	0.26
5.81	1-heptene	-	-	-	-	0.34	0.08
5.97	Furan, 2,5-dimethyl-	1.32	0.07	1.17	0.07	0.80	0.06
6.09	Propanoic acid	-	-	-	-	0.40	0.09
6.84	Toluene	1.93	0.07	2.27	0.31	2.37	0.05
6.95	Cyclopentanone	0.67	0.15	0.87	0.06	0.55	0.03

7.49	2-Cyclopenten-1-one	0.08	0.07	0.75	0.10	0.64	0.18
7.54	Furfural	1.04	0.70	0.51	0.31	0.57	0.09
8.10	Benzene, 1,3-dimethyl-	-	-	0.51	0.14	0.97	0.14
8.35	2-Cyclopenten-1-one, 2-methyl-	1.25	0.20	1.51	0.38	0.77	0.06
8.93	2-Furancarboxaldehyde, 5-methyl-	-	-	1.58	1.18	1.15	0.32
9.18	Phenol	-	-	-	-	1.07	0.19
9.75	Indene	-	-	-	-	0.40	0.20
9.78	Phenol, 2-methyl-	-	-	-	-	0.29	0.08
9.96	Phenol, 3-methyl-	-	-	-	-	1.73	0.38
10.61	1H-Indene, 1-methyl-	-	-	0.03	0.05	0.55	0.09
10.63	6-Hepten-2-one, 7-phenyl-	0.24	0.01	-	-	-	-
10.67	2,5-Cyclohexadiene-1,4-dione, 2,5-dimethyl-	1.11	0.08	-	-	-	-
10.69	Phenol, 4-ethyl-	-	-	-	-	0.54	0.09
12.90	1-Pentadecene	0.33	0.11	0.17	0.02	0.82	0.34

Table S3.3 Carbon yield (%), retention time, and classification of pyrolysis vapors determined by GC-MS/FID/TCD for gumweed during fast pyrolysis at temperatures ranging from 450°C to 550°C

R.T.	Compound Name	MS Quality	Classification 1	Classification 2	Temperature					
					450°C		550°C		650°C	
					Avg.	Stdv.	Avg.	Stdv.	Avg.	Stdv.
1.92	Ethene	83	Alkene	C2	-	-	0.77	0.03	3.28	0.19
2.13	Carbon dioxide	4	Carbon dioxide	Carbon dioxide	11.85	1.3	14.41	0.21	17.21	1.68
2.17	Propene	42	Alkene	C3	0.35	0.03	0.74	0.15	2.84	0.08

2.24	1,2-Propadiene	87	Alkene	C3	-	-	-	-	0.44	0.03
2.31	Acetaldehyde	90	Oxygenate	Carbonyl	0.7	0.01	0.87	0.05	0.98	0.05
2.37	1-Propene, 2-methyl-	53	Alkene	C4	0.66	0.03	0.80	0.31	3.87	0.16
2.73	Acetone	86	Oxygenate	Carbonyl	0.83	0.1	0.89	0.03	1.26	0.05
2.81	Furan	91	Oxygenate	Furan	0.6	0.02	-	-	1.14	0.06
2.92	1,4-Pentadiene	94	Alkene	C5	-	-	0.43	0.04	-	-
3.03	Acetic acid, methyl ester	50	Oxygenate	Acid	0.5	0.02	0.51	0.01	1.4	0.03
3.17	1,3-Cyclopentadiene	87	Alkene	C5	0.14	0.01	0.09	0.12	0.5	0.02
3.41	2-Propenal, 2-methyl-	81	Oxygenate	Alcohol	-	-	-	-	0.56	0.04
3.54	2-Pentene, 4-methyl-, (Z)-	93	Alkane	C6	-	-	-	-	0.75	0.03
3.64	2-Pentanone	59	Oxygenate	Carbonyl	-	-	0.74	0.05	-	-
3.78	5,9-Dodecadien-2-one, 6,10-dimethyl-, (E)-	64	Oxygenate	Carbonyl	-	-	-	-	-	-
3.98	Furan, 2-methyl-	91	Oxygenate	Furan	0.49	0.02	0.25	0.35	0.59	0.02
4	Carbon Monoxide (TCD)	TCD	Carbon Monoxide	Carbon Monoxide	-	-	0.07	0.00	2.59	0.2
4.47	Acetic acid	91	Oxygenate	Acid	1.06	0.04	1.62	0.42	0.55	0.02
4.79	1,3-Cyclopentadiene, 1-methyl-	93	Alkene	C6	-	-	-	-	0.91	0.06
5.07	2-Propanone, 1-hydroxy-	72	Oxygenate	Carbonyl	0.69	0.04	0.78	0.07	-	-
5.13	Benzene	91	Aromatic	1-Ring	-	-	-	-	0.68	0.03
5.97	Furan, 2,5-dimethyl-	76	Oxygenate	Furan	0.53	0.01	-	-	0.51	0.05
6.48	Toluene	94	Aromatic	1-Ring	0.2	0.01	0.34	0.06	1.05	0.06
7.52	1,5-Dimethyl-1,4-cyclohexadiene	95	Alkane	C8	-	-	-	-	0.36	0.07
7.81	Butanoic acid, 3-methyl-	72	Oxygenate	Acid	0.48	0.01	0.54	0.08	-	-
7.92	Butanoic acid, 2-methyl-	58	Oxygenate	Acid	0.51	0.01	0.52	0.03	-	-
8.06	Cyclopentane, 2-ethylidene-1,1-dimethyl-	91	Alkane	C8	0.28	0.02	0.48	0.05	0.49	0.28
8.09	p-Xylene	97	Aromatic	1-Ring	-	-	-	-	0.68	0.12
8.3	1,3,5,7-Cyclooctatetraene	96	Alkene	C8	0.23	0.02	0.30	0.04	0.28	0.02

8.56	1,2-Cyclopentanedione	74	Oxygenate	Carbonyl	0.54	0.06	0.58	0.07	-	-
9.13	Phenol	94	Oxygenate	Phenol	1.14	0.24	1.64	0.10	0.67	0.06
9.31	Benzene, 1,2,3-trimethyl-	76	Aromatic	1-Ring	0.2	0.11	-	-	0.54	0.06
9.66	Limonene	97	Alkene	C10	0.28	0	0.34	0.04	-	-
10.04	Phenol, 3-methyl-	95	Oxygenate	Phenol	0.58	0.06	-	-	0.55	0.03
10.61	1H-Indene, 1-methyl-	95	Aromatic	1-Ring	-	-	-	-	0.59	0.06
10.85	Phenol, 2-methoxy-4-methyl-	70	Oxygenate	Methoxy Phenol	0.47	0.27	-	-	-	-
11.7	Naphthalene, 2-methyl-	93	Aromatic	2-Ring	-	-	-	-	0.4	0.16
11.71	2-Methoxy-4-vinylphenol	95	Oxygenate	Methoxy Phenol	0.66	0.04	0.69	0.05	-	-
11.92	Phenol, 2,6-dimethoxy-	74	Oxygenate	Methoxy Phenol	0.49	0.01	0.52	0.03	-	-
12.11	Naphthalene, 1,2,3,4-tetrahydro-1,1,6-trimethyl-	97	Aromatic	2-Ring	0.22	0.01	0.35	0.02	0.74	0.04
12.55	Naphthalene, 2,7-dimethyl-	94	Aromatic	2-Ring	-	-	-	-	0.31	0.04
12.6	Phenol, 2-methoxy-4-(1-propenyl)-	96	Oxygenate	Methoxy Phenol	0.49	0.03	0.50	0.02	-	-
13.14	1H-Inden-1-one, 2,3-dihydro-3,3,5,7-tetramethyl-	93	Terpenoid	Carbonyl	0.49	0	-	-	0.51	0
13.18	1H-Cycloprop[e]azulene, 1a,2,3,4,4a,5,6,7b-octahydro-1,1,4,7-tetramethyl-, [1aR-(1a.alpha.,4.alpha.,4a.beta.,7b.alpha.)]-	91	Terpenoid	Hydrocarbon	0.43	0.08	0.58	0.05	0.51	0.01
14.02	Phenol, 2,6-dimethoxy-4-(2-propenyl)-	91	Oxygenate	Phenol	0.48	0.03	-	-	-	-
15.2	5,6-Azulenedimethanol, 1,2,3,3a,8,8a-hexahydro-2,2,8-trimethyl-, (3a.alpha.,8.beta.,8a.alpha.)-	45	Terpenoid	Alcohol	1.28	0.03	-	-	-	-
15.39	Cadina-1(10),6,8-triene	94	Terpenoid	Hydrocarbon	1.63	0.15	-	-	-	-
15.41	Benzene, 1-(5,5-dimethyl-1-cyclopenten-1-yl)-2-methoxy-	41	Terpenoid	Ester	-	-	0.99	0.20	-	-

15.46	3-Buten-2-ol, 3-methyl-4-(2,6,6-trimethyl-2-cyclohexen-1-yl)-	64	Terpenoid	Alcohol	0.54	0.01	-	-	-	-
15.56	14-Oxatricyclo[9..2.1.0(1,10)]tetradecane, 2,6,6,10,11-pentamethyl-	97	Terpenoid	Hydrocarbon	0.76	0.16	0.56	0.01	-	-
15.66	1H-Indole-2,3-dione, 7-(3-methylbutyl)-	30	Terpenoid	Carbonyl	0.96	0.11	-	-	-	-
15.92	Cyclopenta[g]-2-benzopyran, 1,3,4,6,7,8-hexahydro-4,6,6,7,8,8-hexamethyl-	62	Terpenoid	Ester	1.01	0.06	-	-	0.45	0.26
16.03	8-Decenoic acid, 5-ethenyl-3,5,9-trimethyl-, methyl ester	56	Terpenoid	Acid	0.58	0.06	-	-	-	-
16.14	Thunbergol	50	Terpenoid	Alcohol	0.62	0.03	-	-	-	-
16.24	Acetic acid, 2-(2,2,6-trimethyl-7-oxa-bicyclo[4.1.0]hept-1-yl)-propenyl ester	84	Terpenoid	Acid	0.53	0.01	-	-	-	-
16.47	Silane, trimethyl[5-methyl-2-(1-methylethyl)phenoxy]-	41	Terpenoid	Ether	0.47	0.01	-	-	0.45	0.01
16.57	Alloaromadendrene oxide-(1)	47	Terpenoid	Ester	0.64	0.05	-	-	-	-
16.76	2-Aziridinone, 1-(1-adamantyl)-3-(1-methylcyclopentyl)-	51	Terpenoid	Carbonyl	0.68	0.02	-	-	-	-
17.07	3-Methoxy-8,14-secoestra-1,3,5(10),9(11)-tetraen-14,17-dione	53	Terpenoid	Ester	0.71	0.03	-	-	-	-
17.23	4-Cyclohexene-1,2-dicarboximide, N-butyl-, cis-	38	Terpenoid	Carbonyl	0.51	0.04	-	-	-	-
17.31	Grindelic acid	62	Terpenoid	Acid	0.53	0.04	-	-	-	-

Table S3.4 FID area percent, and retention time of pyrolysis vapors determined by GC-MS/FID/TCD for gumweed during fast pyrolysis at temperatures ranging from 450°C to 550°C

R.T.	Compound Name	Temperature					
		450°C		550°C		650°C	
		Avg.	Stdv.	Avg.	Stdv.	Avg.	Stdv.

1.92	Ethene	-	-	-	-	9.34	0.42
2.1259	Carbon dioxide	12.80	0.23	17.43	2.92	9.13	0.49
2.17	Propene	1.68	0.28	3.80	0.76	8.64	0.41
2.24	1,2-Propadiene	-	-	-	-	0.77	0.07
2.31	Acetaldehyde	2.04	0.18	3.69	0.28	2.28	0.04
2.37	1-Propene, 2-methyl-	0.40	0.41	-	-	1.30	0.12
2.73	Acetone	2.92	0.68	5.09	0.46	3.40	0.12
2.81	Furan	1.29	0.14	0.23	0.33	2.91	0.23
2.92	1,4-Pentadiene	-	-	2.16	0.18	-	-
3.03	Acetic acid, methyl ester	0.54	0.14	0.40	0.03	2.25	0.25
3.17	1,3-Cyclopentadiene	0.40	0.07	0.64	0.08	1.28	0.11
3.41	2-Propenal, 2-methyl-	-	-	-	-	0.53	0.15
3.54	2-Pentene, 4-methyl-, (Z)-	-	-	-	-	0.99	0.02
3.64	2-Pentanone	-	-	1.85	0.02	-	-
3.78	5,9-Dodecadien-2-one, 6,10-dimethyl-, (E)-	-	-	0.85	0.02	-	-
3.98	Furan, 2-methyl-	0.44	0.12	-	-	0.66	0.04
4.003	Carbon Monoxide (TCD)	1.49	0.17	2.55	0.18	3.26	0.38
4.47	Acetic acid	-	-	-	-	-	-

4.79	1,3-Cyclopentadiene, 1-methyl-	-	-	-	-	0.27	0.05
5.07	2-Propanone, 1-hydroxy-	-	-	2.22	0.43	-	-
5.13	Benzene	-	-	-	-	1.78	0.14
5.97	Furan, 2,5-dimethyl-	0.74	0.04	-	-	0.34	0.17
6.48	Toluene	0.90	0.05	1.48	0.40	3.05	0.03
7.52	1,5-Dimethyl-1,4-cyclohexadiene	-	-	-	-	0.54	0.18
7.81	Butanoic acid, 3-methyl-	0.36	0.01	0.70	0.08	-	-
7.92	Butanoic acid, 2-methyl-	0.63	0.08	0.58	0.04	-	-
8.06	Cyclopentane, 2-ethylidene-1,1-dimethyl-	0.57	0.06	1.62	0.21	0.59	0.51
8.09	p-Xylene	-	-	-	-	1.96	0.51
8.3	1,3,5,7-Cyclooctatetraene	0.28	0.08	0.32	0.02	0.30	0.06
8.56	1,2-Cyclopentanedione	0.80	0.35	0.37	0.52	-	-
9.13	Phenol	-	-	0.56	0.08	-	-
9.31	Benzene, 1,2,3-trimethyl-	0.05	0.09	-	-	1.01	0.11
9.66	Limonene	0.54	0.06	0.73	0.02	-	-
10.04	Phenol, 3-methyl-	1.14	0.58	1.53	0.80	0.49	0.08
10.61	1H-Indene, 1-methyl-	-	-	-	-	0.72	0.15
10.85	Phenol, 2-methoxy-4-methyl-	0.23	0.23	-	-	-	-

11.7	Naphthalene, 2-methyl-	-	-	-	-	0.16	0.01
11.71	2-Methoxy-4-vinylphenol	1.69	0.18	1.60	0.11	-	-
11.92	Phenol, 2,6-dimethoxy-	0.48	0.06	-	-	-	-
12.11	Naphthalene, 1,2,3,4-tetrahydro-1,1,6-trimethyl-	-	-	-	-	0.12	0.06
12.55	Naphthalene, 2,7-dimethyl-	-	-	-	-	0.47	0.09
12.6	Phenol, 2-methoxy-4-(1-propenyl)-	0.47	0.16	0.20	0.28	-	-
13.14	1H-Inden-1-one, 2,3-dihydro-3,3,5,7-tetramethyl-	0.48	0.02	-	-	0.34	0.02
13.18	1H-Cycloprop[e]azulene, 1a,2,3,4,4a,5,6,7b-octahydro-1,1,4,7-tetramethyl-, [1aR-(1a.alpha.,4.alpha.,4a.beta.,7b.alpha.)]-	1.46	0.34	2.39	0.70	1.03	0.05
14.02	Phenol, 2,6-dimethoxy-4-(2-propenyl)-	0.36	0.16	-	-	-	-
15.2	5,6-Azulenedimethanol, 1,2,3,3a,8,8a-hexahydro-2,2,8-trimethyl-, (3a.alpha.,8.beta.,8a.alpha.)-	2.74	0.13	-	-	-	-
15.39	Cadina-1(10),6,8-triene	7.70	0.31	-	-	-	-
15.41	Benzene, 1-(5,5-dimethyl-1-cyclopenten-1-yl)-2-methoxy-	-	-	4.01	1.61	-	-
15.46	3-Buten-2-ol, 3-methyl-4-(2,6,6-trimethyl-2-cyclohexen-1-yl)-	0.83	0.05	-	-	-	-
15.56	14-Oxatricyclo[9..2.1.0(1,10)]tetradecane, 2,6,6,10,11-pentamethyl-	2.36	1.08	0.62	0.09	-	-
15.66	1H-Indole-2,3-dione, 7-(3-methylbutyl)-	3.90	0.61	-	-	-	-
15.92	Cyclopenta[g]-2-benzopyran, 1,3,4,6,7,8-hexahydro-4,6,6,7,8,8-hexamethyl-	4.23	0.13	-	-	0.03	0.04
16.03	8-Decenoic acid, 5-ethenyl-3,5,9-trimethyl-, methyl ester	1.13	0.34	-	-	-	-
16.14	Thunbergol	1.38	0.10	-	-	-	-

16.24	Acetic acid, 2-(2,2,6-trimethyl-7-oxa-bicyclo[4.1.0]hept-1-yl)-propenyl ester	0.72	0.03	-	-	-	-
16.47	Silane, trimethyl[5-methyl-2-(1-methylethyl)phenoxy]-	0.31	0.05	-	-	0.07	0.02
16.57	Alloaromadendrene oxide-(1)	1.55	0.22	-	-	-	-
16.76	2-Aziridinone, 1-(1-adamantyl)-3-(1-methylcyclopentyl)-	1.84	0.08	-	-	-	-
17.07	3-Methoxy-8,14-secoestra-1,3,5(10),9(11)-tetraen-14,17-dione	2.05	0.18	-	-	-	-
17.23	4-Cyclohexene-1,2-dicarboximide, N-butyl-, cis-	0.62	0.22	-	-	-	-
17.31	Grindelic acid	0.73	0.26	-	-	-	-

Table S3.5 Chemicals used for FID calibrations

	Slope	Intercept
Benzene	6.9E-08	0.16
Ethylbenzene	6.7E-08	0.16
Benzene,1,3-dimethyl-	6.7E-08	0.08
Phenol	4.9E-08	0.96
Benzofuran	4.9E-08	0.96
Benzene, 1,3,5-trimethyl-	7.6E-08	0.36
Indene	6.1E-08	0.42
Naphthalene	6.9E-08	0.13
Naphthalene, 2-methyl-	6.9E-08	0.34
Phenanthrene	8.1E-08	0.42
Carbon dioxide (MS Area)	5.5E-07	-17.34
Carbon Monoxide (TCD Area)	2.4E-07	-2.74
Ethene	6.5E-08	0.11
Propene	6.5E-08	0.11
Butene	7.1E-08	-0.18
Pentene	6.8E-08	0.15
Hexene	6.9E-08	0.39

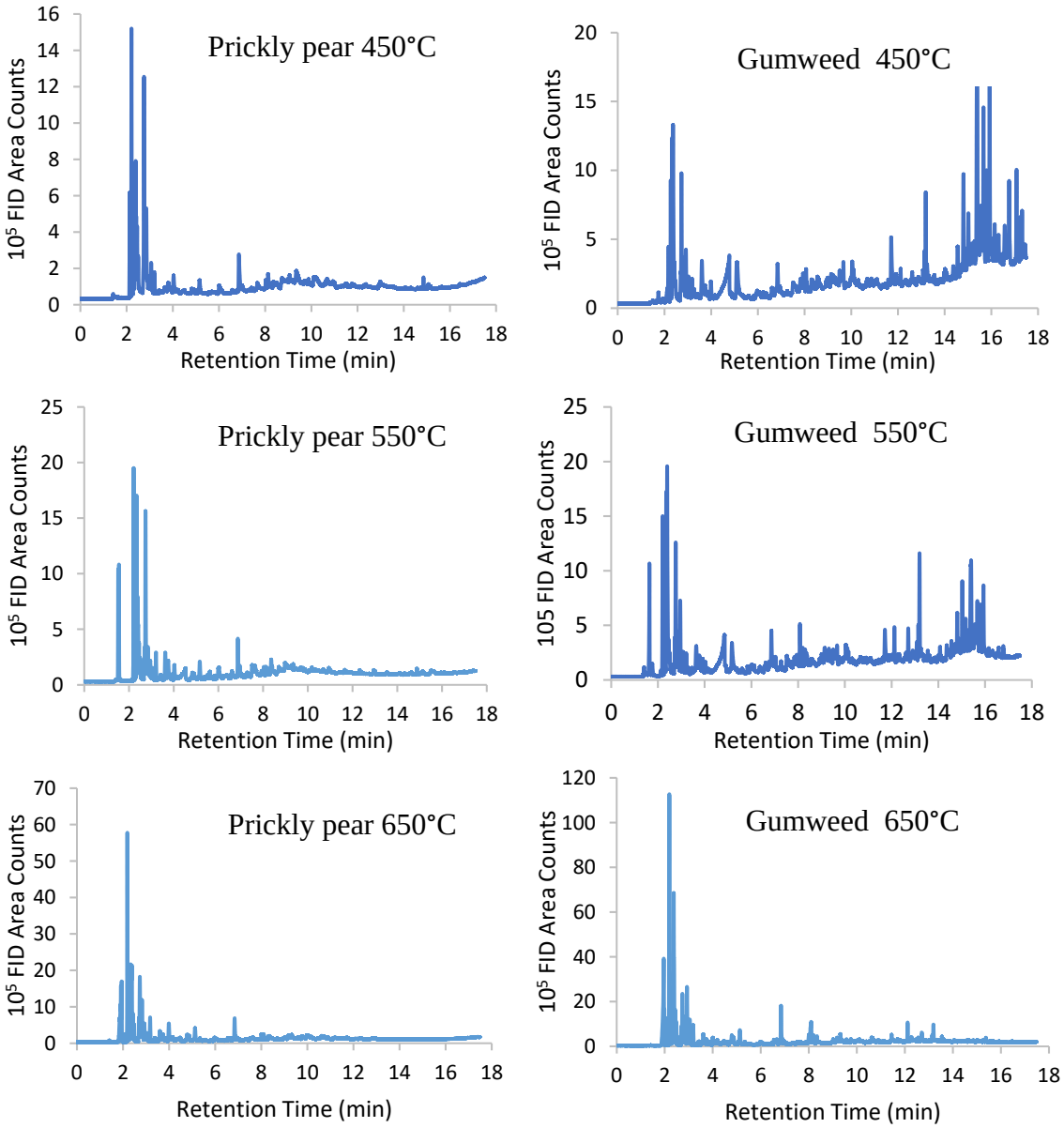

FigureS5.1 FID Chromatograms of prickly pear and gumweed at 450°C - 650°C

Chapter 5

Table S5.1 FTIR Peak assignments

absorbance bands (cm-1)	assignments
3460-3412	O-H stretch
3000-2842	C-H stretch in CH3 or CH2 group
2880-2689	C-H vibration of methyl group of methoxy

1738-1709	C=O stretch in unconjugated ketones, carbonyls and in ester group
1676-1655	C=O stretch in conjugated p-substituent carbonyl and carboxyl
1605-1593	aromatic skeletal vibrations and C=O stretch
1515-1505	aromatic skeletal vibrations and C=O stretch
1470-1460	C-H deformations asymmetric in CH3 and CH2
1430-1422	aromatic skeletal vibrations combined with C-H in-plane deformation
1370-1365	aliphatic C-H stretch in CH3, not in OCH3, phenolic OH
1330-1325	syringyl ring plus condensed guaiacol ring
1270-1266	guaiacol ring plus C=O stretch
1230-1221	C-C, C-O, and C=O stretch
~1166	C-O stretch in ester group (conjugated)
1128-1125	aromatic C-H in-plane deformation (typical for s units) secondary alcohols and C=O stretch
~1086	C-H deformation in secondary alcohols and aliphatic ethers
1035-1030	aromatic C-H in-plane deformation, C-O deformation in primary alcohols, C=O stretch (unconjugated)
~835	C-H out-of-plane in position 2 and 6 of s units, and in all positions of H units

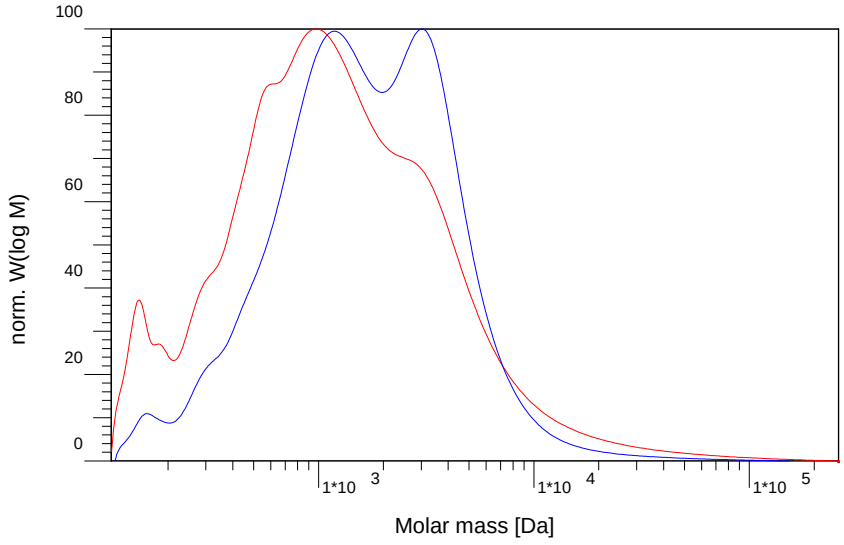

Figure S5.1 Molecular distribution of Poplar-IL lignin (red) and Poplar-EOL lignin (blue)

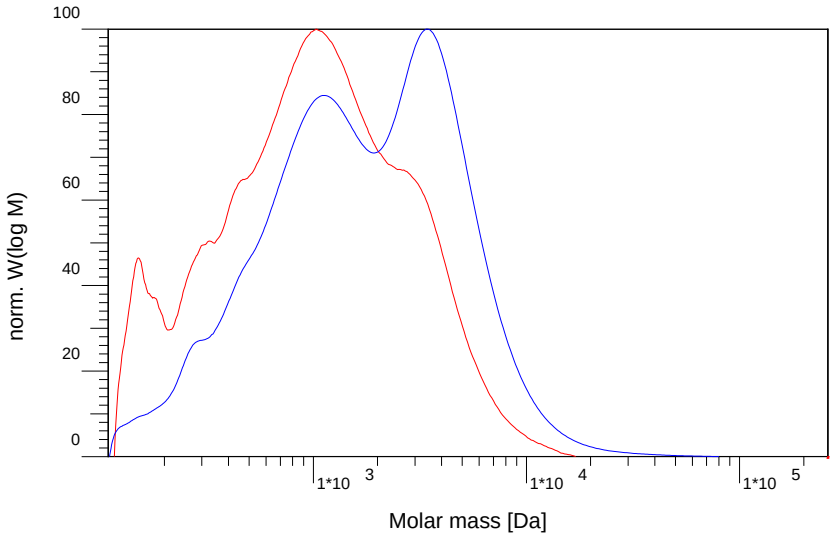

Figure S5.2 Molecular distribution of Douglas fir-IL lignin (red) and Douglas fir-EOL lignin (blue)

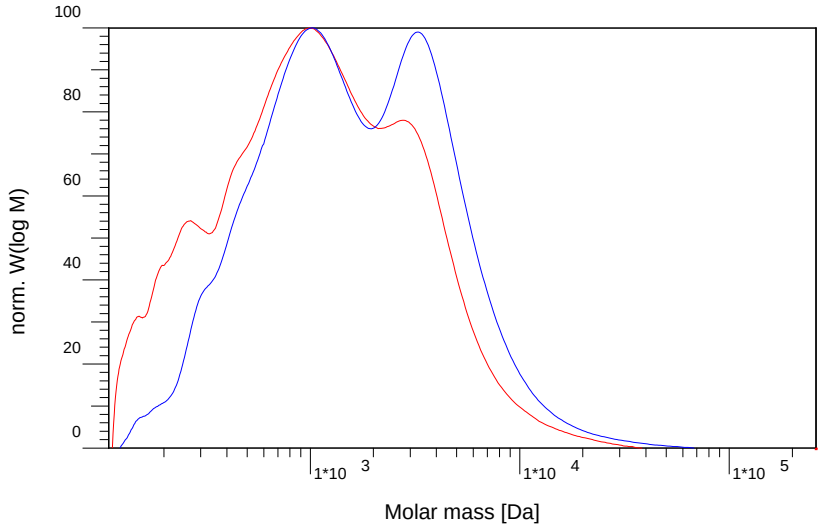

Figure S5.3 Molecular distribution of Eucalyptus-IL lignin (red) and Eucalyptus-EOL lignin (blue)

Table S5.2 Elemental analysis of EOL and IL lignins and raw biomass

	DF			Euc			Pop		
	BM	EOL	IL	BM	EOL	IL	BM	EOL	IL
N	0.09	0.01	2.82	0.16	0.04	2.7	0.13	0.05	2.56
C	45.44	64.82	64.69	45.34	61.8	49.39	45.54	64.84	56.88
H	6.39	5.48	6.25	6.43	5.17	4.86	6.35	5.57	5.76
S	0.02	0.23	2.94	0.01	0.22	3.18	0	0.11	2.88
Other	48.1	29.5	23.3	48.1	32.8	39.9	48.0	29.4	31.9

Table S5.3 Molecular weights (Mw and Mn) and polydispersity index (PDI) of lignins

Lignin Types	Mw (g mol^{-1})		Mn (g mol^{-1})		PDI
	AVG.	SD.	AVG.	SD.	
Poplar-IL	2492	276	683	11	3.65
Poplar-EOL	2313	310	1026	21	2.25
Douglas Fir-IL	1542	62	582	45	2.65
Douglas Fir-EOL	2649	78	984	20	2.69
Eucalyptus-IL	1891	12	655	13	2.89
Eucalyptus-EOL	2731	73	962	49	2.84

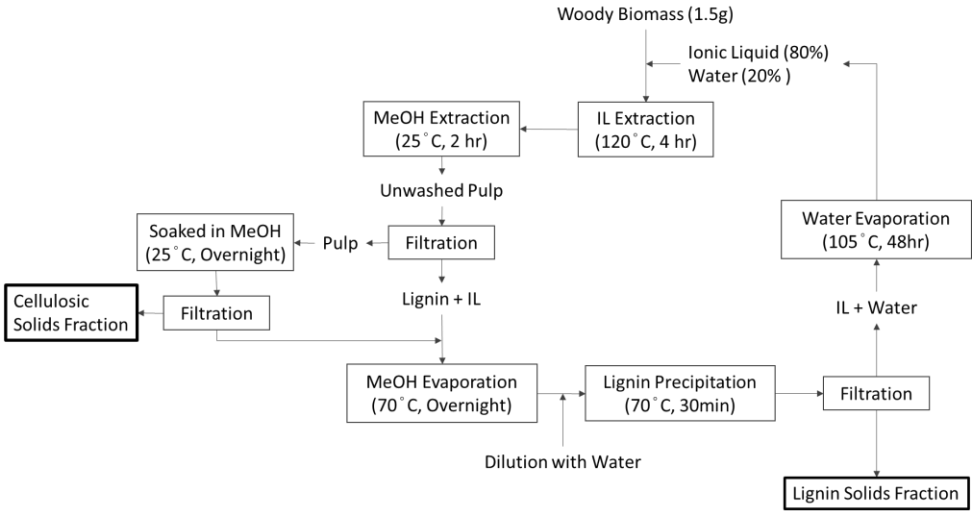

Figure S5.4 Procedure for ionic liquid extraction

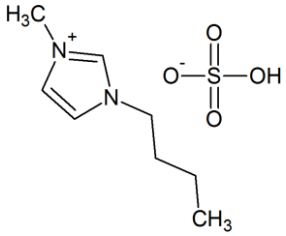

Figure S5.*5* Structure of 1-Butyl-3-methylimidazolium hydrogen sulfide [C4C1im][HSO4]

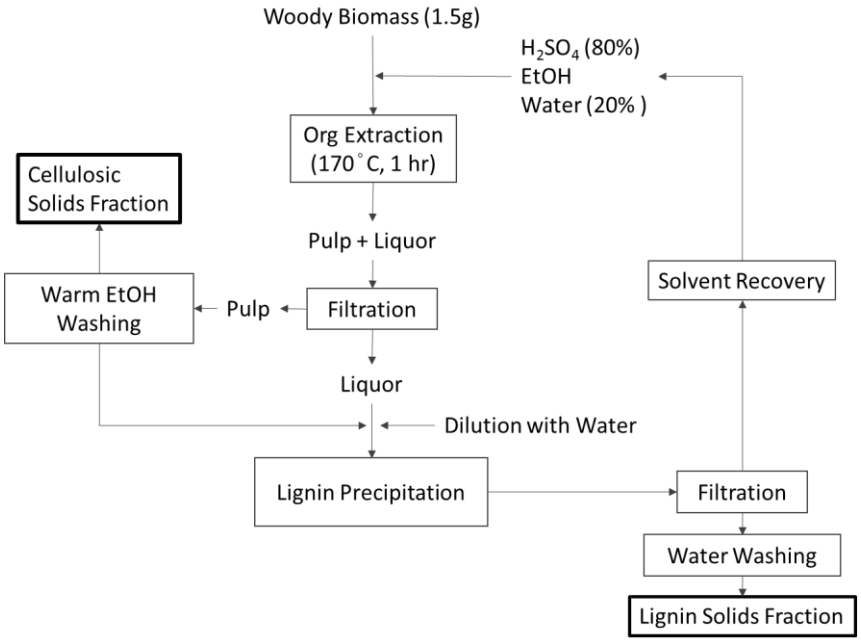

Figure S5.6 Procedure for ethanol organosolv extraction